Mechanisms of hepatocellular toxicity associated with dronedarone and other mitochondrial toxicants

Inauguraldissertation

zur

Erlangung der Würde eines Doktors der Philosophie

vorgelegt der

Philosophisch-Naturwissenschaftlichen Fakultät

der Universität Basel

von

Andrea Debora Felser

aus Nidau, Bern

Basel, 2014

Genehmigt von der Philosophisch-Naturwissenschaftlichen Fakultät

auf Antrag von

Prof. Dr. Stephan Krähenbühl

Prof. Dr. Jörg Huwyler

Basel, den 18.02.2014

Prof. Dr. Jörg Schibler

Dekan der Philosophisch-

Naturwissenschaftlichen Fakultät

Table of contents

Summary

Idiosyncratic drug-induced liver injury is a rare toxic event that typically occurs at therapeutic doses, which are generally safe to the majority of patients. Because there are hardly any reliable preclinical *in vitro* or animal models available to predict this adverse reaction, it represents a substantial problem for the pharmaceutical industry and can have important consequences, such as drug withdrawals or warnings by drug agencies. Although the mechanisms are not fully understood, drug-induced mitochondrial dysfunction and reactive metabolite formation are believed to be major contributors. Severe inhibition of mitochondrial function can trigger accumulation of reactive oxygen species, microvesicular steatosis, hypoglycemia, coma, and death. It is thus important to characterize drugs for their potential interactions with mitochondrial function.

The present work consists of three projects investigating molecular mechanisms of mitochondrial dysfunction *in vitro* and *in vivo*, and is emphasizing on the new antiarrhythmic dronedarone and its structural derivatives.

The aim of the first project was to understand the molecular mechanism of dronedarone-induced hepatotoxicity *in vitro*, and to compare it to amiodarone, a well-known mitochondrial disruptor. We investigated acutely exposed rat liver mitochondria, and primary human hepatocytes and HepG2 cells treated for up to 24h. We performed cytotoxicity experiments, measured the capacity of the respiratory chain and fatty acid β-oxidation, and assessed markers of hepatocyte apoptosis/necrosis. Our investigations demonstrate that similar to amiodarone, dronedarone inhibited the electron transport chain and β-oxidation and uncoupled oxidative phosphorylation of liver mitochondria. We thus suggested that mitochondrial toxicity might explain hepatotoxicity of dronedarone *in vivo*.

The focus of the second project was to expand the knowledge of dronedarone-associated liver toxicity to the *in vivo* situation. We studied hepatotoxicity of dronedarone in wild-type and heterozygous juvenile visceral steatosis mice, a model with higher susceptibility to mitochondrial inhibitors. The animals were treated by oral gavage with two different doses of dronedarone, and mitochondrial function was assessed *in vivo* and *ex vivo*. We found that dronedarone acts as an inhibitor of mitochondrial fatty acid β-oxidation both *in vivo and ex vivo*, whereas the electron

transport chain was not inhibited. Furthermore, juvenile visceral steatosis mice appeared to be more sensitive to the hepatotoxic effects of dronedarone than wild-type mice. We concluded that inhibition of hepatic mitochondrial fatty acid β-oxidation may be an important mechanism of dronedarone-associated hepatotoxicity in humans and underlying defects in hepatic β-oxidation may represent susceptibility factors for this adverse drug reaction.

In the last project we aimed to improve our understanding of the molecular mechanisms of benzbromarone associated liver toxicity. We used HepG2 cells and performed cytotoxicity experiments, measured the capacity of the respiratory chain and fatty acid β-oxidation. In addition, we also investigated adaptive effects on mitochondrial structure. We observed that benzbromarone was associated with uncoupling of oxidative phosphorylation, inhibition of the respiratory chain and inhibition of mitochondrial β-oxidation. Furthermore we found that benzbromarone induced profound changes in mitochondrial network, which may be associated with hepatocyte apoptosis.

Abbreviations

ACS	Acyl-CoA synthetase
ACSL	Long-chain acyl-CoA synthetase
BCA	Bicinchoninic acid
BSA	Bovine serum albumin
ALT	Alanine aminotransferase
ATP	Adenosine triphosphate
ATCC	American type culture collection
BSA	Bovine serum albumin
CACT	Carnitine:acyl-carnitine translocase
CoA	Coenzyme A
CPT1	Carnitine palmitoyltransferase 1
CPT2	Carnitine palmitoyltransferase 2
CYP	Cytochrome P450
DCF	Dichlorofluorescein
DILI	Drug-induced liver injury
DMEM	Dulbecco's Modified Eagle Medium
DMSO	Dimethyl sulfoxide
DPBS	Dulbecco's phosphate buffered saline
ETC	Electron transport chain
ETF	Electron-transfer flavoprotein
$FADH_2$	Flavin adenine dinucleotide
FCCP	Carbonyl cyanide-*4*-(trifluoromethoxy)phenylhydrazone
GSH, GSSG	reduced glutathione, glutathione disulfide
HBSS	Hanks modified salt solution
HEPES	4-(2-hydroxyethyl)-1-piperazineethanesulfonic acid
HPLC	High-performance liquid chromatography

IMM/ or OMM	Inner/ or outer mitochondrial membrane
Jvs	Juvenile visceral steatosis
LCFA	Long-chain fatty acid
MCAD	Medium-chain specific acyl-CoA dehydrogenase
MCFA	Medium-chain fatty acids
MPTP	Mitochondrial permeability transition pore
mtDNA	Mitochondrial DNA
NADH	Nicotinamide adenine dinucleotide
NADPH	Nicotinamide adenine dinucleotide phosphate
Ox/Phos	Oxidative phosphorylation
PGC1α	Proliferator-activated receptor gamma coactivator-1α
PI	Propidium iodide
PPARα	Peroxisome proliferator-activated receptor α
ROS	Reactive oxygen species
RT-PCR	Real-time polymerase chain reaction
SCFA	Short-chain fatty acid
SOD1	Superoxide dismutase 1
SOD2	Superoxide dismutase 2
TBIL	Total bilirubin
TCA cycle	Tricarboxylic acid cycle
TMPD	N,N,N',N'-tetramethyl-p-phenylenediamine
TPP	Tetraphenyl phosphonium

Introduction

Drug-induced liver injury

Drug-induced liver injury (DILI) is a major cause for aborted drug development, post marketing restrictions placed on use of drugs or withdrawals from the market [1]. The reported incidence of DILI attributed to an individual drug is estimated to be between 1 in 10,000 and 1 in 100,000 patients [2]. The hepatotoxicity often remains undetected by clinical Phase III trials since the studies are usually limited to a few thousand people. Only after drug approval and subsequent exposure of a large number of patients to the drug, these rare toxic events occur [3].

DILI has a wide spectrum of manifestations and can trigger diverse types of liver diseases, ranging from asymptomatic mild biochemical abnormalities to severe hepatitis with jaundice. Clinical presentations may include liver transplantation or death of the patient in the most severe cases [4, 5]. In drug development, 'Hy's law' is frequently used to predict serious hepatotoxicity in patients with elevated liver tests. The rule predicts that a drug has a high risk to cause fatal DILI in a larger population if it caused a more than three fold increase in serum alanine aminotransferase (ALT) above the limit of normal together with a more than two fold increase in total bilirubin (TBIL) above the limit of normal in clinical studies [6].

Two different clinical patterns of DILI are distinguished, namely the intrinsic and the idiosyncratic liver toxicity. The intrinsic toxicity, or type A toxicity, leads to a predictable liver injury in a dose-dependent fashion. A typical example is acetaminophen (paracetamol), which leads to a high incidence of elevation of serum ALT levels and acute liver failure, if the daily intake is above the recommended limit of 4g per day. This hepatotoxicity is associated with the formation of a well-characterized and highly reactive intermediate metabolite, *N*-acetyl-p-benzoquinone imine, and is reproducible in animal models [7].

The idiosyncratic toxicity, or type B ("bizarre") toxicity, is host-dependent and not strictly dose-dependent. Typically, idiosyncratic DILI occurs at therapeutic doses that are generally safe to the majority of patients, and often in only few patients (<1%) during drug therapy. In most cases, the underlying mechanisms for the unique susceptibility of few subjects are not completely understood, but do typically not involve

the pharmacological action of the drug [8, 9]. There are hardly any reliable preclinical *in vitro* or animal models available to predict investigational drugs with idiosyncratic DILI before the clinic and these adverse reactions thus represent a major issue for both the pharmaceutical industry and the affected patients [4].

Mechanisms of idiosyncratic liver injury

The reasons for the unique susceptibility of a few patients to idiosyncratic DILI are not completely understood. It might in principle be linked to the drug, the environment, or the patient (Fig. 1) [7]. In a recent retrospective study, the risk of idiosyncratic DILI was shown to be increased when the administered daily dose is higher than 50mg or when the drug undergoes extensive hepatic metabolism [4]. Furthermore, drug-drug interactions could potentially alter the concentration of a drug or its reactive metabolite [7]. Since most drugs require metabolism for pharmacological action and/or removal from the body, the generation of reactive metabolites in the liver might account for some cases of idiosyncratic DILI. Indeed, 62% of drugs withdrawn from the market due to idiosyncratic hepatotoxicity in the last years have been shown to produce reactive metabolites [10].

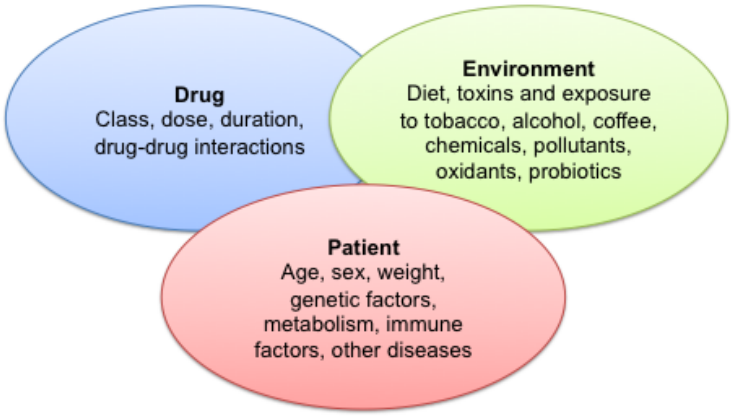

Figure 1: *Potential risk factors involved in the pathogenesis of drug-induced liver injury.* Adapted from Tujios et al. [7]

Possibly the most important susceptibility factors for hepatotoxicity are the patients and their genetic variability. Genetic polymorphisms cause differences in the toxic responses to drugs, such as polymorphisms in bioactivating enzymes, which cause variations in reactive metabolite formation [7, 11]. An example is the enhanced risk of

troglitazone-induced hepatotoxicity in patients harboring the combined glutathione S-transferase GSTT1-GSTM1 null genotype. The deficiency probably leads to the accumulation of a toxic epoxide metabolite of troglitazone and subsequent liver toxicity [12]. Reactive metabolites may furthermore lead to the formation of drug-protein adducts, which can potentially trigger an adaptive immune response to an altered self-protein (hapten) [7, 11].

Another major mechanism believed to be involved in the pathogenesis of idiosyncratic hepatotoxicity is drug-induced mitochondrial dysfunction and the presence of medical conditions that impair mitochondrial function. Drugs that are released on the market do not impair mitochondrial function enough to cause liver injury in most recipients. However, if in a few patients mitochondrial function is already impaired by preexisting conditions, such as inborn mitochondrial cytopathies affecting mitochondrial respiration, mitochondrial β-oxidation defects or mitochondrial alterations associated with the metabolic syndrome, susceptibility to mitochondrial disruptors might be increased. If patients with such inborn or acquired deficiencies take a drug that induces mitochondrial dysfunction, this combination can additively impair mitochondrial function and trigger hepatotoxicity [13]. Sometimes, mitochondrial diseases may therefore be only revealed during drug administration, such as previously latent mitochondrial cytopathy [14, 15] or inborn β-oxidation defect [16, 17] under valproic acid treatment.

Drug-induced mitochondrial toxicity

Although some pharmaceuticals in the past have been designed to uncouple oxidative phosphorylation to cause weight loss, drug-induced mitochondrial dysfunction is often an unintended off-target effect [18]. Mitochondrial toxicity has only recently become more widely acknowledged and is a growing cause for preclinical candidate failures or post marked withdrawals [3]. Numerous mitochondrial off-targets might be responsible for a metabolic failure, and often one drug impairs several mitochondrial targets [18].

Mitochondria-rich organs which are highly aerobically poised, such as the central nervous system, the cardiovascular system, skeletal muscle, or the liver rely heavily on mitochondrial metabolism and are thus particularly susceptible to mitochondrial toxicants [18]. Furthermore, tissues exposed to higher concentrations of the drug, such as the liver due to hepatoportal absorption of oral drugs and their bioactivation, are especially vulnerable to mitochondrial toxicants [3].

General aspects of mitochondrial morphology

Mitochondria are the principal energy-producing organelles of the cell and are composed of two membranes that separate the intermembrane space and the inner mitochondrial matrix (Fig. 2A). The outer mitochondrial membrane (OMM) is smooth and separates the mitochondrion from the cytosol, whereas the inner mitochondrial membrane (IMM) forms multiple invaginations into the matrix compartment, the so-called cristae (Fig. 2B). Both membranes are formed of phospholipid bilayers containing multiple transporting and enzymatic proteins. The OMM is freely permeable for compounds up to 5000 Da and contains cholesterol. In contrast, the IMM is essentially cholesterol-free and highly impermeable but contains several specific transporters, e.g. for respiratory substrates, inorganic phosphate, ADP and ATP. Within the cells, mitochondria are organized as larger, branched structures described as mitochondrial network (Fig. 2C). These structures are in constant motion and can split or fuse [19].

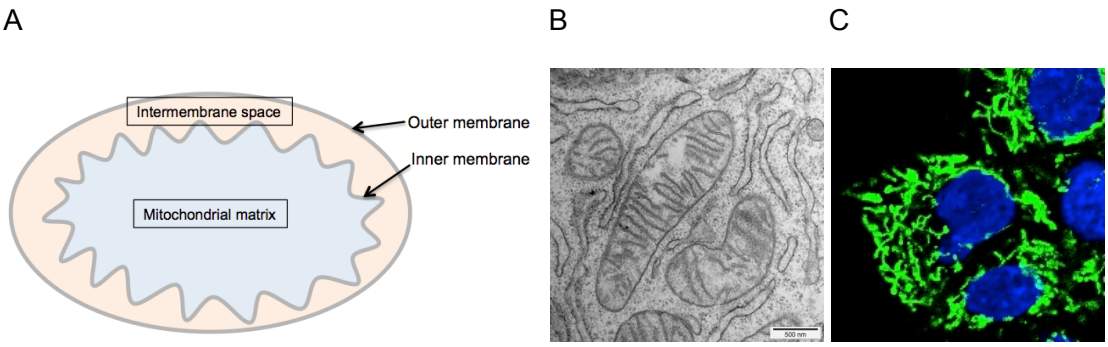

Figure 2: *Mitochondrial morphology*. **A.** Schematic representation of mitochondrial morphology. **B.** Separate mitochondria observed by electron microscopy in HepG2 cells. **C.** Confocal microscopy of mitochondrial network in HepG2 cells stained with TOMM22 antibody (mitochondrial surface marker).

Inhibition of oxidative phosphorylation

General principles

The oxidative phosphorylation (Ox/Phos) is an essential energy-producing process in cells and consists of two functionally independent processes, namely the oxidation of reduced substrates by the electron transport chain (ETC) and the phosphorylation of ADP by inorganic phosphate. In total, the Ox/Phos consists of five complexes (Fig. 3).

Complexes I to IV constitute the ETC, whereas Complex V is the ATP synthase. The ETC is embedded within the inner mitochondrial membrane and each complex is composed of multiple individual protein subunits, which are encoded either by the mitochondrial genome (mtDNA) or the by the nucleus. Two different forms of reducing equivalents are used, namely nicotinamide adenine dinucleotide (NADH) and flavin adenine dinucleotide ($FADH_2$).

The NADH:coenzymeQ oxidoreductase (complex I) catalyzes the electron transfer from NADH to ubiquinone (oxidized form of coenzyme Q) and the succinate:coenzymeQ oxidoreductase (complex II) transfers electrons from succinate via FAD to ubiquinone. Complex II is part of the tricarboxylic acid (TCA) cycle and FAD is a prosthetic group reduced during the oxidation of succinate to fumarate. At the level of coenzymeQ:cytochrome c oxidoreductase (complex III), the electrons of ubiquinol are transferred to cytochrome c (cyt *c*). Finally, at the terminal complex of the electron transport chain, the cytochrome *c* oxidase (complex IV), molecular oxygen (O_2) undergoes a four-electron reduction to water. During this process of electron transport, protons are actively pumped from the mitochondrial matrix to the intermembrane space, creating an electrochemical gradient that approaches 200mV ($\Delta\Psi$) and a pH gradient (alkaline inside). This proton gradient finally drives the F_1F_0-ATP synthase (complex V) to phosphorylate ADP to ATP [18].

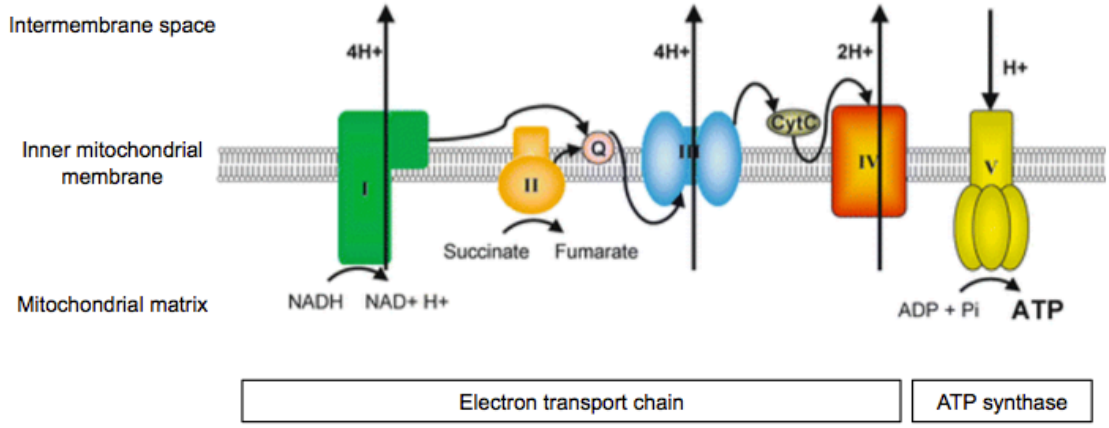

Figure 3: *The respiratory chain.* I, complex I, NADH:coenzymeQ oxidoreductase. II, complex II, succinate:coenzymeQ oxidoreductase. III, complex III, coenzymeQ:cytochrome *c* oxidoreductase. IV, complex IV, cytochrome *c* oxidase. V, complex V, F_1F_0-ATP synthase. Q, ubiquinone. CytC, cytochrome c. NADH, nicotinamide adenine dinucleotide. Adapted from Cuperus et al. [20].

Inhibition of glycolysis and tricarboxylic acid cycle

Different metabolic pathways, such as the glycolysis, the tricarboxylic acid cycle (TCA cycle), and enzymes involved in fatty acid oxidation are directly connected to the respiratory chain, since they provide substrate-derived reducing equivalents (NADH and $FADH_2$) that deliver electrons to the ETC (Fig. 4). Ox/Phos dysfunctions thus not only involve disruptors of the ETC, but also chemicals that interfere with the transport and/or oxidation of reducing substrates [18].

Glycolysis occurs in the cytoplasm and its enzymes convert one glucose molecule to two pyruvates. This degradation yields two ATP and two NADH. Pyruvate may on one hand be further decarboxylated to acetyl-CoA and enter the mitochondrial TCA cycle. On the other hand, it may be reduced to lactate with concomitant oxidation of NADH to NAD^+. The conversion to lactate is anaerobic. A typical response of cells to a loss of ATP production capacity is a compensatory increasing production of lactate, which in humans leads to serum lactic acidosis, a clinical sign of mitochondrial impairment [3].

In the mitochondrial matrix, the TCA cycle oxidizes acetyl-CoA to CO_2. This degradation yields one $FADH_2$, three NADH and one ATP [18]. An example of a direct inhibitior of the TCA cycle is fluoroacetate. Its metabolite, fluorocitrate, is a potent inhibitor of the aconitase enzyme of the tricarboxylic acid cycle, and interferes with the generation and delivery of reducing equivalents into the ETC [21].

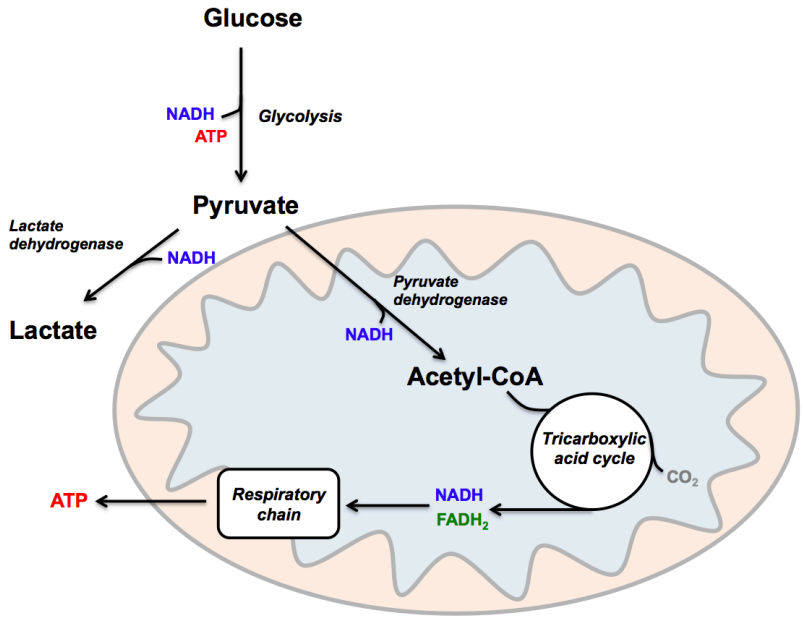

Figure 4: *Glycolysis and the tricarboxylic acid cycle.* Glycolysis and the TCA cycle are directly connected to the respiratory chain. NADH, nicotinamide adenine dinucleotide. $FADH_2$, flavin adenine dinucleotide. ATP, adenosine triphosphate.

Inhibition of the electron transport chain, and uncoupling of Ox/Phos

The function of the ETC depends predominantly on the impermeability of the inner mitochondrial membrane and the catalytic integrity of the respiratory chain complexes. Two different types of interferences with the Ox/Phos are possible, an acute inhibition of the ETC or an uncoupling of the electron transport chain from the ATP synthesis [18].

The direct inhibition of the individual complexes of the ETC leads to inhibition of substrate oxidation and oxygen consumption. Classical inhibitors of each of the five complexes involved in Ox/Phos include rotenone (complex I), malonate (complex II), antimycin A (complex III), cyanide (complex IV), and oligomycin (complex V) (Fig. 5). Depending on the severity, these inhibitions finally diminish or abolish ATP production

and may trigger cell death through apoptosis. Possible metabolic consequences in patients are hyperlactic acidemia and hypoglycemia [18].

Uncouplers are often hydrophobic weak acids, such as phenols or amides, and have a 'protonophoric' activity, which means that they may carry a proton into the mitochondrial matrix due to their permeability through the inner mitochondrial membrane. Classical examples are carbonyl cyanide-*4*-(trifluoromethoxy)phenylhydrazone (FCCP) or 2,4-dinitrophenol (DNP). The uncoupling of the electron transport from the ATP synthesis dissipates the pH gradient and mitochondrial membrane potential. Uncoupling results thus in stimulation of substrate oxidation and oxygen consumption, and the energy generated is dissipated as heat (hyperpyrexia) instead of ATP [18].

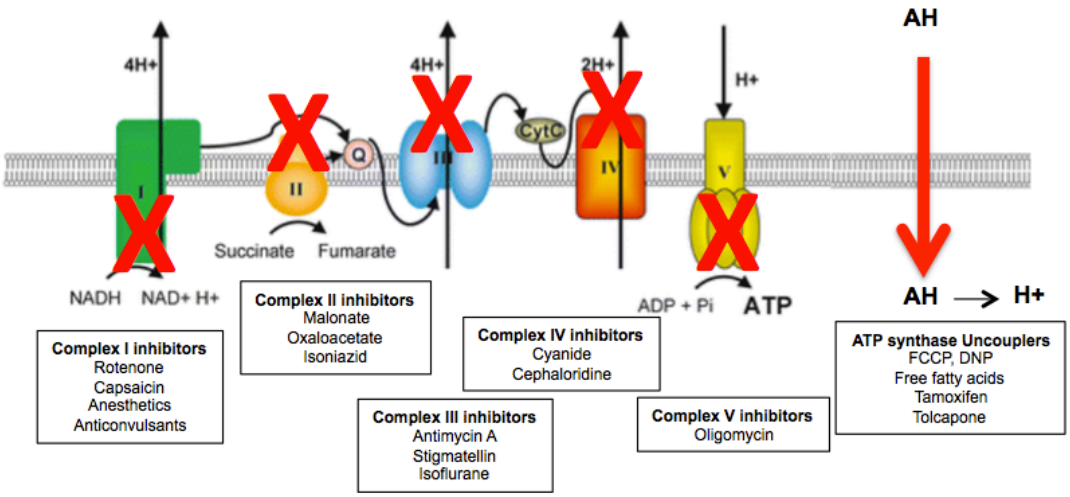

Figure 5: *Inhibitors and uncouplers of the respiratory chain.* FCCP, carbonyl cyanide-*4*-(trifluoromethoxy)phenylhydrazone. DNP, 2,4-dinitrophenol. Adapted from Cuperus et al. [20].

Production of reactive oxygen species

Mitochondria are one of the major reactive oxygen species (ROS) producers and it is estimated that approximately 90% of cellular ROS is derived from the mitochondrial ETC [22]. Three important forms of cellular ROS are superoxide anions (O_2^-), hydrogen peroxide (H_2O_2), and hydroxyl free radicals (OH•). Superoxide is generated in mitochondria as a byproduct of Ox/Phos. Analysis of isolated mitochondria revealed that mainly two ROS-forming sites in the mitochondrial ETC, namely complex I and complex III, are responsible for superoxide formation [23, 24]. Superoxide generated

by the respiratory chain appears on both sides of the inner mitochondrial membrane and can be decomposed by the enzyme superoxide dismutase (SOD) (Fig. 6). SOD catalyzes the dismutation of two superoxide anion radicals to H_2O_2 ($2O_2^- + 2H^+ -> H_2O_2 + O_2$). The SOD1 isoform (or Cu,Zn-SOD) is present in the cytoplasm and mitochondrial intermembrane space, whereas the SOD2 isoform (or Mn-SOD) is abundant in the mitochondrial matrix. If superoxide is not quickly dismutated, it may react with nitric oxide (NO) to form peroxynitrite ($ONOO^-$), which damages DNA and proteins. This first line of defense is important for the correct maintenance of a normal function of mitochondria-rich organs and is underscored by the fact that homozygous SOD2-knockout mice die during the first few weeks after birth [23, 25].

The next step in the protective mechanism against ROS is the removal of H_2O_2. In contrast to a limited permeability of the superoxide radical, H_2O_2 may readily cross biological membranes. In the presence of ferrous ions (Fe^{2+}), H_2O_2 reacts nonenzymatically in the Fenton reaction, generating extremely reactive hydroxyl radicals ($H_2O_2 + Fe^{2+} -> HO• + OH^- + Fe^{3+}$), which may directly damage proteins, lipids and DNA. H_2O_2 can be deactivated to water and oxygen by the enzyme catalase, which is mainly expressed in peroxisomes ($2H_2O_2 -> 2H_2O + O_2$). Alternatively, glutathione peroxidases remove H_2O_2 by using two molecules of reduced glutathione (GSH) as an electron acceptor, and oxidizing it to the glutathione disulfide (GSSG). GSSG is then reduced back into GSH by the enzyme GSH reductase by using nicotinamide adenine dinucleotide phosphate (NADPH) as cofactor. Glutathione peroxidases are expressed in the mitochondrial matrix as well as in the cytosol [19, 22].

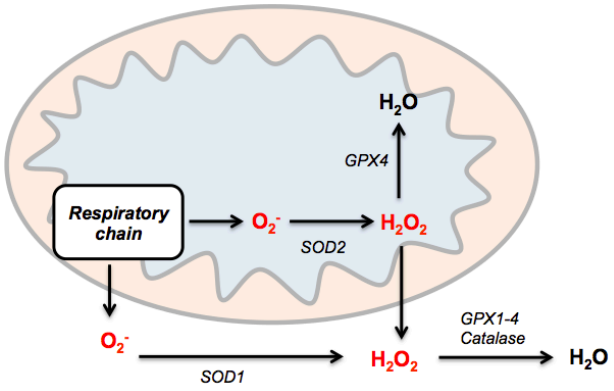

Figure 6: *Mitochondrial ROS production and antioxidant mechanisms.*
SOD, superoxide dismutase. GPX, glutathione peroxidase.

Under normal conditions, these ROS-metabolizing processes are sufficient to keep superoxide and H_2O_2 concentrations at physiological submicromolar levels. However, inhibitors of the ETC, such as rotenone or antimycin A, increase the generation of ROS and electrons passing through the ETC may leak out to molecular oxygen (O_2) to form superoxide [23]. Although lower levels of ROS formation are required for normal cell homeostasis and cell adaptation, high quantities of ROS lead to oxidative stress and induce cell death [26].

In contrast to an inhibition of the ETC, uncoupling of the Ox/Phos leads to a higher efficiency of the ETC in order to re-establish the proton gradient. Therefore, during uncoupling the ROS production of the ETC is usually not increased and might even be reduced [27].

Inhibition of fatty acid transport and oxidation

General principles

The mitochondrion is the main site of fatty acid degradation and involves the fatty acid translocation into the mitochondrial matrix and their β-oxidation. Short-chain (C_4-C_6) and medium-chain (C_6-C_{14}) fatty acids can freely cross the mitochondrial outer and inner membranes, and are activated into acyl-CoA thioesters by short- and medium-chain acyl-CoA synthetases in the mitochondrial matrix (Fig. 7) [28]. In contrast, long-chain fatty acids (C_{14}-C_{18}) require a specific carnitine shuttle system involving a four-step process in order to access the mitochondria matrix. First, the long-chain fatty acid is activated to an acyl-CoA thioester by the action of the enzyme long-chain acyl-CoA synthetase located in the outer mitochondrial membrane (OMM). In a next step, the long-chain acyl-CoA is esterified into an acyl-carnitine derivative, a reaction catalyzed by carnitine palmitoyltransferase 1 (CPT1) in the OMM. The produced acyl-carnitine is then translocated across the inner mitochondrial membrane into the mitochondrial matrix by the carnitine:acyl-carnitine translocase (CACT). Finally, carnitine palmitoyltransferase 2 (CPT2), which is located on the inner side of the IMM, is responsible for the conversion of the acylcarnitine back to carnitine and acyl-CoA [28]. CPT1 is considered as the rate-limiting step in this translocation and plays a key regulatory role in committing long-chain fatty acid towards oxidation, instead of esterification into triglycerides or fatty acid synthesis. CPT1 is regulated by an inhibition of malonyl-CoA, the first product in cytosolic fatty acid synthesis [29, 30].

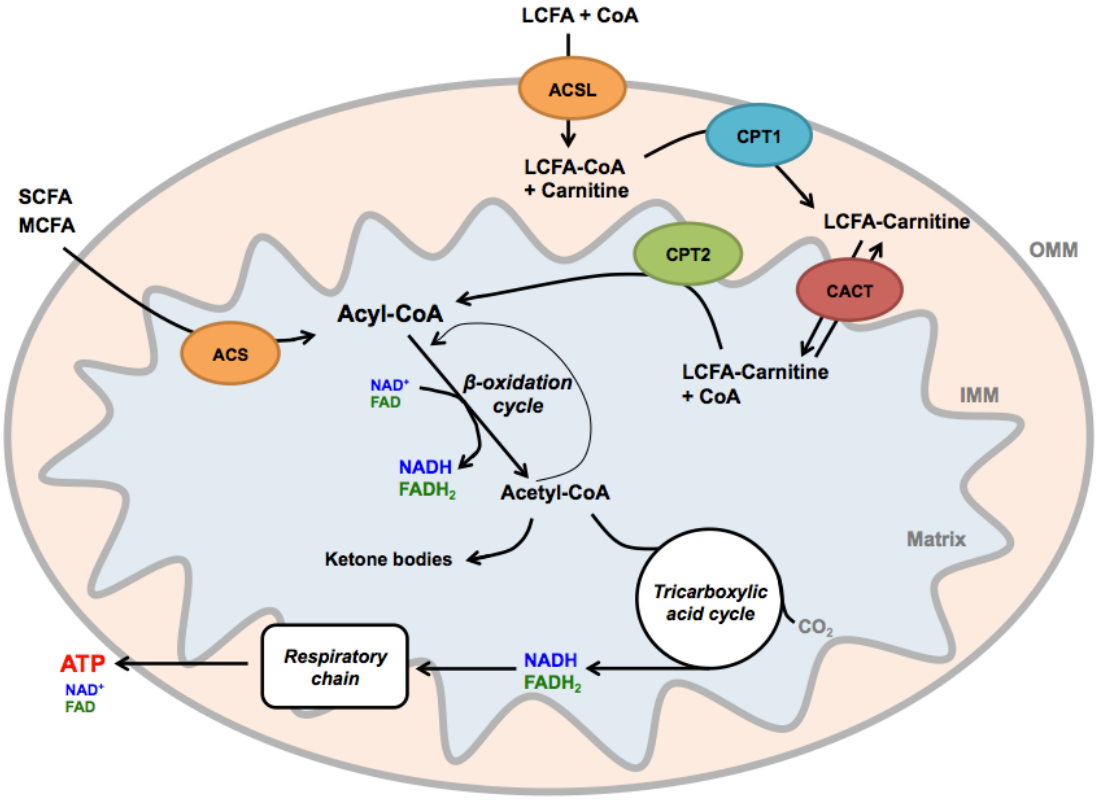

Figure 7: *Fatty acid transport and β-oxidation.* SCFA, short-chain fatty acid. MCFA, medium-chain fatty acids. LCFA, long-chain fatty acid. CoA, coenzyme A. ACS, short- and medium-chain acyl-CoA synthetase. ACSL, long-chain acyl-CoA synthetase. CPT1, carnitine palmitoyltransferase 1. CACT, carnitine:acyl-carnitine translocase. CPT2, carnitine palmitoyltransferase 2. OMM, outer mitochondrial membrane. IMM, inner mitochondrial membrane.

In the mitochondrial matrix, acyl-CoA thioesters can in a next step undergo the β-oxidation cycle. The mitochondrial fatty acid β-oxidation cycle involves four enzymes and progressively shortens fatty acids by two carbons. The first reaction is the dehydrogenation of the fatty acyl-CoA to 2-*trans*-enoyl-CoA by acyl-CoA dehydrogenases. Different isoforms of the enzyme are known, namely very-long-chain, long-chain, medium-chain and short-chain dehydrogenases. This reaction requires FAD as a cofactor. In the second reaction, 2-*trans*-enoyl-CoA is hydrated to L-3-hydroxyacyl-CoA, a reaction catalyzed by enoyl-CoA hydratase. The third reaction is catalyzed by L-3-hydroxyacyl-CoA dehydrogenase and involves the dehydrogenation into 3-ketoacyl-CoA. This reaction requires NAD^+ as cofactor. In the last reaction, the enzyme thiolase finally cleaves 3-ketoacyl-CoA and generates an acetyl-CoA and an acyl-CoA shortened by two carbon atoms. The shortened acyl-CoA derivative may

finally enter a new cycle of β-oxidation and acetyl-CoA either enters the TCA cycle or condenses into ketone bodies (mainly acetoacetate and β-hydroxybutyrate). NADH generated by the dehydrogenation is reoxidized by Complex I of the respiratory chain, whereas $FADH_2$ delivers electrons to the electron-transfer flavoprotein (ETF), which is then oxidized by ETF-ubiquinone oxidoreductase, and gives electrons to the respiratory chain by reducing coenzyme Q in Complex III. Fatty acid β-oxidation is thus directly connected to the respiratory chain [28].

Causes and consequences of decreased β-oxidation

Several mechanisms decreasing fatty acid oxidation are known. Drugs may for example directly impair the activity of enzymes involved in the mitochondrial uptake of fatty acids or sequester important cofactors [31]. An example is troglitazone, an inhibitor of mitochondrial acyl-CoA synthetases [32], or amiodarone, an inhibitor of carnitine palmitoyltransferase 1 activity [33]. Other drugs, such as valproic acid, impair fatty acid oxidation through the generation of coenzyme A and L-carnitine esters, which results in the depletion of these cofactors and thus inhibits the entry of long-chain fatty acids into the mitochondria [34, 35]. Finally, some drugs directly inhibit mitochondrial β-oxidation cycle, such as glucocorticoids, which are known to inhibit the acyl-CoA dehydrogenase [36]. Importantly, mitochondrial fatty acid oxidation can also be secondarily impaired as a result of severe inhibition of the ETC, since the mitochondrial respiratory chain allows constant regeneration of FAD and NAD+ required for the enzymatic reactions of acyl-CoA dehydrogenase and 3-hydroxyacyl-CoA dehydrogenase in the β-oxidation cycle (Fig. 7) [8].

Severe and prolonged impairment of mitochondrial β-oxidation leads to accumulation of free fatty acids that can impair mitochondrial function through different mechanisms [28]. On one hand, they can remain in their free form and reinforce mitochondrial dysfunction through uncoupling of the mitochondrial respiration, thus further decreasing energy production [37]. On the other hand, fatty acids can be esterified into triglycerides, whose accumulation causes steatosis (fatty liver). Two types of steatosis are distinguished, namely macro- and microvesicular. Macrovesicular steatosis, where hepatocytes contain a single large vacuole of fat, mainly triglycerides, is a relatively benign condition and is often associated with a mild increase in serum transaminases. Frequent causes are human alcohol abuse, obesity and diabetes. In contrast, the presence of microvesicular steatosis implies a more severe disease, where

hepatocytes are filled by numerous small lipid vesicles thus involving severe impairment of mitochondrial fatty acid β-oxidation. Typically, serum transaminases and blood ammonia levels are increased, and disease may progress rapidly from banal symptoms, such as anorexia and nausea, to acute liver failure and death [28].

The impairment of mitochondrial β-oxidation of fatty acids deprives the cell of an important source of energy during fasting episodes, since fat oxidation is the principal source of ATP in the liver in the fasting state [38]. Furthermore, inhibition of β-oxidation leads to an imbalance between increased extrahepatic catabolism of glucose and a decreased hepatic production of glucose (Fig. 8). The decreased ketogenesis forces extrahepatic tissues to use glucose instead, whereas at the same time the impaired β-oxidation inhibits pyruvate carboxylase activity, the first step in hepatic gluconeogenesis. This combination may cause severe hypoglycemia during fasting episodes [31].

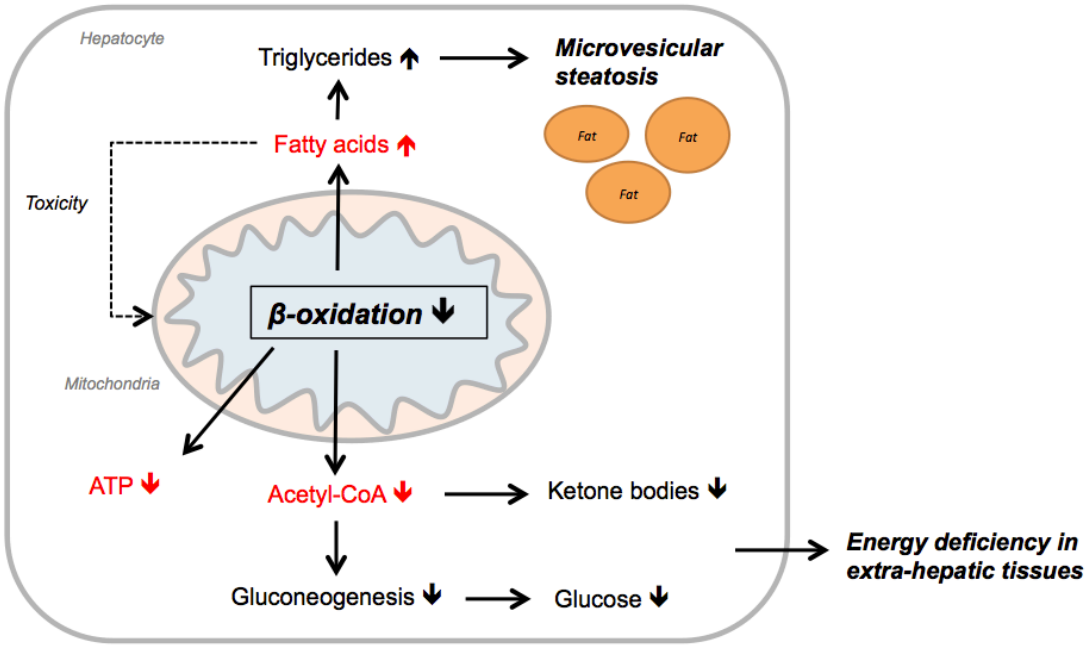

Figure 8: *Consequences of inhibition of mitochondrial fatty acid β-oxidation.* Severe impairment of mitochondrial fatty acid oxidation can induce accumulation of fatty acids and triglycerides, and lower production of ATP, ketone bodies and glucose. Adapted from Begriche et al. [8].

Mitochondrial adaptations to drugs

Various different adaptive mechanisms may occur in mitochondria in response to cellular stress in order to limit mitochondrial injury and dysfunction (Fig. 9A).

Firstly, damaged or dysfunctional mitochondria may be removed by increased rates of mitophagy (mitochondrial autophagy, degradation) and/ or mitochondrial biogenesis may be enhanced in order to replace injured or damaged mitochondria [39]. A concept called mitochondrial hormesis proposes that mitochondrial biogenesis may be triggered by low doses of reactive oxygen species (ROS) in order to re-establish homeostasis [40]. The proliferator-activated receptor gamma coactivator-1α (PGC1α) plays a key regulatory role in mitochondrial biogenesis. Furthermore, it participates in the induction of several antioxidant enzymes [41] and may bind to the peroxisome proliferator-activated receptor α (PPARα) in order to transcriptionally activate nuclear genes encoding fatty acid metabolizing enzymes [31].

A next possible adaptive response is that the respiratory capacity might be increased by mitochondrial remodeling of the respiratory chain. The increased mitochondrial respiration ensures an easier flow of electrons along the respiratory chain and decreases the accumulation of superoxide. As an example, Han et al. described that chronic alcohol feeding in mice causes increased incorporation of respiratory chain complexes (I, IV, V) in the liver as an adaptive response to the increased metabolic stress [42].

Finally, drugs may cause diverse changes in mitochondrial morphology, since mitochondria constantly undergo fusion-fission to exchange respiratory-complexes, mitochondrial DNA (mtDNA) and other constituents. Metabolic and toxic stresses, e.g. increased mitochondrial reactive oxygen species (ROS) generation, can affect mitochondrial fusion-fission rates [39]. As an example, embryonic fibroblasts adapt during starvation through a decreased mitochondrial fission to produce elongated mitochondria that have greater cristae surfaces and are more resistant to mitophagy [43]. In contrast, mitochondrial fission typically occurs during apoptotic cell death [44].

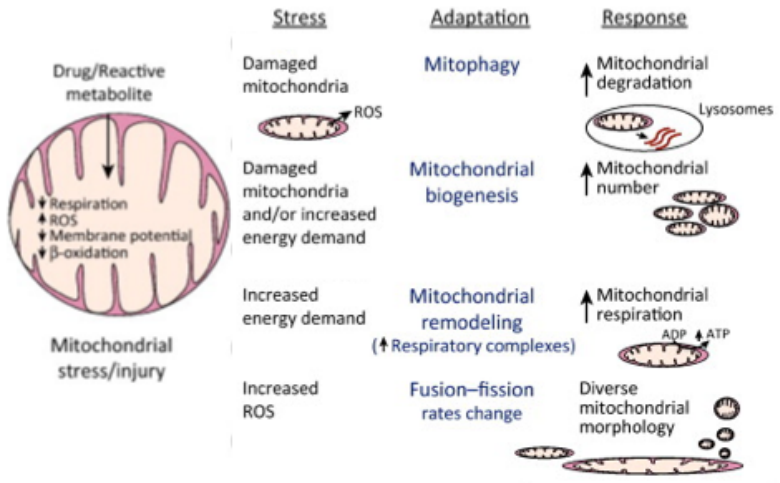

Figure 9. Possible mitochondrial adaptations induced by cellular stress. Adapted from Han et al. [39].

Role of mitochondria in cell viability and death

Mitochondria play an important role in cell survival and cell death. Apoptosis represents a complex sequence of events proceeding by two partially independent routes, namely the death receptor pathway, which is initiated by ligation of death receptors at the cell surface, and the mitochondrial pathway. The latter is known to be induced by excessive production of reactive oxygen species and originates from the release of cytochrome c from the mitochondria into the cytosol, activation of proapoptotic proteins and mitochondrial permeability transition pore (MPTP) opening [19].

Cytochrome c is located on the outer surface of the inner mitochondrial membrane. During apoptosis it is released to the cytosol, where it interacts with apoptosis protease-activating factor 1 (apaf-1), to form a multiprotein complex called apoptosome. The apoptosome triggers the activation of caspase-9, an initiator caspase that activates capase-3 and other effector caspases. The effector caspases are responsible for the degradation of the cell in the terminal phase of apoptosis [13, 19].

The mitochondrial permeability transition pore (MPTP) can be opened by diverse stimuli, including ROS, accumulation of free fatty acids or an increase in the ratio GSSG/GSH, and is located in the contact sites between the outer and inner mitochondrial membranes. It is formed by a complex assembly of proteins originating from the matrix (cyclophilin D), the inner membrane (adenine nucleotide translocase), and outer mitochondrial membrane (porin). In its open state it enables free passage of

compounds up to 1500Da between the mitochondrial matrix and the cytosol, and causes massive reentry of protons through the IMM, leading to an interruption of mitochondrial ATP synthesis. The pore opening also causes matrix expansion and results in large-scale mitochondrial swelling, up to rupture of the OMM [13, 19].

In contrast to apoptotic cell death, which reflects a programmed cell death that needs a certain cellular ATP content, necrotic cell death reflects an uncontrolled cell damage, which usually results from major cell injury (e.g. loss of osmotic balance between intra- and extracellular fluids), acute metabolic disruption with ATP depletion, or selective permeability of cell membranes (e.g. mitochondrial permeabilization). These processes result in a rupture of the plasma membrane and loss of intracellular proteins. A switch between apoptotic and necrotic cell death depends thus on the mitochondrial energy state or the extent of mitochondrial impairment. In general, cell depletion of ATP is a stimuli towards cell necrosis [45, 46].

Preclinical methods to investigate drug-induced mitochondrial dysfunction in liver

Several *in vitro* and *in vivo* investigations can be performed to detect mitochondrial dysfunction. In the following section, commonly used models are described and limitations specified.

In vitro models

A number of *in vitro* models, such as isolated mitochondria and hepatic cell models, are available to detect and understand drug-induced mitochondrial dysfunction in liver. A convenient approach is to first assess the effects of the drugs in isolated liver mitochondria, and then to check the effects of the drug in a human liver cell line [47]. Since numerous mitochondrial targets might be responsible for a metabolic failure, and often one drug impairs several mitochondrial targets, attempts to model drug-induced mitochondrial dysfunction must be multifaceted [18]. Table 1 summarizes some of the currently used endpoints to assess mitochondrial dysfunction *in vitro* [47].

Mitochondrial dysfunction can be assessed in isolated liver mitochondria by acutely exposing them to the drug of interest and measuring basic processes of oxidative

phosphorylation and fatty acid oxidation. However, this system has some limitations, since the mitochondria are not present in a physiological environment and the drug may also interact with other organelles or the plasma membrane. Furthermore, isolated mitochondria potentially overpredict drug effects because compounds have unlimited access and are not metabolized [48].

Table 1. *Examples of* in vitro *investgations to detect drug-induced mitochondrial dysfunction.* TPP, tetraphenylphosphonium, MPTP, mitochondrial permeability transition pore. Adapted from Labbe et al. [47].

Isolated liver mitochondria	Oxygen consumption and respiratory chain complex activity Fatty acid oxidation with radiolabelled fatty acids Determination of $\Delta\Psi m$ (TPP selective electrode, fluorescent probe) Ca^{2+}- induced swelling (MPTP)
Hepatic cells	Oxygen consumption and respiratory chain complex activity Lactic acid in incubation medium Fatty acid oxidation with radiolabelled fatty acids Determination of neutral lipids (coloration with oil red O, fluorescent probe) Determination of $\Delta\Psi m$ (fluorescent probe) mtDNA levels by qPCR

Working with intact hepatocytes has thus a higher physiological relevance than working with isolated organelles [48]. The use of primary human hepatocytes is considered as the gold standard when the presence of metabolic activity is required, since these cells express P450 enzymes and have detoxifying capacities. Primary hepatocytes however are limited in their use, because these cells are scarce, expensive and have only a limited viability over time (up to 72 hours) in a classical monolayer [49].

Commonly used hepatic cell lines for cell-based mitochondrial assays are tumor-derived immortalized cell lines (e.g. the human hepatoma cell line HepG2). This cell lines have the advantage of being readily available and easy to use. However, the use of tumor-derived cells may not truly reflect primary cell behavior [48]. On one hand, they are not capable of metabolizing drugs, because they lack the functional expression of almost all relevant human liver P450 enzymes [50]. On the other hand, tumor-derived cell lines are adapted to rapid growth and generate their energy from glycolysis rather than mitochondrial Ox/Phos. Cell culture medium of these cell lines

thus usually contains high glucose concentration (25 mM glucose, a more than fivefold higher concentration than physiological level) [51, 52]. This glucose-induced suppression of Ox/Phos is called “Crabtree effect” (Fig. 10), and in such cells, mitochondrial toxicants have little effect on cell growth and death [51, 53].

In order to circumvent such resistance, tumor-derived immortalized cell lines can either be grown in a low glucose culture medium (and adding higher amounts of TCA intermediates, e.g. L-glutamine), or glucose can be replaced by galactose. If cells are growing in a medium containing galactose instead of glucose, they require an investment of two ATPs in order to enter glycolysis, but complete glycolysis to pyruvate yields only two ATPs. These cells must thus rely on mitochondrial Ox/Phos to obtain ATP, which makes them more vulnerable to mitochondrial toxicants [51, 54]. Another experimental condition for mitochondrial toxicity testing is to add an excess of free fatty acids to human liver cell lines, to show accumulation of intracellular lipids induced by steatogenic drugs [55] [56]. Overall, if drug-induced mitochondrial dysfunction is aimed to be assessed on immortalized cell lines, it is of high importance to carefully choose the culture conditions, since results can be greatly affected.

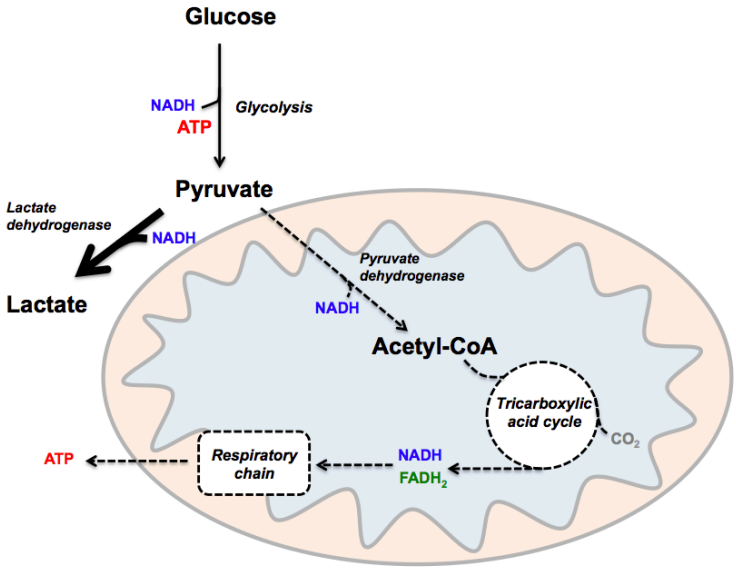

Figure 10: *The Crabtree effect.* Despite abundant oxygen and fully functional mitochondria, pyruvate is converted to lactate and oxidative phosphorylation is suppressed. Anaerobic glycolysis is inefficient and is capturing ca. 5-6% of the potential energy in the glucose substrate, when fully oxidized via Ox/Phos. However, flux rates through the glycolytic pathway can be dramatically accelerated, so that inefficiency is offset by an abundance of substrate [51, 57].

Animal models

Although predictive cell based models might be useful, they still lack the *in vivo* complexity of cell-cell interactions. Animal models are thus more likely to capture the complexity of idiosyncratic liver reactions [58-60].

It is considerably more difficult to study mitochondrial injury *in vivo*, since there are only limited numbers of noninvasive endpoints that can be assessed. Table 2 summarizes some of the currently used endpoints to assess mitochondrial liability *in vivo* and *ex vivo* in animal studies. Mitochondrial injury can be attributed *in vivo* by exhalation assays of ^{14}C-labelled or nonradioactive ^{13}C-enriched substrates. For instance, whole body fatty acid oxidation can be assessed after the administration of ^{14}C- or ^{13}C-labelled fatty acid by measuring the [^{14}C]CO_2 exhalation [61, 62]. In this assay, ^{14}C-labelled fatty acids of different lengths, such as octanoic acid or palmitic acid, can be used to determine whether fatty acid oxidation affects the whole oxidative process or only some chain length-specific processes [63]. These methods are typically used in combination with *ex vivo* approaches.

Animals used in standard preclinical safety studies are normal healthy wild-type animal models that do not mimic critical interindividual differences, such as genetic and environmental predispositions. Especially mild mitochondrial damage is not readily detectable in such models since individual cells contain hundreds or thousands of mitochondria and respond to a toxic insult only if a certain critical threshold has been reached. These models are thus often refractory to drugs that produce hepatotoxicity only in susceptible humans [58-60]. Different models with an inherited or acquired abnormality in mitochondrial function have been developed to increase the susceptibility to mitochondrial disruptors.

One approach utilizes direct chemically induced modifications of mitochondrial function, and such animal models are primarily used to study mechanisms of mitochondrial pathology [60]. An example is the acquired carnitine deficiency in animals chronically exposed to the carnitine analog trimethylhydrazinium propionate, which leads to massive inhibition of mitochondrial fatty acid β-oxidation and hepatic steatosis [64, 65].

A second approach involves transgenic or other techniques to induce mitochondrial dysfunction. Two promising animal models with preexisting mitochondrial abnormality, namely heterozygous mitochondrial superoxide dismutase mice and heterozygous juvenile visceral steatosis mice, were recently used to study idiosyncratic liver injury due to an increased susceptibility to mitochondria-targeting drugs [60].

Table 2. *Commonly used endpoints in animal models to assess mitochondrial liability.* AST, aspartate aminotransferase; ALT, alanine aminotransferase; $\Delta\Psi m$, mitochondrial transmembrane potential. Adapted from Boelsterli et al. [60].

Clinical chemistry	Plasma AST activity relative to ALT activity, plasma lactate level Ketone bodies Acyl-carnitine derivatives
Histopathology, electron microscopy	Microvesicular steatosis Alterations in mitochondrial structure, loss of cristae, megamitochondria, change in abundance
Tissue analysis	ATP content, lipid content Mitochondrial GSH/GSSG Mitochondrial/ cytosolic cytochrome c translocation
Functional assays *in vivo*	Whole body fatty acid (^{14}C- or ^{13}C-palmitate or octanoate) oxidation assay
Functional assays with *ex vivo* isolated cells or mitochondria	Oxygen consumption and respiratory chain complex activity Fatty acid oxidation with radiolabelled fatty acids Determination of $\Delta\Psi m$ Ca^{2+}- induced swelling (MPTP)

Heterozygous mitochondrial superoxide dismutase ($SOD2^{+/-}$) mice

This mouse model has a heterozygous deficiency in the mitochondrial manganese superoxide dismutase (SOD2). Whereas homozygous SOD2 mutant mice die within the first 10 days of life and suffer from a dilated cardiomyopathy [25], the heterozygous animals are phenotypically normal, but show increased oxidative stress [66, 67]. $SOD2^{+/-}$ mice treated with troglitazone for 14 to 28 days developed increased ALT activity, increased hepatic superoxide concentration, and hepatic necrosis whereas wild-type mice did not [66, 67]. Similarly, the $SOD2^{+/-}$ mice model could unmask the mitochondrial toxicity of nimesulide [68]. In summary, the mouse model is more

susceptible to drug-induced mitochondrial liver injury and seems to be especially sensitive to drugs that enhance mitochondrial oxidative stress [58].

Heterozygous juvenile visceral steatosis (jvs$^{+/-}$) mice

Heterozygous juvenile visceral steatosis mice are carnitine deficient through an impaired renal reabsorption. Jvs$^{+/-}$ mice treated with 100mg/kg/day valproic acid for 14 days developed hepatotoxicity, but wild-type mice did not. They had decreased mitochondrial oxidative function, reduced carnitine concentration in liver, increases in serum ALT and ALP activities, and histopathological changes in form of microvesicular steatosis and apoptosis [62]. These results showed that mitochondrial alterations in fatty acid oxidation might be a risk factor for idiosyncratic liver injuries [58].

Mitochondrial toxicants – benzofuran derivatives

Members of diverse drug classes have been reported to inhibit mitochondrial function. In this section, a specific group of structural analogs associated with hepatotoxicity and mitochondrial dysfunction will be introduced, namely the group of benzofuran derivatives (Fig. 11).

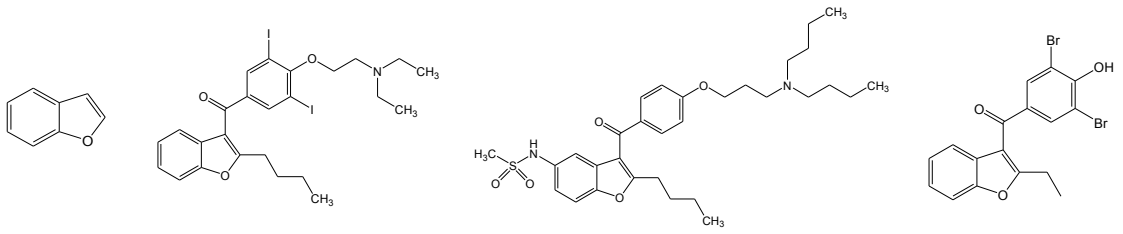

Figure 11. *Structures of benzofuran derivatives.*

Amiodarone

Amiodarone is an antiarrhythmic drug, which is widely used [69, 70] and causes multiple potentially severe adverse reactions, including hepatotoxicity with symptoms that range from benign increases in transaminases to potentially fatal hepatitis and cirrhosis [71-74].

Amiodarone is a well-known mitochondrial toxicant [28, 75-78]. It is highly lipophilic and can accumulate in tissues including hepatocytes. It is a cationic amphiphilic drug, with a lipophilic moiety and an amine function, which can be protonated (Fig. 11). The uncharged lipophilic form easily crosses the outer mitochondrial membrane and is protonated in the acidic mitochondrial intermembrane space [31]. The cationic compound can enter the mitochondrial matrix, most probably thanks to charge delocalization and the high electrochemical potential across the inner mitochondrial membrane, causing a transient uncoupling of Ox/Phos [75]. Besides Ox/Phos uncoupling, amiodarone accumulation in the mitochondrial matrix leads to high intramitochondrial drug concentrations [79]. At these high concentrations, amiodarone inhibits mitochondrial fatty acid β-oxidation causing micro- and/or macrovesicular steatosis and inhibits the ETC causing accumulation of superoxide anion radicals [75, 80]. This impairment leads to hepatocyte necrosis or apoptosis and secondarily to inflammation and cytokine induction, and may progress the steatosis to steatohepatitis [31]. Furthermore, amiodarone is metabolized by N-desalkylation of the side-chain by cytochrome P450 (CYP) 3A4, and it is known that the N-desalkylated metabolites are toxic [78, 81].

Dronedarone

Dronedarone is a new antiarrhythmic drug with an amiodarone-like non-iodinated benzofuran structure, carrying an additional methylsulfonamide group that decreases its lipophilicity (Fig. 11) [82]. The drug was specifically designed to minimize amiodarone-associated adverse reactions [83].

However, shortly after its introduction to the market, dronedarone became implicated in evere hepatic injury and a post marketing warning was issued [84-87]. So far, the underlying mechanisms of dronedarone-induced hepatotoxicity are not fully understood. Recently, Serviddio et al. [88] published a study in which they investigated liver toxicity of dronedarone in isolated mitochondria from treated rats. They reported

that dronedarone uncoupled Ox/Phos, but was not associated with inhibition of the ETC or increased ROS production. Similar to amiodarone, dronedarone is metabolized by CYP3A4 by N-desalkylation [89]. However, it is currently not known if the N-desalkylated metabolites are hepatotoxic.

Benzbromarone

Benzbromarone is a uricosuric drug, used in the treatment of gout and is a structural analog of amiodarone and dronedarone (Fig. 11) [31]. In humans, benzbromarone can cause hepatocellular liver injury [90-93] and was withdrawn from the market in 2003 because of continuing concerns about hepatotoxicity.

The mechanisms of benzbromarone induced liver injury are not fully understood, but due to the structural similarity to amiodarone, they are believed to be due to effects on mitochondrial function. In isolated rat liver mitochondria and rat hepatocytes benzbromarone acutely uncouples Ox/Phos, inhibits the ETC and mitochondrial β-oxidation, and triggers the mitochondrial permeability transition [76, 94]. Benzbromarone is metabolized in the liver by CYP3A4 and CYP2C9. In a recent study, Kobayashi et al. showed that benzbromarone and the CYP3A4 metabolite 1'-hydroxy-benzbromarone have cytotoxic effects in a human hepatocellular carcinoma cell line [95, 96]. The hepatotoxic effects of benzbromarone might thus be associated to the parent compound as well as to its 1'-hydroxy metabolite [95].

Aim of the thesis

The main purpose of this thesis was to investigate molecular mechanisms of drug-induced mitochondrial dysfunction. We were interested in the new antiarrhythmic dronedarone, as well as its structural analog benzbromarone, both causing rare but severe idiosyncratic liver injury in patients. The thesis had three specific aims developed in three studies.

The aim of our first study was to understand the molecular mechanism of dronedarone-induced hepatotoxicity *in vitro*. Since dronedarone has an amiodarone-like benzofuran structure and amiodarone is a well-known mitochondrial disruptor, we aimed to compare both antiarrhythmic drugs regarding their effect on mitochondrial function. We performed an analysis in isolated rat liver mitochondria, primary human hepatocytes, and the human hepatoma cell line HepG2. After acute drug exposure or treatments up to 24h, we performed cytotoxicity experiments, measured the capacity of the respiratory chain as well as fatty acid β-oxidation, and assessed markers of hepatocyte apoptosis and necrosis.

The goal of the second study was to expand the knowledge of dronedarone-associated liver toxicity to the *in vivo* situation. From our *in vitro* study, we hypothesized that the inhibition of mitochondrial function might be an important factor leading to dronedarone-induced liver injury *in vivo*. Since only few patients were affected by hepatic injury, we tested dronedarone not only in wild-type mice, but also in heterozygous juvenile visceral steatosis mice, a model with higher susceptibility to mitochondrial disruptors. The animals were treated by oral gavage with two different doses of dronedarone, and mitochondrial function was assessed *in vivo* and *ex vivo*.

The third project aimed to investigate the molecular mechanisms of benzbromarone-associated hepatotoxicity, a structural analog of amiodarone and dronedarone. Benzbromarone is a known mitochondrial disruptor in isolated rat liver mitochondria and hepatocytes. However, it is unclear if the findings in rodent mitochondrial and hepatocytes are also observable in a human liver cell line. The principle aim of this study therefore was to investigate the specific mechanisms by which benzbromarone impairs mitochondrial function in HepG2 cells. Furthermore, we were also interested to investigate adaptive effects on mitochondrial morphology.

Paper one

Mechanisms of hepatocellular toxicity associated with dronedarone – a comparison to amiodarone

[*†]Felser A, [*†]Blum K, [*†‡]Lindinger PW, [*†‡]Bouitbir J, [*†‡]Krähenbühl S

[*]Clinical Pharmacology & Toxicology, University Hospital Basel, Switzerland.

[†]Department of Biomedicine, University of Basel, Switzerland.

[‡]Swiss Center of Applied Human Toxicology (SCAHT).

Toxicological Sciences, 2013, 131(2): 480-90

Abstract

Dronedarone is a new antiarrhythmic drug with an amiodarone-like benzofuran structure. Shortly after its introduction, dronedarone became implicated in causing severe liver injury. Amiodarone is a well-known mitochondrial toxicant.

The aim of our study was to investigate mechanisms of hepatotoxicity of dronedarone *in vitro* and to compare them with amiodarone. We used isolated rat liver mitochondria, primary human hepatocytes and the human hepatoma cell line HepG2, which were exposed acutely or up to 24h. After exposure of primary hepatocytes or HepG2 cells for 24h, dronedarone and amiodarone caused cytotoxicity and apoptosis starting at 20µM and 50µM, respectively. The cellular ATP content started to decrease at 20µM for both drugs, suggesting mitochondrial toxicity. Inhibition of the respiratory chain required concentrations of approximately 10µM, and was caused by an impairment of complexes I and II for both drugs. In parallel, mitochondrial accumulation of reactive oxygen species was observed. In isolated rat liver mitochondria, acute treatment with dronedarone decreased the mitochondrial membrane potential, inhibited complex I and uncoupled the respiratory chain. Furthermore, in acutely treated rat liver mitochondria and in HepG2 cells exposed for 24h, dronedarone started to inhibit mitochondrial β-oxidation at 10µM and amiodarone at 20µM.

Similar to amiodarone, dronedarone is an uncoupler and an inhibitor of the mitochondrial respiratory chain and of β-oxidation both acutely and after exposure for 24h. Inhibition of mitochondrial function leads to accumulation of ROS and fatty acids, eventually leading to apoptosis and/or necrosis of hepatocytes. Mitochondrial toxicity is an explanation for hepatotoxicity of dronedarone *in vivo*.

Introduction

Amiodarone is a well-established antiarrhythmic drug [1, 2], which is associated with several potentially severe adverse reactions [3, 4]. Importantly, it is a hepatic mitochondrial toxicant [2, 5, 6], which has been described to uncouple oxidative phosphorylation, to inhibit enzyme complexes of the electron transport chain and to impair fatty acid β-oxidation [7-11]. Mitochondrial β-oxidation and oxidative phosphorylation are fundamental physiological processes as evidenced by inherited impairment of these pathways, which can affect the function of many organs, including the liver [12]. Patients treated with amiodarone for several months or years may thus suffer from micro- and/or macrovesicular steatosis, a disease that may progress to steatohepatitis and may eventually be fatal [5, 13].

Dronedarone, a structural analog of amiodarone, was specifically designed to minimize the adverse reactions associated with amiodarone [14]. As shown in Figure 1, dronedarone is a non-iodinated amiodarone derivative carrying a methylsulfonamide group at the benzofurane ring that decreases its lipophilicity. Similar to amiodarone, dronedarone is metabolized by N-desalkylation of the basic side-chain by cytochrome P450 (CYP) 3A4 [15]. Although the N-desalkylated metabolites are toxic for amiodarone [11, 16], this is currently not known for dronedarone.

Shortly after its introduction, severe hepatic injury has been reported in two patients treated with dronedarone, eventually leading to liver transplantation [17]. Recently, Serviddio et al. [18] published a study in which they investigated liver mitochondrial toxicity of dronedarone and amiodarone *in vivo* in rats. Similar to previous studies [7, 9, 10], amiodarone inhibited the activity of complex I of the respiratory chain, uncoupled oxidative phosphorylation and was associated with increased reactive oxygen species (ROS) production and lipid peroxidation. In contrast, dronedarone only uncoupled oxidative phosphorylation, but was not associated with inhibition of the respiratory chain or increased ROS production.

In this study, we aimed to investigate and to better understand the mechanisms of cytotoxicity of dronedarone *in vitro* using isolated rat liver mitochondria, primary human hepatocytes and HepG2 cells, a well-characterized human hepatoma cell line [16]. We compared the toxic effects associated with dronedarone with those of amiodarone. Because the two drugs are structurally related (Fig. 1) and both can cause hepatic injury, we hypothesized that their mechanism of toxicity may be similar. The systems used allowed to study the toxicity acutely and after different exposure periods as well as after cytochrome P450 (CYP) induction.

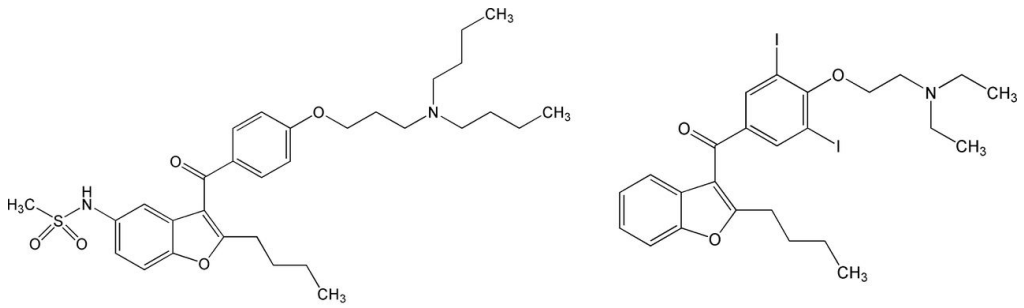

Figure 1. *Chemical structures of dronedarone and amiodarone.*

Materials and Methods

Chemicals

Dronedarone hydrochloride was extracted from commercially available tablets (brand name Multaq®) from ReseaChem life science GmbH (Burgdorf, Switzerland). The manufacturer declared the substance 99% pure by high-performance liquid chromatography (HPLC) and confirmed the structure by ^{1}H-NMR analysis. Amiodarone hydrochloride was purchased from Sigma-Aldrich (Buchs, Switzerland). Stock solutions were prepared in DMSO and stored at -20°C. All other chemicals used were purchased from Sigma-Aldrich or Fluka (Buchs, Switzerland), except where indicated.

Cell lines and cell culture

The human hepatoma cell line HepG2 was provided by ATCC (Manassas, USA) and maintained in Dulbecco's Modified Eagle Medium (DMEM, with 1.0g/l glucose, 4mM L-glutamine, and 1mM pyruvate) from Invitrogen (Basel, Switzerland). The culture medium was supplemented with 10% (v/v) heat-inactivated fetal calf serum, 2mM GlutaMax, 10mM HEPES buffer and non-essential amino acids. Cell culture supplements were all purchased from GIBCO (Paisley, UK). Cells were kept at 37°C in a humidified 5% CO_2 cell culture incubator and were passaged using trypsin. The cell number was determined using a Neubauer hemacytometer and viability using the trypan blue exclusion method.

Cryo-preserved primary human hepatocytes were purchased from Becton Dickinson (BD Gentest, Woburn, MA, USA). They were recovered and cultured according to the protocol of the manufacturer. Induction of CYP3A4 was achieved by preincubation of recovered primary human hepatocytes with 20µM rifampicin for 72h [16].

Rat liver mitochondria

Male Sprague-Dawley rats were kept in the animal facility of the University Hospital Basel (Basel, Switzerland) in a temperature-controlled environment with a 12h light/dark cycle and food and water ad libitum. Animal procedures were conducted in accordance with the institutional guidelines for the care and use of laboratory animals. The mean rat weight was 433±79g and the mean liver weight 12±4g. Rats were sacrificed by pentobarbital overdose (100mg/rat) and liver mitochondria were isolated by differential centrifugation according to the method of Hoppel et al. [19]. The mitochondrial protein content was determined using the bicinchoninic acid (BCA) protein assay kit from Merck (Darmstadt, Germany).

Cytotoxicity

Cytotoxicity was determined using ToxiLight® BioAssay Kit (Lonza, Basel, Switzerland) according to the manufacturer's manual. This assay measures the release of adenylate kinase, a marker for loss of cell membrane integrity, using a firefly luciferase system. After drug incubation, 100µl assay buffer was added to 20µl supernatant from drug-treated cell culture medium, and luminescence was measured after incubation in the dark for 5min, using a Tecan M200 Pro Infinity plate reader (Männedorf, Switzerland).

Intracellular ATP content

Intracellular ATP was determined using CellTiterGlo® Luminescent cell viability assay (Lonza, Basel, Switzerland), in accordance with the manufacturer's manual. In brief, 100µl assay buffer was added to each 96-well containing 100µl culture medium. After incubation in the dark for 30min, luminescence was measured using a Tecan M200 Pro Infinity plate reader (Männedorf, Switzerland).

Annexin V and propidium iodide staining

Apoptosis and necrosis were investigated using Annexin V and propidium iodide staining (Invitrogen, Basel, Switzerland). Cells were treated with the test compounds for 24h and stained with 1µl Annexin V-Alexa Fluor 647 and 1µl propidium iodide 100µg/ml in 100µl Annexin V binding buffer (10mM Hepes, 140mM NaCl, 2.5mM $CaCl_2$ in H_2O, pH 7.4). Cells were incubated for 15min at room temperature (RT) and analyzed by flow cytometry using a CyAn ADP cytometer (Beckman coulter, Marseille, France). Data were analyzed using FlowJo 9.3.2 software (Tree Star, Ashland, OR, USA).

Caspase 3/7 assay

Caspase 3/7 activity was determined using the luminescent Caspase-Glo® 3/7 Assay (Promega, Wallisellen, Switzerland). The assay was conducted according to the manufacturer's protocol.

Cytochrome c release

Quantitative determination of cytochrome c was performed as described by Waterhouse and Trapani [20]. HepG2 cells (100,000) were harvested and permeabilized with digitonin (10µg/ml in Dulbecco's phosphate buffered saline (DPBS) without calcium) at room temperature for 20min. Cells were fixed in paraformaldehyde (4% in DPBS) for 20min at room temperature and were washed with blocking buffer (BSA 10% in DPBS) for 1h and incubated over night at 4°C with 1:1000 purified mouse anti-cytochrome c monoclonal antibody (BD Pharmingen, Basel, Switzerland) in blocking buffer. Cells were washed with blocking buffer and incubated for 1h with 1:1000 alexa 488-labeled secondary antibody (Alexa fluor 488 goat anti-mouse IgG, Invitrogen, Basel, Switzerland). After an additional washing step with DPBS, the cell suspensions were examined by flow cytometry. Since the selective permeabilization of the plasma membrane allows cytoplasmic cytochrome c to diffuse out of the cell, mitochondrial release of cytochrome c into the cytoplasm leads to a low cellular cytochrome c content.

Cellular oxygen consumption using the Seahorse XF24 analyzer

Cellular respiration was measured using a Seahorse XF24 analyzer (Seahorse Biosciences, North Billerica, MA, USA). HepG2 cells were seeded in Seahorse XF 24-well culture plates at 20,000 cells/well in DMEM growth medium and allowed to adhere overnight. Cells were treated with the drugs for 24h. Before the experiment, the medium was replaced with 750µl unbuffered medium using a XF Prep Station (Seahorse Biosciences, North Billerica, MA, USA) and cells were equilibrated for 40min at 37°C in a CO_2-free incubator. Basal oxygen consumption was determined in the presence of glutamate/pyruvate (4mM and 1mM, respectively). After inhibition of mitochondrial phosphorylation by adding oligomycin (1µM), the mitochondrial electron transport chain was stimulated maximally by the addition of the uncoupler carbonyl cyanide p-(trifluoromethoxyl)-phenyl-hydrozone (FCCP, 1µM). Finally, the extramitochondrial respiration was determined after the addition of the complex I inhibitor rotenone (1µM).

Respiration by permeabilized HepG2 cells and isolated mitochondria

The activity of specific enzyme complexes of the respiratory chain was analyzed using an Oxygraph-2k high-resolution respirometer equipped with DatLab software (Oroboros Instruments, Innsbruck, Austria). Freshly isolated rat liver mitochondria or HepG2 cells were suspended in MiR06 (mitochondrial respiration medium containing 0.5mM EGTA, 3mM $MgCl_2$, 60mM K-lactobionate, 20mM taurine, 10mM KH_2PO_4, 20mM HEPES, 110mM sucrose, 1 g/L fatty acid-free bovine serum albumin (BSA), and 280 U/ml catalase, pH 7.1) and transferred to the pre-calibrated oxygraph chambers.

Activities of complexes I and II were assessed in isolated rat liver mitochondria using L-glutamate/malate (10mM and 2mM, respectively) as substrates, followed by the addition of adenosine diphosphate (ADP, 2.5mM) and succinate/rotenone (10mM and 0.5µM, respectively). The oxidative leak, a measure for uncoupling, was determined by assessing the residual oxygen consumption after addition of oligomycin (1µM). Uncoupling was achieved by the addition of FCCP (1µM).

The activities of complexes I, II, III and IV were assessed in HepG2 cells permeabilized with digitonin (10µg/1 million cells). In a first run, complexes I and III were analyzed using L-glutamate/malate as substrate followed by the addition of ADP and the inhibitor rotenone. Afterwards, duroquinol (500µM, Tokyo Chemical Industry, Tokyo, Japan) was added to investigate complex III and inhibited with antimycin A (2.5µM). In a second run, complexes II and IV were analyzed using succinate/rotenone as substrate,

followed by the addition of ADP and the inhibitor antimycin A. Afterwards N,N,N',N'-tetramethyl-p-phenylenediamine (TMPD)/ascorbate (0.5mM and 2mM, respectively) was added to investigate complex IV and inhibited with KCN (1mM).

We confirmed the integrity of the outer mitochondrial membrane by showing the absence of a stimulatory effect of exogenous cytochrome c (10µM) on respiration. Respiration was expressed as oxygen consumption per mg protein. Protein concentrations were determined using the Pierce bicinchoninic acid (BCA) protein assay kit from Merck (Darmstadt, Germany).

Mitochondrial membrane potential

The mitochondrial membrane potential was determined as described by Kaufmann et al. [9] with some modifications. Freshly isolated rat liver mitochondria were washed with incubation buffer containing 137mM sodium chloride, 4.74mM potassium chloride, 2.56mM calcium chloride, 1.18mM potassium phosphate, 1.18mM magnesium chloride, 10mM HEPES, and 1g/L glucose (pH 7.4). Then, mitochondria were incubated at 37°C in incubation buffer containing 0.5µl/ml [phenyl-^{3}H]-tetraphenylphosphonium bromide (40Ci/mmol, Anawa trading SA, Wangen, Switzerland). After 15min, the suspension was centrifuged and the mitochondrial pellet resuspended in fresh non-radioactive incubation buffer. Afterwards, mitochondria were treated with test substances for 1h at 37°C and centrifuged. After the incubation, radioactivity of the mitochondrial pellet was measured on a Packard 1900 TR liquid scintillation analyzer.

Mitochondrial accumulation of reactive oxygen species

HepG2 cells were stained with Hoechst 33342 trihydrochloride trihydrate (final concentration 20µg/ml DMEM, Invitrogen) for 30min at 37°C, followed by the addition of MitoSOX red (final concentration 5µM in DMEM, Invitrogen) and dronedarone (5µM, 10µM, 20µM) or amiodarone (10µM, 20µM, 50µM). Real-time accumulation of superoxide was analyzed over 6h using a Cellomics ArrayScan VTI HCS Reader (Thermo scientific, Pittsburg, PA).

mRNA expression of superoxide dismutase 1 and superoxide dismutase 2

The mRNA expression of SOD1 and SOD2 was assessed using real-time PCR as described previously [21]. HepG2 cells were treated for 24h and RNA was extracted and purified using the Qiagen RNeasy mini extraction kit (Qiagen, Hombrechtikon, Switzerland). The purity and quantity of RNA were evaluated with the NanoDrop 2000 (Thermo Scientific, Wohlen, Switzerland) and cDNA was synthesized from 10µg RNA using the Qiagen omniscript system. The real-time PCR was performed in triplicate using SYBR green (Roche Diagnostics, Rotkreuz, Basel). We used primers specific for the cytosolic SOD1 (forward: 5'-TGGCCGATGTGTCTATTGAA-3', reverse: 5'-ACCTTTGCCCAAGTCATCTG-3') and mitochondrial SOD2 (forward: 5'-GGTTGTTCACGTAGGCCG-3', reverse: 5'-CAGCAGGCAGCTGGCT-3') and calculated relative quantities of specifically amplified cDNA with the comparative-threshold cycle method. GAPDH was used as endogenous reference (forward: 5′-CATGGCCTTCCGTGTTCCTA-3′; reverse: 5′-CCTGCTTCACCACCTTCTTGA-3′) and no-template and no-reverse-transcription controls were used to exclude non-specific amplification [21].

Mitochondrial β-oxidation

Metabolism of [1-^{14}C] palmitic acid (60 mCi/mmol; PerkinElmer, Schwerzenbach, Switzerland) was assessed via the formation of ^{14}C-acid–soluble β-oxidation products. Experiments were performed as previously described [9] with some modifications. Isolated rat liver mitochondria were incubated for 15min in the presence of the test compounds in assay buffer (200µM Na-palmitate, 0.1pCi/ml [1-^{14}C] palmitic acid (60mCi/mmol), 70mM sucrose, 43mM KCl, 3.6mM $MgCl_2$, 7.2mM KH_2PO_4, 36mM TRIS, 2mM ATP, 500µM L-carnitine, 150µM coenzyme A, 50mM acetoacetate, 170µM BSA essentially fatty acid free, pH 7.4) at 37°C in a thermomixer at 600 rpm (Eppendorf, Switzerland). HepG2 cells were permeabilized with digitonin (10µg/million cells) after drug exposure for 24 h and incubated for 1 h in the same assay buffer. The reactions were stopped by adding 400µl 20% perchloric acid, and samples were precipitated for 20min on ice before centrifugation (10,000 g, 2 min). Radioactivity was measured in the supernatant.

Intracellular lipid accumulation

Experiments were performed as described by Donato et al. [22]. HepG2 cells were exposed for 24h to exogenous lipids (DMEM containing 62µM of a 2:1 mixture of oleate and palmitate). Cells were treated with toxicants in lipid-free medium for 24h and intracellular lipid accumulation was measured using BODIPY 493/503 (final concentration 3.75ng/ml), a non-polar derivative of the BODIPY fluorophore [22]. Cell suspensions were stained for 30min at 37°C in HBSS buffer in the dark, before examining by flow cytometry without any additional washing step. In order to exclude non-viable cells, propidium iodide was added and the analysis was restricted to live-cell populations.

Statistical methods

Data are given as the mean ± standard error of the mean (SEM) of at least three independent experiments. Statistical analyses were performed using GraphPad Prism 5 (GraphPad Software, La Jolla, CA, US). One-way analysis of variance (ANOVA) was used for comparisons of more than two groups, followed by the comparisons between incubations containing toxicants and the control group using Dunnett's posttest procedure. Differences between induction experiments were compared using two-way ANOVA followed by Bonferroni's post hoc test. P-values <0.05 (*) or <0.01 (**) were considered significant.

Results

Cytotoxicity in primary human hepatocytes and HepG2 cells

In primary human hepatocytes, dronedarone caused adenylate kinase release starting at a concentration of 20µM after treatment for 6 or 24h, whereas amiodarone was not toxic up to 100µM (Fig. 2A). In HepG2 cells, dronedarone and amiodarone were both toxic starting at 50 and 100µM, respectively (Fig. 2B). Intracellular ATP started to decrease at 20µM for both dronedarone and amiodarone after exposure for 6 or 24h, suggesting that mitochondria were affected before cytotoxicity could be demonstrated (Fig. 2C). CYP3A4 induction by rifampicin increased the cytotoxicity of both 100µM amiodarone (42%) and 20µM dronedarone (21%). Considering the only small increase in dronedarone-associated cytotoxicity with CYP3A4 induction, the following studies were carried out with the parent compounds only.

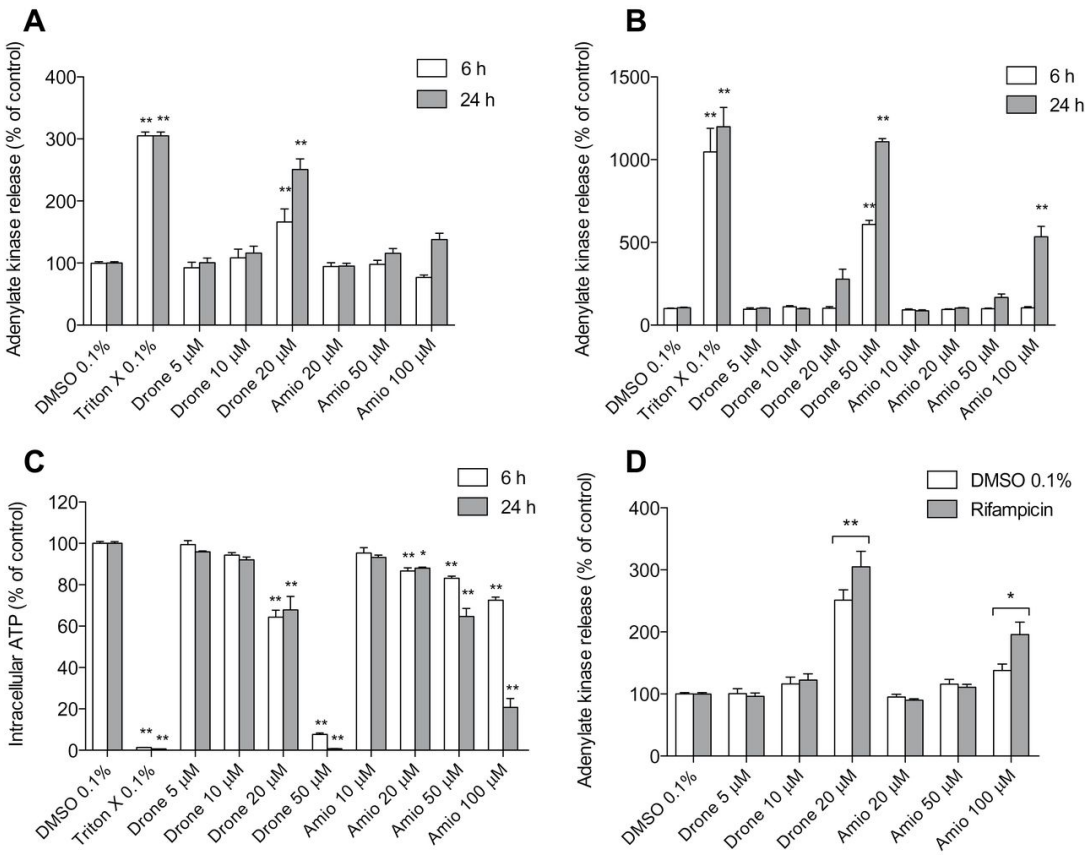

Figure 2. *Cytotoxicity and effect on intracellular ATP content.* Cytotoxicity was assessed using the Toxi-Light assay. **A**. Cytotoxicity in primary human hepatocytes after drug exposure for 6 or 24h. **B**. Cytotoxicity in HepG2 cells after drug exposure for 6 or 24h. **C.** Intracellular ATP content in HepG2 cells expressed as a percentage of the values obtained for DMSO (control). **D**. Effect of pretreatment with rifampicin on cytotoxicity. Primary human hepatocytes were pretreated with rifampicin and then exposed to dronedarone or amiodarone for 24h. CYP induction by rifampicin was associated with a 21% increase in cytotoxicity for dronedarone and a 42% increase for amiodarone. If not indicated otherwise, cytotoxicity data are expressed as percent increase compared with DMSO control. Drone: dronedarone, Amio: amiodarone. Data represent the mean ± SEM of at least three independent experiments. *p<0.05 versus DMSO control. **p<0.01 versus DMSO control.

Acute effects on isolated rat liver mitochondria

Reduced cellular ATP content was compatible with impaired mitochondrial function, which has been reported previously for amiodarone [7, 10, 11]. As shown in Fig. 3A, both amiodarone and dronedarone reduced the membrane potential of isolated rat liver mitochondria, confirming this assumption. Both toxicants impaired concentration dependently the maximal function of the electron transport chain in the presence of

oligomycin and FCCP and acted as uncouplers of oxidative phosphorylation as evidenced by an increase of the respiratory leak in the presence of oligomycin (Fig. 3B and 3C). Further investigation of oxidative phosphorylation revealed a concentration-dependent decrease of state 3 respiration in the presence of L-glutamate/malate by both toxicants (Fig. 4A and 4B). With succinate as substrate, the inhibition was less pronounced, showing only for amiodarone a significant inhibition of state 3 respiration at 50µM (Fig. 4A and 4B).

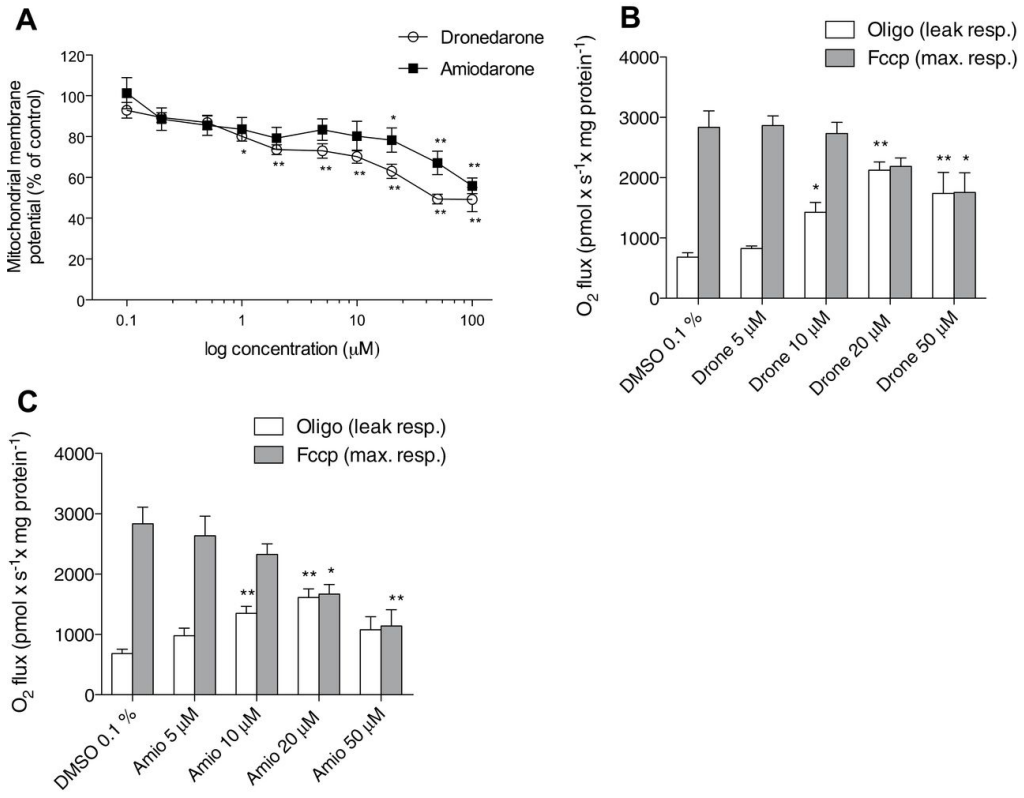

Figure 3. *Effect on membrane potential and oxidative metabolism of freshly isolated rat liver mitochondria.* **A.** Mitochondria were labeled with [^{3}H]-tetraphenylphosphonium bromide, and mitochondrial accumulation of radioactivity was determined. DMSO served as control and was set at 100%. **B.** and **C.** Acute effect of dronedarone and amiodarone on the respiratory leak (respiration in the presence of oligomycin) and maximal (FCCP-induced) respiration after acute drug exposure. Drone, dronedarone; Amio, amiodarone; Oligo, oligomycin. Data represent the mean ± SEM of at least three individual preparations. *p<0.05 versus control. **p<0.01 versus control.

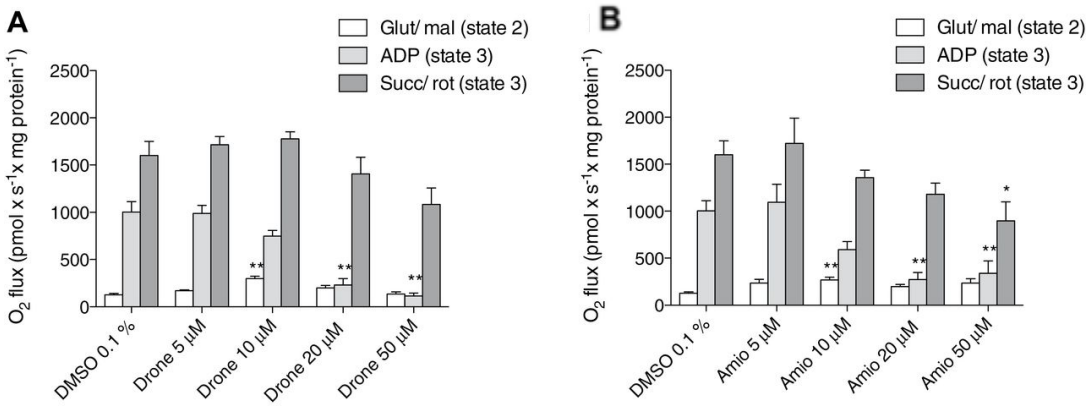

Figure 4. *Acute effect of dronedarone and amiodarone on oxidative metabolism of freshly isolated rat liver mitochondria.* Glut/mal, glutamate/malate; Succ/rot, succinate/rotenone; Drone, dronedarone; Amio, amiodarone. Data represent the mean ± SEM. *p<0.05 versus control. **p<0.01 versus control.

Subacute mitochondrial toxicity in HepG2 cells

The oxygen consumption of intact HepG2 cells was assessed at drug concentrations that were not cytotoxic in previous experiments. Figures 5A and 5B show oxygen consumption of HepG2 cells after treatment with vehicle (DMSO), dronedarone (5µM, 10µM) or amiodarone (5µM, 10µM) for 24h. A concentration of 5µM did not significantly decrease basal and maximal respiration for both drugs, whereas the higher concentration tested decreased basal and maximal (uncoupled) respiration for both drugs significantly (Fig. 5C). The respiratory leak after the addition of oligomycin was not increased by the toxicants (Fig. 5C), suggesting that dronedarone and amiodarone had no uncoupling effect in HepG2 cells exposed for 24h at these low concentrations.

In order to investigate the mechanism of decreased oxygen consumption, the respiratory capacities through the complexes of the electron transport chain were analyzed using high-resolution respirometry. After exposure to 10µM dronedarone or amiodarone for 24h, the respiratory capacities through complexes I and II were decreased for both drugs (Fig. 5D).

As expected from toxicants inhibiting complex I [23], mitochondrial superoxide accumulated in HepG2 cells when exposed to the toxicants (Fig. 6A and 6B). At the same time, mRNA expression of mitochondrial SOD2 was increased, whereas the expression of the cytoplasmic SOD1 remained unchanged (Fig. 6C), underscoring that dronedarone and amiodarone mainly affect mitochondria.

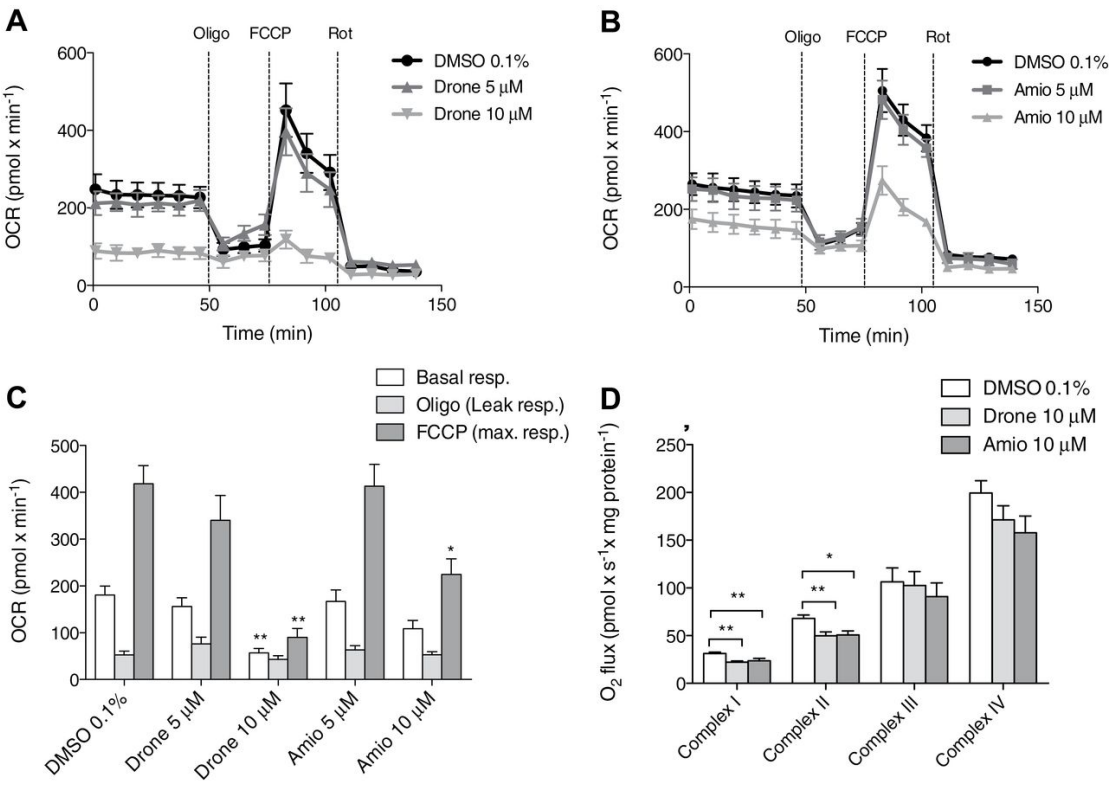

Figure 5. *Subacute effect of dronedarone and amiodarone on oxidative metabolism of HepG2 cells.* **A.** and **B.** Oxygen consumption rate after 24 h exposure for dronedarone or amiodarone measured on the Seahorse XF24 analyzer. **C.** Basal respiration, oxidative leak, and maximal respiration after 24 h drug exposure measured on the Seahorse XF24 analyzer. **D.** Respiratory capacity through complexes I, II, III, and IV after 24 h drug exposure measured on the Oxygraph-2k high-resolution respirometer. Drone, dronedarone; Amio, amiodarone; Oligo, oligomycin. Data present the mean ± SEM. *p < 0.05, **p < 0.01 versus control.

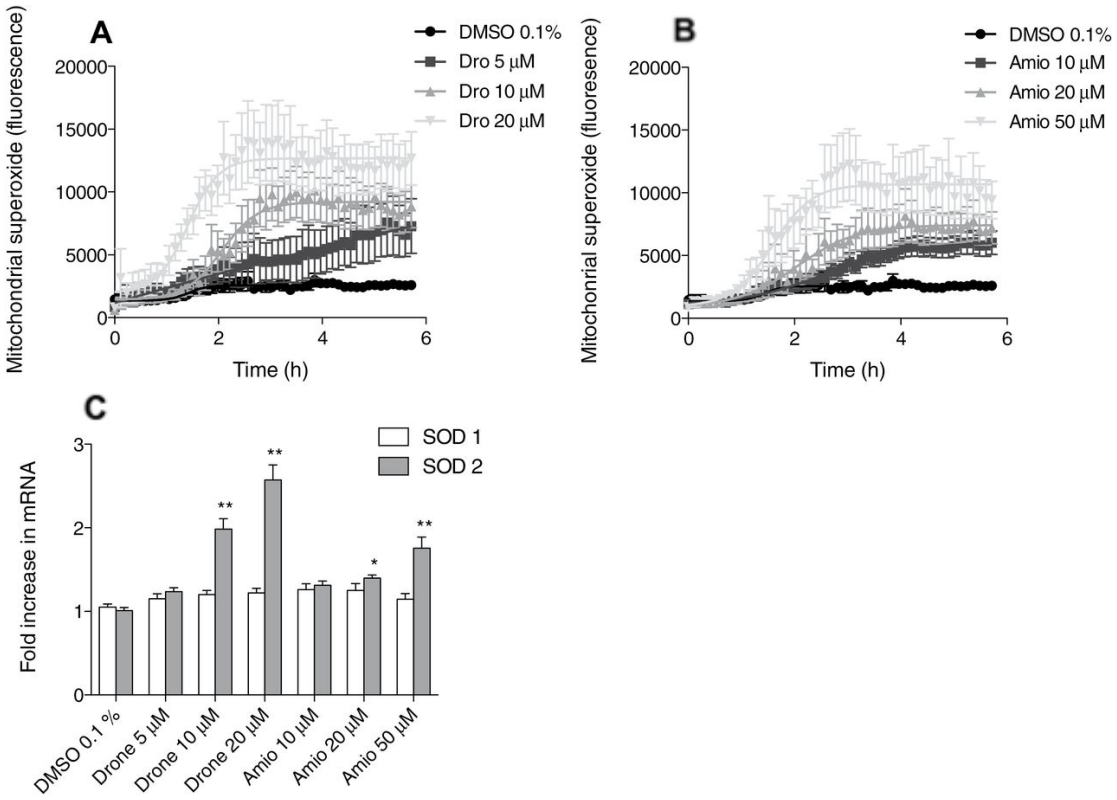

Figure 6. *Mitochondrial ROS production and SOD expression by HepG2 cells.* **A.** and **B.** Mitochondrial ROS accumulation in the presence of dronedarone or amiodarone for 24 h. **C.** mRNA expression of SOD1, SOD2 in HepG2 cells after exposure to dronedarone or amiodarone for 24 h. Drone: dronedarone, Amio: amiodarone. Data present the mean ± SEM. *p<0.05, **p<0.01 versus control.

Effect on mitochondrial β-oxidation and cellular accumulation of fatty acids

Mitochondrial β-oxidation was monitored by the formation of acid-soluble β-oxidation products from palmitate in isolated rat liver mitochondria after acute exposure to dronedarone and amiodarone. Dronedarone started to inhibit β-oxidation by isolated rat liver mitochondria at 20µM and amiodarone at 100µM (Fig. 7A). In permeabilized HepG2 cells after 24h drug exposure, dronedarone started to inhibit mitochondrial β-oxidation at 10µM and amiodarone at 20µM (Fig. 7B). As a consequence, intracellular lipid accumulation was significant after exposure to 20µM dronedarone or 50µM amiodarone for 24h.

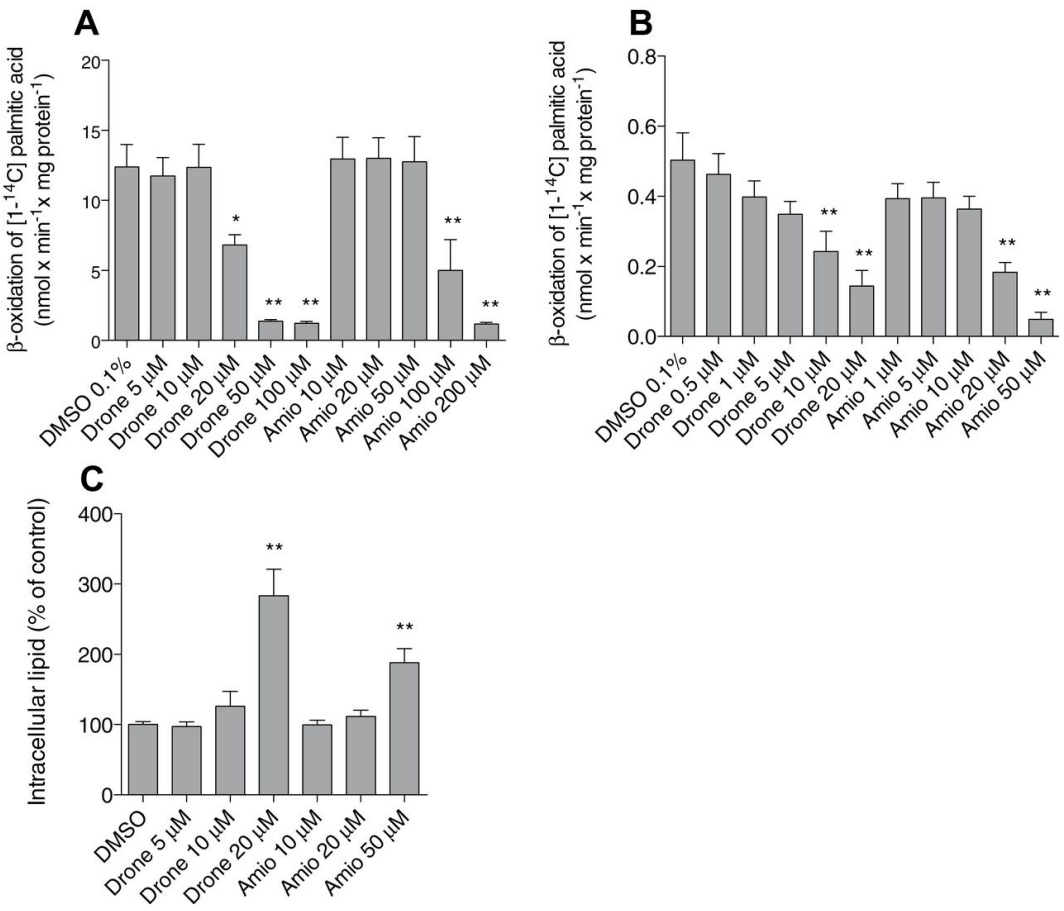

Figure 7. *Effect on mitochondrial β-oxidation and intracellular fat accumulation.* **A.** Freshly isolated rat liver mitochondria were exposed to test compounds and acute inhibition of the rate of β-oxidation was determined. **B.** HepG2 cells were exposed to test compounds for 24 h and β-oxidation was determined in permeabilized cells. **C.** Intracellular triglyceride accumulation in HepG2 cells after drug exposure for 24 h. Drone, dronedarone; Amio, amiodarone. Data present the mean ± SEM. *p<0.05 versus control. **p<0.01 versus control.

Mechanisms of cell death in HepG2 cells

In order to investigate the mechanism of cell death, externalization of phosphatidylserine was analyzed using Annexin V and disintegration of cell membranes with PI. Flow cytometric analysis of HepG2 cells revealed a progressive increase of early and late apoptotic cells with increasing concentrations of dronedarone or amiodarone (Fig. 8A). The activity of caspases 3/7, key mediators of apoptosis, was increased after treatment with 20µM dronedarone for 6 or 24h, and after treatment with 50µM amiodarone for 24h (Fig. 8B). Furthermore, the release of cytochrome c from mitochondria was significant after 6 or 24h of incubation with 5µM dronedarone and

with 20μM or 5μM amiodarone, respectively (Fig. 8C). Mitochondrial release of cytochrome c is a marker of permeabilization of the mitochondrial outer membrane, activating the intrinsic apoptotic pathway [24].

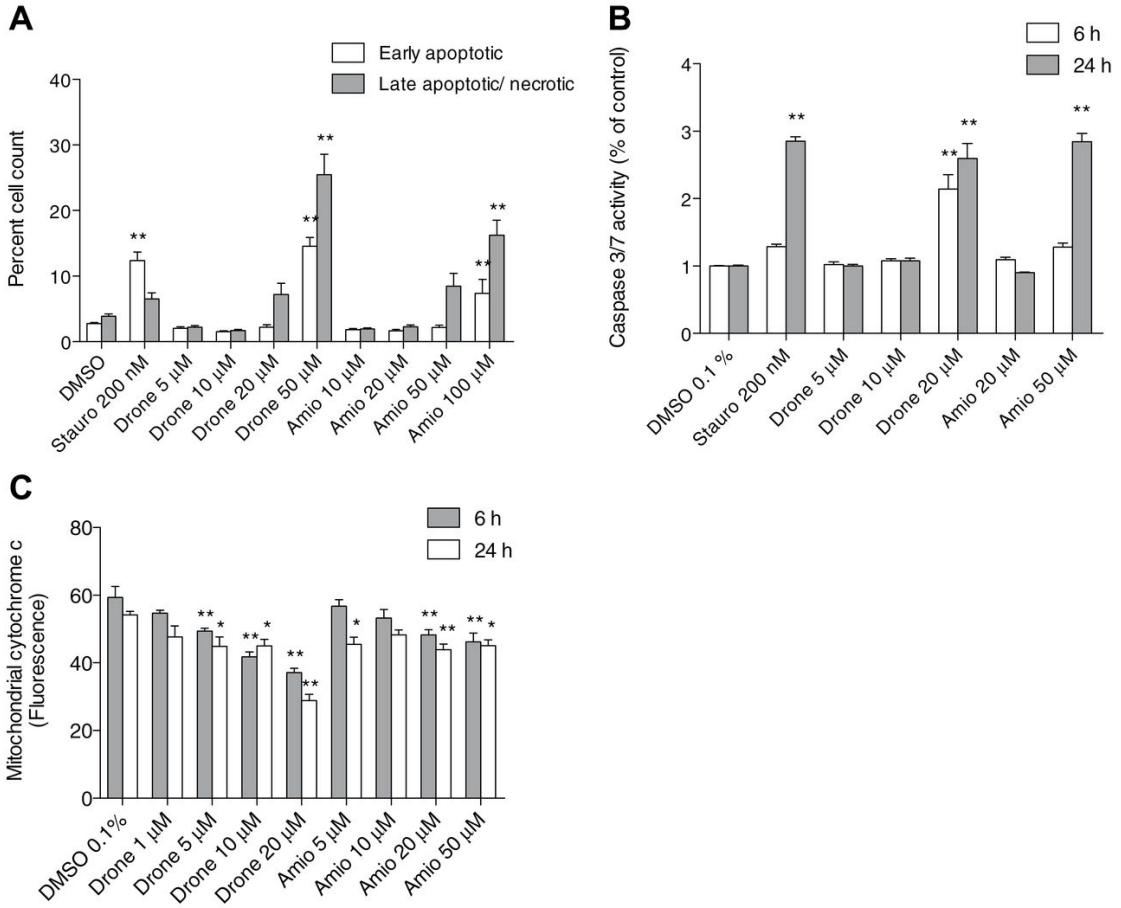

Figure 8. *Mechanisms of cell death.* **A.** Annexin V binding and PI uptake by HepG2 cells which were exposed for 24 h to test compounds. The samples were analyzed using flow cytometry. Early apoptotic populations are stained only with annexin V and late apoptotic represent annexin V and PI double-stained populations, undergoing necrosis or later stages of apoptosis. Staurosporine was used as a positive control for apoptosis. Data are presented as percent cell count. **B.** Caspase 3/7 activity after drug exposure for 6 and 24 h, expressed as percent increase compared with DMSO control. **C.** Mitochondrial cytochrome c content after drug exposure for 6 and 24 h expressed as fluorescence intensity measured by flow cytometry. Stauro: staurosporine, Drone: dronedarone, Amio; amiodarone. Data represent the mean ± SEM of at least three independent experiments. *p<0.05 versus DMSO control **p<0.01 versus DMSO control.

Discussion

Our investigations demonstrate that both dronedarone and amiodarone are uncouplers and inhibitors of the mitochondrial respiratory chain and also inhibit mitochondrial β-oxidation. Furthermore, exposure to dronedarone and amiodarone was associated with cellular superoxide accumulation and lipid storage, eventually leading to apoptosis and/or necrosis.

Both compounds tested were toxic for isolated liver mitochondria, primary human hepatocytes and HepG2 cells. They impaired mitochondrial function starting at concentrations between 10 and 20μM, whereas cytotoxicity was observed at higher concentrations, namely 20μM for dronedarone and 50μM for amiodarone. At therapeutic dosages, amiodarone reaches plasma concentrations in the range of approximately 2μM [25]. In liver, amiodarone concentrations are 10 to 20 times higher than in plasma [26], suggesting that the results of the current study are clinically relevant. This assumption is supported by the observation that in 104 patients treated with amiodarone and followed prospectively, 25 developed an increase in serum transaminases and 3 out of these 25 patients symptomatic liver injury [6]. For dronedarone, plasma concentrations reached at therapeutic dosages are in the range of 0.2μM [15], which is approximately 50 times lower than the lowest concentration where we started to observe mitochondrial toxicity. Dronedarone is almost completely absorbed and its bioavailability is only 15% [27], suggesting that the hepatic concentrations may be higher than in plasma. This may be even more so in patients with low hepatic CYP3A4 activity, in particular in patients treated concomitantly with CYP3A4 inhibitors, because dronedarone is metabolized mainly by CYP3A4 [15, 28]. Although dronedarone was at least as toxic as amiodarone in this study, slightly less patients appear to develop liver injury during treatment with dronedarone compared with amiodarone. In large clinical studies, between 0.6% and 13.6% of the patients treated with dronedarone have been reported to develop liver injury [29-31]. The large variation can be explained by different definitions of liver injury and by the patients included into the studies. No patient in these studies developed symptomatic liver injury. The apparently lower hepatic toxicity of dronedarone compared to amiodarone may at least partially be explained by the assumption that the tissue accumulation of dronedarone is less accentuated than for amiodarone due to the lower lipophilicity of dronedarone [27]. As a consequence, as discussed above, only specific patients may reach high enough hepatic concentrations which lead to hepatocyte damage.

Our data suggest that the toxicity of dronedarone is mainly caused by the parent compound. In comparison to amiodarone, the N-dealkylated metabolites appear to play

a less important role for the toxicity (Fig. 2D). The question concerning the toxicity of the N-dealkylated metabolites is clinically important, because, as we have shown in an *in vitro* study for amiodarone, CYP3A4 induction is a risk factor for hepatotoxicity, since the N-dealkylated metabolites are even more hepatotoxic than amiodarone [11, 16]. For dronedarone, this question can only be answered accurately, however, when toxicological studies can be carried out with the corresponding N-dealkylated metabolites.

The toxicity of dronedarone and amiodarone on the electron transport chain was quite similar. Both drugs inhibited complex I and uncoupled oxidative phosphorylation in isolated liver mitochondria in a concentration-dependent manner. Amiodarone inhibited also complex II, a finding observed for dronedarone only in HepG2 cells, but not in isolated rat liver mitochondria. For amiodarone, such findings have already been described in previous studies [7, 10, 11]. For dronedarone, they are not surprising, taking into account its structure with a benzofurane ring carrying a butyl side-chain. These structural properties have been described in a previous study from our laboratory as being sufficient for mitochondrial toxicity [9]. Importantly, the effects of both drugs on mitochondrial respiration were observed at lower concentrations than those required for cytotoxicity; taking into account the concentration-dependency, it is likely that mitochondrial toxicity is a major reason for the cytotoxicity of these compounds. In contrast to our study, Serviddio et al.[18] had not observed an inhibition of enzyme complexes of the electron transport chain in liver mitochondria isolated from rats treated with dronedarone. This discrepancy with our study may be explained by the observation that small molecules such as drugs can diffuse out of the mitochondria during the isolation procedure [32]. In our experiments, we used either isolated mitochondria which were exposed to a known drug concentration or permeabilized hepatocytes, in which the local environment of the mitochondria should not have changed much during the experimental procedures. Alternatively, the exposure in the study of Serviddio et al. [18] may have been lower than in our *in vitro* investigations. In their study, Serviddio et al. used a dosage of approximately 40mg dronedarone per kg body weight and they did not determine serum or tissue concentrations.

Besides affecting the electron transport chain, dronedarone and amiodarone also efficiently inhibited mitochondrial β-oxidation. Steatosis during the treatment with amiodarone is well established [5, 13] and may be a result from impaired β-oxidation [8, 9]. A likely mechanism how amiodarone inhibits β-oxidation is by inhibiting carnitine palmitoyltransferase 1 [33], which is considered to be rate-limiting for β-oxidation. In contrast to amiodarone, the effects of dronedarone on the individual steps of β-oxidation are currently not known. The inhibition of mitochondrial β-oxidation has

several consequences. As shown in the current and in previous investigations [32, 34], free fatty acids, acyl-CoAs and triglycerides accumulate and may be toxic in hepatocytes. Accumulating free fatty acids have been described to uncouple oxidative phosphorylation, increase ROS production and to induce mitochondrial permeability transition, eventually leading to apoptosis [35].

Both inhibition of the electron transport chain (especially complexes I and/or III) [23, 36] and inhibition of β-oxidation [9] are associated with increased mitochondrial production of ROS. In the presence of inhibitors of complex I or III, electrons may escape from the electron transport chain and react with molecular oxygen to form superoxide [36]. Under normal conditions, superoxide is degraded by intramitochondrial antioxidative systems such as glutathione peroxidase and superoxide dismutase [37, 38]. The observed increase of the mRNA expression of mitochondrial SOD2 after treatment with 20μM dronedarone or 50μM amiodarone can therefore be regarded as a compensatory mechanism to counteract increased mitochondrial ROS production. The lacking increase of cytosolic SOD1 mRNA expression suggests that ROS production was primarily intramitochondrial. An increase of mitochondrial ROS production is a trigger for opening of the mitochondrial membrane permeability transition pore, which is associated with cytochrome c release into the cytoplasm and induction of apoptosis and/or necrosis [24]. Mitochondrial release of cytochrome c and apoptosis could clearly be demonstrated in our study.

In conclusion, our investigations demonstrate that dronedarone inhibits the electron transport chain and β-oxidation and uncouples oxidative phosphorylation of liver mitochondria. Inhibition of complex I and of β-oxidation is associated with increased mitochondrial ROS production, which triggers mitochondrial membrane permeability transition and apoptosis. These findings may explain liver toxicity observed in predisposed patients.

Financial support

This study was supported by a grant from the Swiss National Science Foundation to SK (SNF 31003A-132992).

References

1. Julian, D.G., et al., *Randomised trial of effect of amiodarone on mortality in patients with left-ventricular dysfunction after recent myocardial infarction: EMIAT. European Myocardial Infarct Amiodarone Trial Investigators.* Lancet, 1997. **349**(9053): p. 667-74.

2. Morse, R.M., et al., *Amiodarone-induced liver toxicity.* Ann Intern Med, 1988. **109**(10): p. 838-40.

3. Mason, J.W., *Amiodarone.* N Engl J Med, 1987. **316**(8): p. 455-66.

4. Stelfox, H.T., et al., *Monitoring amiodarone's toxicities: recommendations, evidence, and clinical practice.* Clin Pharmacol Ther, 2004. **75**(1): p. 110-22.

5. Lewis, J.H., et al., *Histopathologic analysis of suspected amiodarone hepatotoxicity.* Hum Pathol, 1990. **21**(1): p. 59-67.

6. Lewis, J.H., et al., *Amiodarone hepatotoxicity: prevalence and clinicopathologic correlations among 104 patients.* Hepatology, 1989. **9**(5): p. 679-85.

7. Fromenty, B., et al., *Dual effect of amiodarone on mitochondrial respiration. Initial protonophoric uncoupling effect followed by inhibition of the respiratory chain at the levels of complex I and complex II.* J Pharmacol Exp Ther, 1990. **255**(3): p. 1377-84.

8. Fromenty, B. and D. Pessayre, *Inhibition of mitochondrial beta-oxidation as a mechanism of hepatotoxicity.* Pharmacol Ther, 1995. **67**(1): p. 101-54.

9. Kaufmann, P., et al., *Mechanisms of benzarone and benzbromarone-induced hepatic toxicity.* Hepatology, 2005. **41**(4): p. 925-35.

10. Spaniol, M., et al., *Toxicity of amiodarone and amiodarone analogues on isolated rat liver mitochondria.* J Hepatol, 2001. **35**(5): p. 628-36.

11. Waldhauser, K.M., et al., *Hepatocellular toxicity and pharmacological effect of amiodarone and amiodarone derivatives.* J Pharmacol Exp Ther, 2006. **319**(3): p. 1413-23.

12. Krahenbuhl, S., et al., *Microvesicular steatosis, hemosiderosis and rapid development of liver cirrhosis in a patient with Pearson's syndrome.* J Hepatol, 1999. **31**(3): p. 550-5.

13. Simon, J.B., et al., *Amiodarone hepatotoxicity simulating alcoholic liver disease.* N Engl J Med, 1984. **311**(3): p. 167-72.

14. Dobrev, D. and S. Nattel, *New antiarrhythmic drugs for treatment of atrial fibrillation.* Lancet, 2010. **375**(9721): p. 1212-23.

15. Patel, C., G.X. Yan, and P.R. Kowey, *Dronedarone.* Circulation, 2009. **120**(7): p. 636-44.

16. Zahno, A., et al., *The role of CYP3A4 in amiodarone-associated toxicity on HepG2 cells.* Biochem Pharmacol, 2011. **81**(3): p. 432-41.

17. Anonymous, *In brief: FDA warning on dronedarone (Multaq).* Med Lett Drugs Ther, 2011. **53**(1359): p. 17.

18. Serviddio, G., et al., *Mitochondrial oxidative stress and respiratory chain dysfunction account for liver toxicity during amiodarone but not dronedarone administration.* Free Radic Biol Med, 2011. **51**(12): p. 2234-42.

19. Hoppel, C., J.P. DiMarco, and B. Tandler, *Riboflavin and rat hepatic cell structure and function. Mitochondrial oxidative metabolism in deficiency states.* J Biol Chem, 1979. **254**(10): p. 4164-70.

20. Waterhouse, N.J. and J.A. Trapani, *A new quantitative assay for cytochrome c release in apoptotic cells.* Cell Death Differ, 2003. **10**(7): p. 853-5.

21. Mullen, P.J., et al., *Susceptibility to simvastatin-induced toxicity is partly determined by mitochondrial respiration and phosphorylation state of Akt.* Biochim Biophys Acta, 2011. **1813**(12): p. 2079-87.

22. Donato, M.T., et al., *Cytometric analysis for drug-induced steatosis in HepG2 cells.* Chem Biol Interact, 2009. **181**(3): p. 417-23.

23. Drose, S. and U. Brandt, *Molecular mechanisms of superoxide production by the mitochondrial respiratory chain.* Adv Exp Med Biol, 2012. **748**: p. 145-69.

24. Antico Arciuch, V.G., et al., *Mitochondrial regulation of cell cycle and proliferation.* Antioxid Redox Signal, 2012. **16**(10): p. 1150-80.

25. Lafuente-Lafuente, C., et al., *Amiodarone concentrations in plasma and fat tissue during chronic treatment and related toxicity.* Br J Clin Pharmacol, 2009. **67**(5): p. 511-9.

26. Wyss, P.A., M.J. Moor, and M.H. Bickel, *Single-dose kinetics of tissue distribution, excretion and metabolism of amiodarone in rats.* J Pharmacol Exp Ther, 1990. **254**(2): p. 502-7.

27. Hoy, S.M. and S.J. Keam, *Dronedarone.* Drugs, 2009. **69**(12): p. 1647-63.

28. Dorian, P., *Clinical pharmacology of dronedarone: implications for the therapy of atrial fibrillation.* J Cardiovasc Pharmacol Ther, 2010. **15**(4 Suppl): p. 15S-8S.

29. Connolly, S.J., et al., *Dronedarone in high-risk permanent atrial fibrillation.* N Engl J Med, 2011. **365**(24): p. 2268-76.

30. Hohnloser, S.H., et al., *Effect of dronedarone on cardiovascular events in atrial fibrillation.* N Engl J Med, 2009. **360**(7): p. 668-78.

31. Singh, B.N., et al., *Dronedarone for maintenance of sinus rhythm in atrial fibrillation or flutter.* N Engl J Med, 2007. **357**(10): p. 987-99.

32. Spaniol, M., et al., *Mechanisms of liver steatosis in rats with systemic carnitine deficiency due to treatment with trimethylhydraziniumpropionate.* J Lipid Res, 2003. **44**(1): p. 144-53.

33. Kennedy, J.A., S.A. Unger, and J.D. Horowitz, *Inhibition of carnitine palmitoyltransferase-1 in rat heart and liver by perhexiline and amiodarone.* Biochem Pharmacol, 1996. **52**(2): p. 273-80.

34. Begriche, K., et al., *Drug-induced toxicity on mitochondria and lipid metabolism: mechanistic diversity and deleterious consequences for the liver.* J Hepatol, 2011. **54**(4): p. 773-94.

35. Rial, E., et al., *Lipotoxicity, fatty acid uncoupling and mitochondrial carrier function.* Biochim Biophys Acta, 2010. **1797**(6-7): p. 800-6.

36. Liu, Y., G. Fiskum, and D. Schubert, *Generation of reactive oxygen species by the mitochondrial electron transport chain.* J Neurochem, 2002. **80**(5): p. 780-7.

37. Troy, C.M. and M.L. Shelanski, *Down-regulation of copper/zinc superoxide dismutase causes apoptotic death in PC12 neuronal cells.* Proc Natl Acad Sci U S A, 1994. **91**(14): p. 6384-7.

38. Bouitbir, J., et al., *Opposite effects of statins on mitochondria of cardiac and skeletal muscles: a 'mitohormesis' mechanism involving reactive oxygen species and PGC-1.* Eur Heart J, 2012. **33**(11): p. 1397-407.

Paper two

Hepatic toxicity of dronedarone in mice: role of mitochondrial β-oxidation

[*†]Felser A, [*†]Stoller A, [*†]Morand R, [*†]Schnell D, [*†]Donzelli M, [§‡]Terracciano L [*†‡]Bouitbir J, [*†‡]Krähenbühl S

[*]Clinical Pharmacology & Toxicology, University Hospital Basel, Switzerland.
[†]Department of Biomedicine, University of Basel, Switzerland.

[§]Institute of Pathology, University Hospital Basel, Switzerland.

[‡] Swiss Centre for Applied Human Toxicology (SCAHT)

Abstract

Dronedarone is an amiodarone-like antiarrhythmic drug associated with severe liver injury. Since dronedarone inhibits the mitochondrial respiratory chain and β-oxidation *in vitro*, we hypothesized that mitochondrial toxicity may also explain dronedarone-induced hepatotoxicity *in vivo*. We therefore studied hepatotoxicity of dronedarone (200mg/kg/day for 2 weeks or 400mg/kg/day for 1 week by intragastric gavage) in heterozygous juvenile visceral steatosis ($jvs^{+/-}$) and wild-type mice. $Jvs^{+/-}$ mice have reduced carnitine stores and are sensitive for mitochondrial β-oxidation inhibitors.

Treatment with dronedarone 200mg/kg/day had no effect on body weight, serum transaminases and bilirubin, and hepatic mitochondrial function in both wild-type and $jvs^{+/-}$ mice. In contrast, dronedarone 400mg/kg/day was associated with a 10 to 15% drop in body weight, and a 3 to 5-fold increase in transaminases and bilirubin in wild-type mice and, more accentuated, in $jvs^{+/-}$ mice. *In vivo* metabolism of intraperitoneal ^{14}C-palmitate was impaired in wild-type, and, more accentuated, in $jvs^{+/-}$ mice treated with 400mg/kg/day dronedarone compared to vehicle-treated mice. Impaired β-oxidation was also found in isolated mitochondria *ex vivo*. A likely explanation for these findings was a reduced activity of carnitine palmitoyltransferase 1a in mitochondria from dronedarone-treated mice. In contrast, dronedarone did not affect the activity of the respiratory chain *ex vivo*.

We conclude that dronedarone inhibits mitochondrial β-oxidation *in and ex vivo*, but not the respiratory chain. $Jvs^{+/-}$ mice appear to be more sensitive to the effects of dronedarone on mitochondrial β-oxidation than wild-type mice. The results suggest that inhibition of mitochondrial β-oxidation is an important mechanism of hepatotoxicity associated with dronedarone.

Introduction

Dronedarone, a structural analogue of amiodarone, was introduced as a new antiarrhythmic drug for the treatment of atrial fibrillation or flutter in the year 2009. Amiodarone is a well characterized hepatic toxicant which causes symptoms that range from benign increases in transaminases to potentially fatal hepatitis and cirrhosis [1]. Although dronedarone has been claimed to possess an improved hepatic safety profile compared to amiodarone, only shortly after its introduction, two cases of severe liver injury requiring emergency liver transplantation have been reported [2, 3]. These reports were followed by warnings by regulatory authorities about possible severe hepatotoxicity in patients treated with dronedarone.

The underlying mechanisms of dronedarone-associated hepatotoxicity are currently not fully understood. Amiodarone is a well-known mitochondrial toxicant that inhibits both mitochondrial β-oxidation and oxidative phosphorylation [4-7]. In our previous *in vitro* study [8], we therefore compared dronedarone and amiodarone for their effects on mitochondrial function and found that dronedarone has at least the same potential as amiodarone to inhibit the respiratory chain complexes I and II and mitochondrial β-oxidation. Furthermore, a study in rats performed by Serviddio et al. suggested that dronedarone is not a direct inhibitor of the mitochondrial respiratory chain *in vivo* [9]. We therefore hypothesized that inhibition of mitochondrial β-oxidation may play a more important role in the hepatotoxic potential of dronedarone *in vivo*.

Since severe hepatotoxicity of dronedarone can be considered as an idiosyncratic reaction needing susceptibility factors for its manifestation [10], we decided to study the toxicity of dronedarone not only in wild-type mice, but also in mice with impaired β-oxidation. Based on our previous experience with valproic acid [11], we choose $jvs^{+/-}$ mice as a model with impaired hepatic β-oxidation. Carnitine is an essential cofactor for hepatic β-oxidation [12] and $jvs^{+/-}$ mice have reduced plasma and tissue carnitine stores due to a mutation in the gene coding for OCTN2, the renal carnitine carrier [13]. Homozygous $jvs^{-/-}$ mice are characterized by liver steatosis and other features of impaired β-oxidation due to carnitine deficiency such as growth retardation and cardiac hypertrophy, and do not survive without carnitine supplementation [14, 15]. Heterozygous ($jvs^{+/-}$) mice have carnitine plasma and tissue levels which are approximately half that of wild-type mice and can survive without carnitine supplementation [16].

The specific questions that we wanted to answer in our study were 1. is dronedarone hepatotoxic *in vivo* in mice, 2. if yes, which are the principle mechanisms and 3. are $jvs^{+/-}$ mice more sensitive to dronedarone than the corresponding wild-type mice.

Materials and methods

Animals

The experiments were performed with 9 to 12 weeks old male C57BL/6 (wild-type) or heterozygous juvenile visceral steatosis mice ($jvs^{+/-}$). $Jvs^{+/-}$ mice were originally obtained from Prof. Masahisa Horiuchi (University of Kagoshima, Kagoshima, Japan). The genotype of the breeding pairs and offsprings was analyzed by a TaqMan allelic discrimination method as described previously [11]. Experiments were reviewed and accepted by the cantonal veterinary authority and were performed in agreement with the guidelines for care and use of laboratory animals.

Study design and dronedarone administration

Dronedarone was administered as a suspension in water-macrogol 400 (50:50 v/v) at a concentration of 20mg/ml by oral gavage. The 200mg/kg dronedarone dose was administered for 14 days once daily. The 400mg/kg dose was administered twice daily (every 12h 200mg/kg) for 7 days.

Based on body surface area (BSA) conversion according to Reagan-Shaw et al. [17], the daily dose of 200mg/kg corresponds approximately to a human adult daily equivalent dose of 500mg/m^2 (corresponding to 400mg twice-daily with a mean human adult BSA of 1.6m^2). The animals received water and food *ad libitum* during the entire study, but were starved over night before sacrifice.

Reagents

Dronedarone HCl was extracted from commercially available tablets (Multaq®, Sanofi) from ReseaChem life science GmbH (Burgdorf, Switzerland). 1-^{14}C palmitic acid was purchased from Perkin Elmer (Schwerzenbach, Switzerland), and L-(N-^{14}C-methyl)-carnitine, 1-^{14}C palmitoylcarnitine, and palmitoyl-L-(N-^{14}C-methyl)-carnitine from American Research Chemicals (Anawa, Wangen, Switzerland). All other chemicals used in this study were purchased from Sigma Aldrich (Buchs, Switzerland) if not indicated differently.

Characterization of the animals

The animals were characterized by their body, liver, and heart weight. Mouse plasma was analyzed for the activity of alanine aminotransferase, total bilirubin and creatine kinase using routine biochemical tests. Plasma concentrations of carnitine and acetylcarnitine were determined with an established LC-MS/MS method as described previously [18]. Plasma β-hydroxybutyrate was analyzed using a commercially available colorimetric assay kit (Cayman, MI, USA).

Histological analysis of liver tissue

Liver samples were treated with 4% formaldehyde or frozen in isopentane. Staining with hematoxylin-eosin or immunohistochemistry for cleaved caspase-3 was performed as described previously on formaldehyde conserved liver samples [11]. Lipid accumulation was investigated by Oil red O staining and performed on isopentane frozen sections. Oil red O was freshly diluted (3:2 in distilled water) from a stock solution in isopropanol (0.5g in 100ml) and sections were incubated for 15min. After incubation, the slides were rinsed with 60% isopropanol, counterstained with hematoxylin and coverslipped in aqueous mountant. The stained sections were examined by light microscopy and investigated for pathological changes in the liver.

mRNA expression

RNA was extracted and purified using the Qiagen RNeasy mini extraction kit (Qiagen, Hombrechtikon, Switzerland) and RNA quality was evaluated with the NanoDrop 2000 (Thermo Scientific, Wohlen, Switzerland). The Qiagen omniscript system was used to synthesize cDNA from 10µg RNA. The expression of mRNA was assessed using SYBR Green real-time PCR (Roche Diagnostics, Rotkreuz, Basel). We used primers specific for Bcl2 (forward: 5'-AGTACCTGAACCGGCATCTG-3', reverse: 5'-GGGGCCATATAGTTCCACAAA-3') and Bax (forward: 5'-GTGAGCGGCTGCTTGTCT-3', reverse: 5'-GGTCCCGAAGTAGGAGAGGA-3'). Quantification was performed using the comparative-threshold cycle method. Beta actin (forward: 5'-CATGGCCTTCCGTGTTCCTA-3', reverse: 5'-CCTGCTTCACCACCTTCTTGA-3') was used as endogenous reference.

Immunoblotting

Expression of cleaved caspase-3 and CPT1a were checked by Western blotting using monoclonal antibodies (cleaved caspase-3 from Cell signaling technology, USA, and CPT1a from Abcam, UK). We homogenized frozen liver samples with a Micro-dismembrator S (Sartorius, Göttingen, Germany) during 1min at 2000rpm, resuspended the tissue in protein extraction reagent (T-PER, Thermo scientific, Wohlen, Switzerland) containing a protease inhibitor cocktail (Roche AG, Basel, Switzerland) and collected the supernatant. We separated 20µg protein on a commercially available 4-12% gradient NuPAGE Bis-Tris gel (Invitrogen, CA, USA) in the presence of molecular weight standards (Gibco, Paisly, UK), transferred the proteins onto a polyvinylidene fluoride membrane, and probed with the specific antibodies. Appropriate secondary antibodies coupled to horseradish peroxidase were applied and chemiluminescence substrate (GE Healthcare, Buckinghamshire, UK) was used for quantification. Densitometric analysis was performed using ImageJ software (Bethesda, USA).

In vivo metabolism of palmitate

A trace amount of 1-^{14}C palmitic acid (3 µCi/kg, 60 µCi/µmol) was diluted in thistle oil and administered i.p. at 0 min. The mice were placed in a cylindrical vessel attached to a vacuum pump and breath samples were collected over 100min. Exhaled $^{14}CO_2$ was pulled through ethanol (to dry the exhaled breath) followed by a solution containing 4M ethanolamine in ethanol. The exhaled $^{14}CO_2$ was quantified by liquid scintillation counting using a scintillation fluid for organic compounds (GE Healthcare, Buckinghamshire, UK) [11].

Isolation of liver mitochondria

Fresh liver tissue was quickly removed and immersed in ice-cold isolation buffer (200mM mannitol, 50mM sucrose, 1mM Na_4EDTA, 20mM HEPES, pH 7.4). Liver mitochondria were isolated by differential centrifugation as described previously [19]. The mitochondrial protein content was determined using the bicinchoninic acid protein assay reagent from Thermo Scientific (Wohlen, Switzerland).

Oxygen consumption and mitochondrial membrane potential

Activities of complexes I and II of the respiratory chain were analyzed using an Oxygraph 2k high resolution respirometer equipped with DatLab software (Oroboros Instruments, Innsbruck, Austria). Freshly isolated liver mitochondria were resuspended in mitochondrial respiration medium MiR06 [8]. Complex I (NADH dehydrogenase) was assessed using L-glutamate and L-malate (10 and 2mM, respectively) as substrates, followed by the addition of ADP (2.5mM). Complex II (succinate dehydrogenase) was assessed using 10mM succinate as a substrate after having blocked complex I with 0.5µM rotenone. The integrity of the outer mitochondrial membrane was assessed by showing the absence of a stimulatory effect of exogenous cytochrome c (10µM) on respiration. The mitochondrial membrane potential was assessed using the Oroboros 2k-MultiSensor system (Oroboros Instruments) with an electrode selective for tetraphenylphosphonium (TPP) in the presence of succinate, rotenone and oligomycin (2.5µM). The membrane potential ($\Delta\Psi$) was calculated using a TPP calibration curve (1µM to 3µM), and using a modified Nernst equation [20].

β-oxidation of palmitic acid

Mitochondrial oxidation of 1-^{14}C palmitic acid by freshly isolated liver mitochondria was assessed in the presence of saturating concentrations of cold palmitic acid and co-substrates. The metabolism of 1-^{14}C palmitic acid was quantified as the formation of ^{14}C-acid-soluble β-oxidation products. Isolated mouse liver mitochondria (250µg protein) were preincubated for 10min in 450µl assay buffer (70mM sucrose, 43mM KCl, 3.6mM $MgCl_2$, 7.2mM KH_2PO_4, 36mM Tris, 2mM ATP, 500µM L-carnitine, 150µM coenzyme A, 5mM acetoacetate, pH 7.4) at 37°C in a thermomixer at 600rpm (Eppendorf, Switzerland). The reaction was started by addition of 50µl of radioactive substrate mix containing 200µM Na-palmitate (final concentration), 25pCi [1-^{14}C] palmitic acid, and 170µM BSA (fatty acid free). The reactions were stopped after 15min by adding 100µl 20% perchloric acid. After centrifugation (7000g, 2min), radioactivity was measured in the supernatant by liquid scintillation counting.

Activity of carnitine palmitoyltransferase 1

The activity of carnitine palmitoyltransferase (CPT) 1 was assessed by the formation of palmitoyl-^{14}C-carnitine from palmitoyl-CoA and ^{14}C-carnitine as prescribed previously [21] with some modifications. Mitochondria (250µg protein) were incubated for 10min in

450µl assay buffer (80mM KCl, 50mM MOPS, 10mg/ml BSA defatted, 5mM EGTA, 25mM *N*-ethylmaleimide, pH 7.4) at 37°C in a thermomixer at 600rpm. The reaction was started by the addition of 50µl radioactive substrate mix containing L-carnitine (final concentration 400 µM), 25pCi ^{14}C-L-carnitine and palmitoyl-CoA (final concentration 200 µM). The reaction was terminated after 10min by adding 100µl of concentrated HCl. The samples (600 µl) were transferred into an extraction vial, and 1.4ml butanol-saturated distilled water and 1ml water-saturated n-butanol was added. The tubes were shaken for 10min at 200rpm and centrifuged at 2000rpm for 10min. The upper (butanol) phase was transferred into a new extraction tube containing 2ml of butanol-saturated water and the extraction repeated. Finally, the upper butanol-phase, containing the lipophilic palmitoyl-^{14}C-L-carnitine, was separated and the radioactivity determined by liquid scintillation counting.

Acute treatment of isolated liver mitochondria and activity of fatty acid metabolism

Untreated freshly isolated C57BL/6 (wild-type) liver mitochondria were acutely exposed to dronedarone and amiodarone concentrations ranging between 10 to 100µM for 10min at 37°C before starting the assays.

The metabolism of 1-^{14}C palmitic acid and 1-^{14}C palmitoyl-L-carnitine were assessed as described above, but the assay buffer of palmitoyl-L-carnitine metabolism contained no L-carnitine (70mM sucrose, 43mM KCl, 3.6mM $MgCl_2$, 7.2mM KH_2PO_4, 36mM Tris, 2mM ATP, 150µM coenzyme A, 5mM acetoacetate, pH 7.4), and the reaction was started by the addition of a radioactive substrate mix containing palmitoyl-L-carnitine (200µM final assay concentration), containing 25pCi [1-^{14}C] palmitoylcarnitine.

The activity of the long-chain acyl-CoA synthetase (ACSL) was investigated by assessing the rate of ^{14}C-palmitoyl-CoA formation as prescribed previously [22].

The activity of carnitine palmitoyltransferase 2 (CPT2) was measured by the formation of ^{14}C-carnitine from CoASH and palmitoyl-^{14}C-carnitine. Mitochondria (250µg protein) were incubated for 10min in 450µl assay buffer (80mM KCl, 50mM MOPS, 10mg/ml BSA defatted, 1mM EGTA, pH 7.4) at 37°C in a thermomixer at 600rpm. The reaction was started by the addition of 50µl radioactive substrate mix containing CoASH (final concentration 2mM), malonyl-CoA (final concentration 200µM), palmitoyl-L-carnitine (final concentration 1mM), and 25pCi palmitoyl-^{14}C-carnitine. The reactions were stopped after 5min by adding 100µl 20% perchloric acid. After centrifugation (7000g, 2min), radioactivity was measured in the supernatant by liquid scintillation counting.

The activities of mitochondrial acyl-CoA dehydrogenases were determined spectrophotometrically at 37°C as described by Hoppel et al. [19]. Long-chain, medium-chain, and short-chain acyl-CoA dehydrogenase were assessed using palmitoyl-, octanoyl-, and butyryl-CoA (final concentrations 100, 50, and 50µM, respectively) as substrates.

Statistical analysis

Data are represented as mean ± standard error of the mean (SEM). Statistical analyses were performed using two-way analysis of variance (ANOVA) followed by a Bonferroni's post test (GraphPad Prism 5, Graph Pad Software, Inc., San Diego, CA, USA). Comparisons of acute treatments between one control group and several treatment groups were performed by one-way ANOVA followed by Dunnett's post test. Statistical significance is indicated as *$p<0.05$ or **$p<0.01$.

Results

Characterization of the animals

A daily dose of 200mg/kg dronedarone for 14 days had no significant effect on the body weight, whereas 400mg/kg for 7 days was associated with a 10% drop in wild-type and a 15% drop in $jvs^{+/-}$ mice body weight (Table 1). The food intake by mice treated with 400mg/kg dronedarone was decreased compared to vehicle-treated control mice, explaining the decrease in body weight. Liver and heart weight adjusted to body weight were not affected by treatment with dronedarone.

Plasma activities of alanine aminotransferase (ALT) and creatine kinase (CK) as well as the plasma concentration of total bilirubin were not different from control mice in animals treated with 200mg/kg dronedarone per day (Table 2). In contrast, wild-type mice treated with 400mg/kg dronedarone had a 4-fold increase in ALT and a 3-fold increase in total bilirubin, and $jvs^{+/-}$ mice a 5-fold increase in ALT and a 4-fold increase in total bilirubin compared to vehicle-treated control mice. In contrast, plasma CK activity was not different from vehicle-treated control mice in mice treated with 400mg/kg dronedarone. In comparison to wild-type mice, $jvs^{+/-}$ mice had significantly lower plasma free carnitine and acetylcarnitine concentrations, reflecting deficient renal carnitine reabsorption [13].

Table 1. *Animal and organ weights.* The animal weight was recorded at start and end of the study, and organ weights were normalized to the body weight at study end. Wild-type and jvs$^{+/-}$ mice treated orally with 200mg/kg dronedarone (Drone) for 14 days or 400mg/kg for 7 days or vehicle control (Vehicle). Statistical differences were calculated with a two-way ANOVA followed by a Bonferroni post test. bw, body weight; nd, not determined.

	200 mg/kg/day				**400 mg/kg/day**			
	Wild-type		Jvs$^{+/-}$		Wild-type		Jvs$^{+/-}$	
	Vehicle	Drone	Vehicle	Drone	Vehicle	Drone	Vehicle	Drone
Body weight, start of study (g)	28.7 ± 0.3	27.8 ± 0.9	28.9 ± 0.9	28.0 ± 0.5	27.6 ± 1.3	27.7 ± 1.0	28.5 ± 1.2	27.5 ± 0.6
Body weight, end of study (g)	29.8 ± 0.3	27.9 ± 0.8	30.0 ± 0.9	28.3 ± 0.8	27.6 ±1.1	24.7 ± 0.7*	28.9 ± 1.3	23.5 ± 0.7**
Average food intake (g/animal/day)	nd	nd	nd	nd	3.4 ± 0.2	2.4 ± 0.2**	3.5 ± 0.2	2.3 ± 0.2**
Liver weight (mg/g bw)	34 ± 2	40 ± 2	38 ± 2	36 ± 1	39 ± 1	37 ± 1	41 ± 2	37 ± 1
Heart weight (mg/ g bw)	4.7 ± 0.1	4.5 ± 0.1	4.5 ± 0.1	4.4 ± 0.1	4.3 ± 0.1	4.6 ± 0.2	4.3 ± 0.1	4.7 ± 0.2

Table 2. *Plasma parameters.* Alanine transaminase (ALT), total bilirubin (bilirubin), creatine kinase (CK), free carnitine and acetylcarnitine were determined in mouse plasma. Statistical differences were calculated with a two-way ANOVA followed by a Bonferroni post test. *p<0.05, or **p<0.01 indicate difference between dronedarone treated mice in comparison to their respective controls. †p<0.05, or ††p<0.01 indicate difference between jvs$^{+/-}$ mice in comparison to wild-type mice.

	200 mg/kg/day				**400 mg/kg/day**			
	Wild-type		Jvs$^{+/-}$		Wild-type		Jvs$^{+/-}$	
	Vehicle	Drone	Vehicle	Drone	Vehicle	Drone	Vehicle	Drone
Alanine transaminase (U/L)	17 ± 2	23 ± 2	18 ± 3	23 ± 2	21 ± 1	91 ± 24**	23 ± 2	109 ± 22**
Bilirubin (µmol/L)	1.3 ± 0.2	1.1 ± 0.2	1.1 ± 0.3	1.3 ± 0.2	0.8 ± 0.1	2.3 ± 0.5**	0.8 ± 0.1	3.0 ± 0.4**
Creatine kinase (U/L)	386 ± 161	552 ± 193	540 ± 115	644 ± 173	601 ± 84	448 ± 91	663 ± 147	1091 ± 400
Free carnitine (µmol/L)	32.0 ± 3.1	26.3 ± 2.6	19.5 ± 2.2††	19.9 ± 3.1†	28.4 ± 2.3	35.2 ± 2.3	19.2 ± 1.7††	20.9 ± 2.1††
Acetylcarnitine (µmol/L)	12.9 ± 1.8	13.6 ± 2.3	6.0 ± 0.8†	8.5 ± 1.6	11.7 ± 1.1	13.5 ± 2.6	6.6. ± 0.7†	12.4 ± 1.9*

Histological changes in the liver

Liver histology of wild-type and jvs$^{+/-}$ mice treated with 200mg/kg dronedarone per day was not different from the respective vehicle-treated control mice (data not shown). As shown in supplemental Fig. 1, haematoxylin-eosin stained liver sections of wild-type and jvs$^{+/-}$ mice treated with 400mg/kg dronedarone per day were negative for inflammation, necrosis or steatosis. In agreement with the serum transaminase activity, staining of hepatocytes for cleaved caspase 3 was increased in wild-type or jvs$^{+/-}$ mice treated with 400mg/kg dronedarone per day, suggesting apoptosis (Fig. 1A-D). This finding was confirmed by increased protein expression of cleaved caspase 3 (Fig. 1E) and an increased Bax/Bcl2 mRNA expression ratio in livers of mice treated with 400mg/kg dronedarone per day (Fig. 1F).

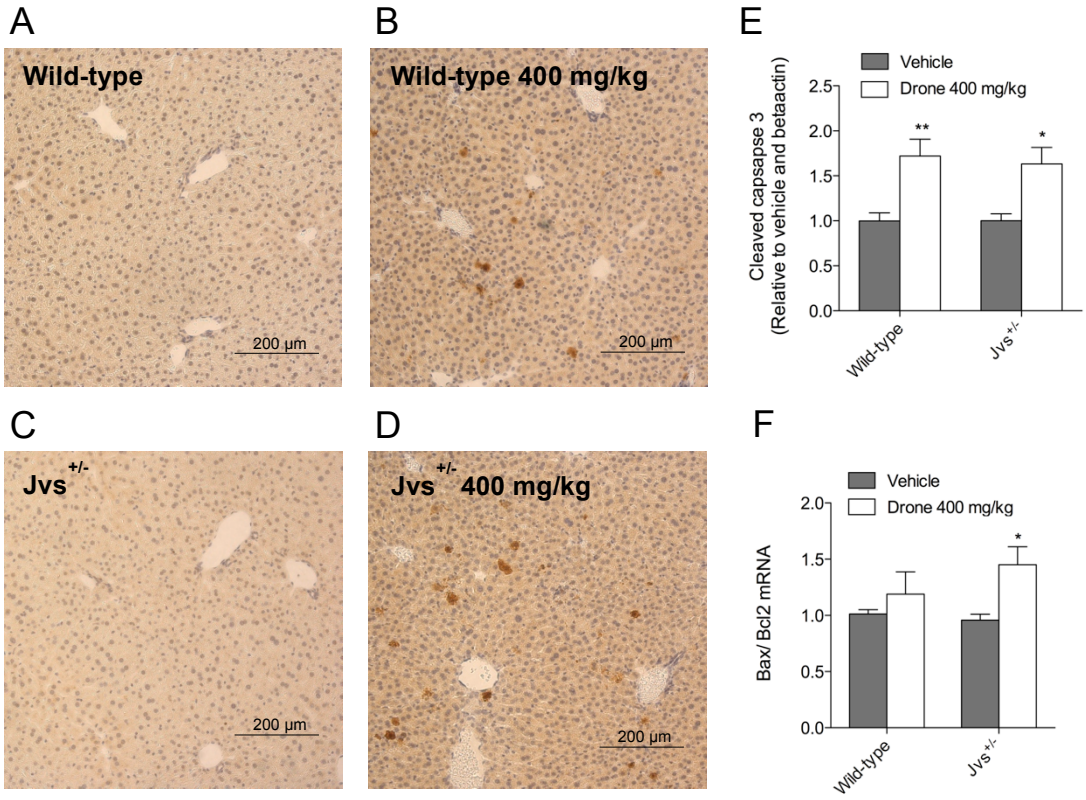

Figure 1. *Assessment of hepatocyte apoptosis associated with dronedarone.* **A-D.** Liver sections stained for cleaved caspase 3 of wild-type mice treated with vehicle (A) or dronedarone 400mg/kg (B) and jvs$^{+/-}$ mice treated with vehicle (C) or dronedarone 400mg/kg (D). E. Cleaved caspase 3 assessed by Western blot. **F.** mRNA expression of Bax/Bcl2 in liver tissue. Statistical differences were calculated with a two-way ANOVA followed by a Bonferroni post test.

In vivo oxidation of palmitate

Since our previous *in vitro* study has shown that hepatocellular fatty acid metabolism is impaired at dronedarone concentrations in the low µmolar range [8], we investigated hepatic metabolism of palmitate *in vivo*. The breakdown of an i.p. administered 1-^{14}C palmitic acid tracer was analyzed by collecting $^{14}CO_2$ breath samples over time. Wild-type animals treated with 400mg/kg dronedarone per day had a significantly decreased $^{14}CO_2$ peak exhalation 30min after tracer injection compared to control mice (Fig. 2 and Table 3). In agreement with this finding, jvs$^{+/-}$ mice treated with 400mg/kg dronedarone per day not only had a numerically lower peak exhalation, but also a significantly slower $^{14}CO_2$ production compared to vehicle-treated control mice (Fig. 2 and Table 3). Impaired metabolism of fatty acids was also reflected by a numerically lower serum β-hydroxybutyrate concentration after overnight starvation in mice treated with 400mg/kg dronedarone per day (Fig 2 D). In contrast to these findings, fat accumulation in livers of wild-type or jvs$^{+/-}$ mice treated with 400mg/kg dronedarone per day could not be demonstrated by Oil red O staining of liver sections (Suppl. Fig. 2).

Table 3. *Quantitative results of in vivo metabolism of 1-^{14}C palmitic acid.* Wild-type and jvs$^{+/-}$ mice were given oral treatment with 400mg/kg/day dronedarone or vehicle for 7 days. 1-^{14}C-palmitic acid (3µCi/kg, 57.0mCi/mmol in thistle oil) was administered i.p. and exhaled $^{14}CO_2$ was quantified over 100min. Statistical differences were calculated with a two-way ANOVA followed by a Bonferroni post test.

	400 mg/kg/day			
	Wild-type		Jvs$^{+/-}$	
	Vehicle	Drone	Vehicle	Drone
Peak exhalation (percentage of injected dose/10 min)	14.4 ± 0.7	11.2 ± 1.1*	12.3 ± 1.4	11.6 ± 1.0
T_{max} (min)	28 ± 2	29 ± 1	29 ± 1	39 ± 3 **
AUC (10-100min)	580 ± 28	499 ± 46	512 ± 50	593 ± 44

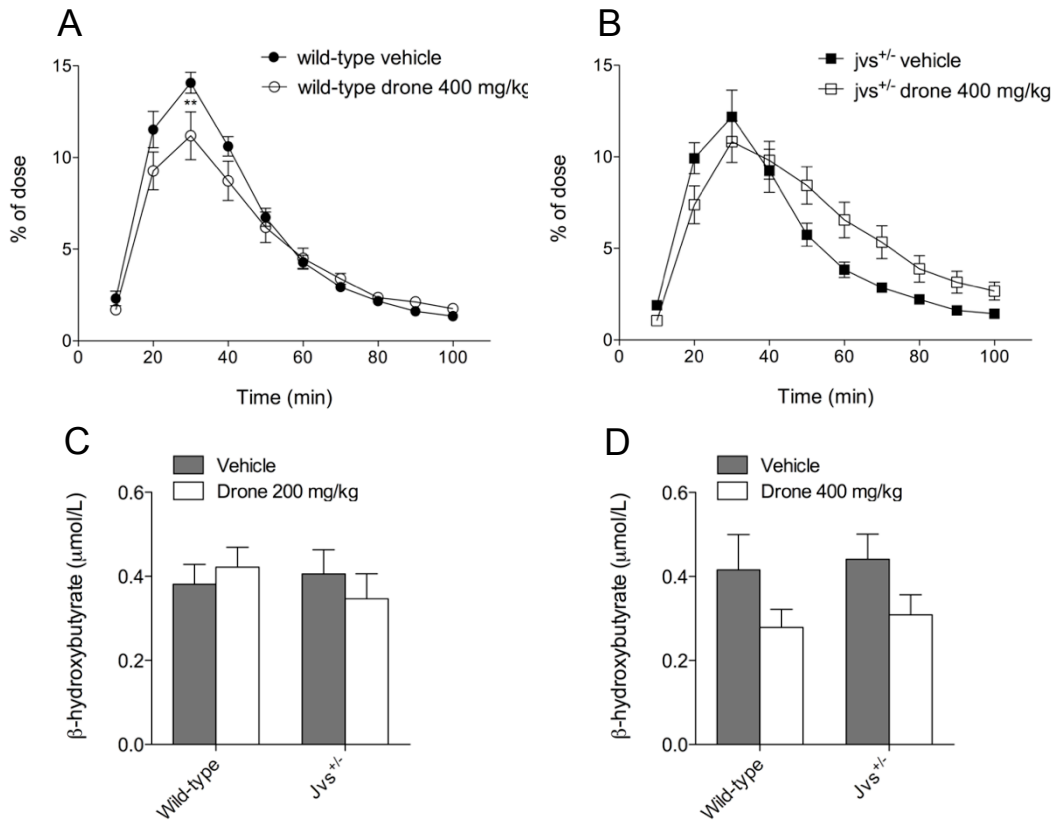

Figure 2. *In vivo metabolism of 1-^{14}C palmitate and ketone bodies in plasma.* **A, B.** Exhalation time curves of $^{14}CO_2$ in wild-type (A) or jvs$^{+/-}$ mice (B) treated with vehicle or 400mg/kg dronedarone. Quantitative results of this experiment are shown in Table 3. **C, D.** β-hydroxybutyrate plasma level in wild-type or jvs$^{+/-}$ mice treated with 200mg/kg (C) or 400mg/kg per day (D). Statistical differences were calculated with a two-way ANOVA followed by a Bonferroni post test.

Metabolic function of intact liver mitochondria

Dronedarone has been shown *in vitro* to be an inhibitor of both the respiratory chain complexes I and II and mitochondrial β-oxidation [8]. Since impaired hepatic fatty acid metabolism (as reflected by altered $^{14}CO_2$ exhalation after i.p. administration of ^{14}C-palmitate) can be a consequence of a decreased function of both the activity of the respiratory chain or β-oxidation [12], we examined these pathways *ex vivo* in isolated liver mitochondria in more detail. Treatment with 200mg/kg or 400mg/kg dronedarone per day did neither impair the membrane potential, nor the activity of the respiratory chain complexes I and II of liver mitochondria isolated from wild-type or jvs$^{+/-}$ mice (Fig. 3A,B and Suppl. Fig. 3A,B). The activity of mitochondrial β-oxidation of 1-^{14}C palmitic acid was not altered in liver mitochondria from mice treated with 200mg/kg

dronedarone per day (Fig. 3C), whereas the activity was decreased by 15% in liver mitochondria from wild-type or jvs$^{+/-}$ mice treated with 400mg/kg dronedarone per day compared to vehicle treated control mice (Fig. 3D).

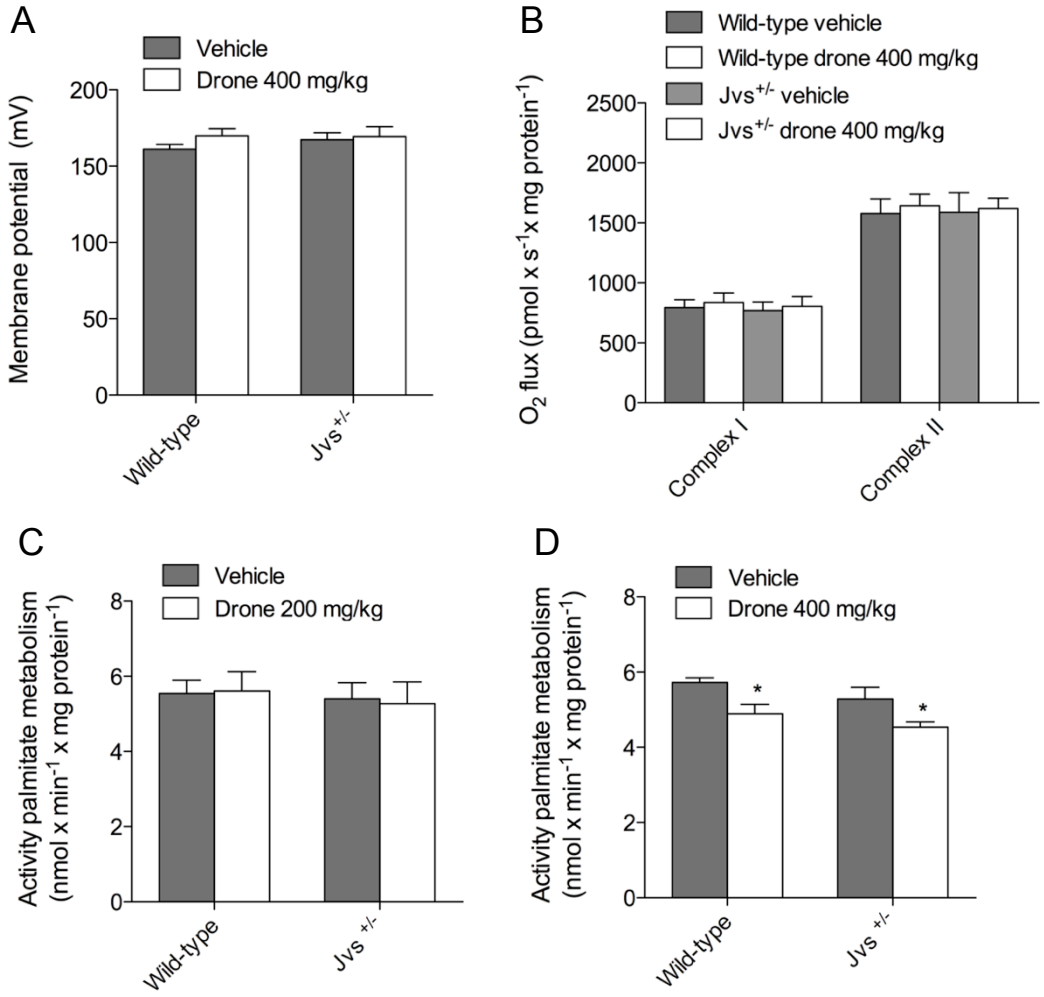

Figure 3. *Characterization of isolated mouse liver mitochondria.* **A.** Mitochondrial membrane potential in mitochondria from animals treated with 400mg/kg. **B.** Respiratory capacity through complexes I and II in mitochondria from animals treated with 400mg/kg. **C, D.** Metabolism of 1-^{14}C palmitic acid in mitochondria from animals treated with 200mg/kg (C) or 400mg/kg (D). Statistical differences were calculated with a two-way ANOVA followed by a Bonferroni post test.

In order to find out the reason for impaired liver mitochondrial β-oxidation in mice treated with 400mg/kg dronedarone per day, we assessed the function and protein expression of carnitine palmitoyltransferase 1a (CPT1a), the rate limiting enzyme of hepatic fatty acid β-oxidation [12]. As expected, CPT1a activity was not affected by a treatment of 200mg/kg dronedarone per day (Fig. 4A), but was decreased by 15% in liver mitochondria from mice treated with 400mg/kg dronedarone per day (Fig. 4B). In contrast to CPT1a activity, dronedarone treatment did not affect protein expression of CPT1a in livers of wild-type or jvs$^{+/-}$ mice treated with 400mg/kg dronedarone per day (Fig. 4C and D).

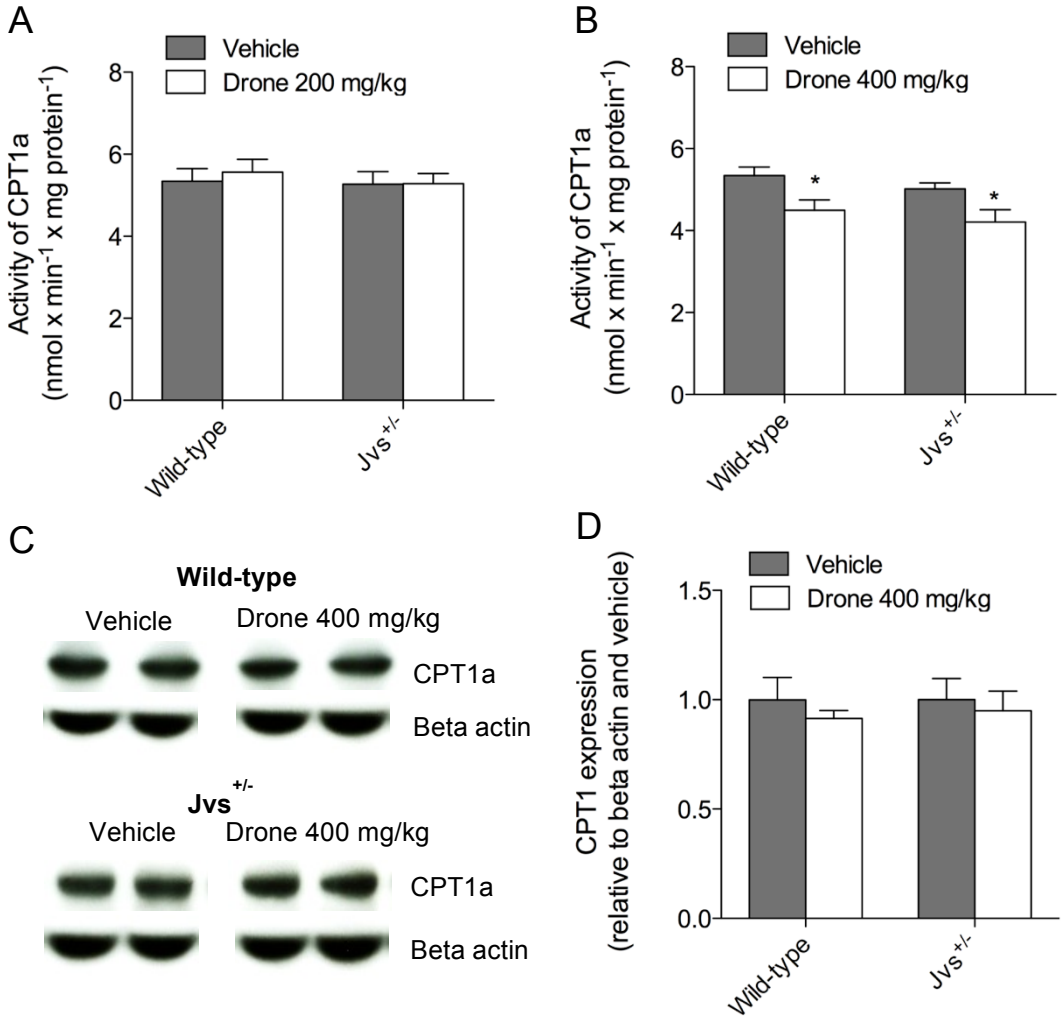

Figure 4. *Mechanism of inhibition of fatty acid metabolism.* **A, B.** Activity of carntine palmitoyltransferase 1a (CPT1a) in mitochondria from animals treated with 200mg/kg (A) and 400mg/kg (B). **C, D.** Protein expression of CPT1a in wild-type and jvs$^{+/-}$ mice treated with 400mg/kg. Statistical differences were calculated with a two-way ANOVA followed by a Bonferroni post test.

Acute inhibition of fatty acid oxidation in liver mitochondria

Mitochondrial β-oxidation of long-chain fatty acids (LCFAs, e.g. palmitic acid) is a complex process involving multiple enzymes. In order to localize the inhibition of fatty acid metabolism more precisely we investigated the effects of acute exposures to dronedarone on isolated liver mitochondria and compared the findings to amiodarone. The translocation of LCFAs into the mitochondrial matrix space depends on the transformation of the free fatty acid to the corresponding acylcarnitine (e.g. palmitoylcarnitine) (Fig. 5A). In freshly isolated mouse liver mitochondria exposed acutely to different concentrations of dronedarone or amiodarone, we found that both drugs inhibited palmitic acid (Fig. 5B) as well as palmitoylcarnitine metabolism (Fig. 5C) starting at 50μM. These findings suggested that dronedarone and amiodarone inhibit not only the conversion of palmitate to palmitoylcarnitine, but also the downstream metabolism of palmitoylcarnitine (see Fig. 5A). We then assessed the activity of the enzymes involved in fatty acid transport and showed that CPT1a was inhibited by dronedarone and amiodarone starting at 50 μM (Fig. 5E), but not the long-chain acyl-CoA synthetase (ACSL) (Fig. 5D) or CPT2 (Fig. 5F). Next, we assessed the activity of the first enzymes in the β-oxidation cycle, namely the acyl-CoA dehydrogenase, and found that amiodarone inhibited the long-chain dehydrogenase starting at 50 μM (Fig. 5G), whereas dronedarone had no inhibitory effect on acyl-CoA dehydrogenases (Fig. 5G,H,I).

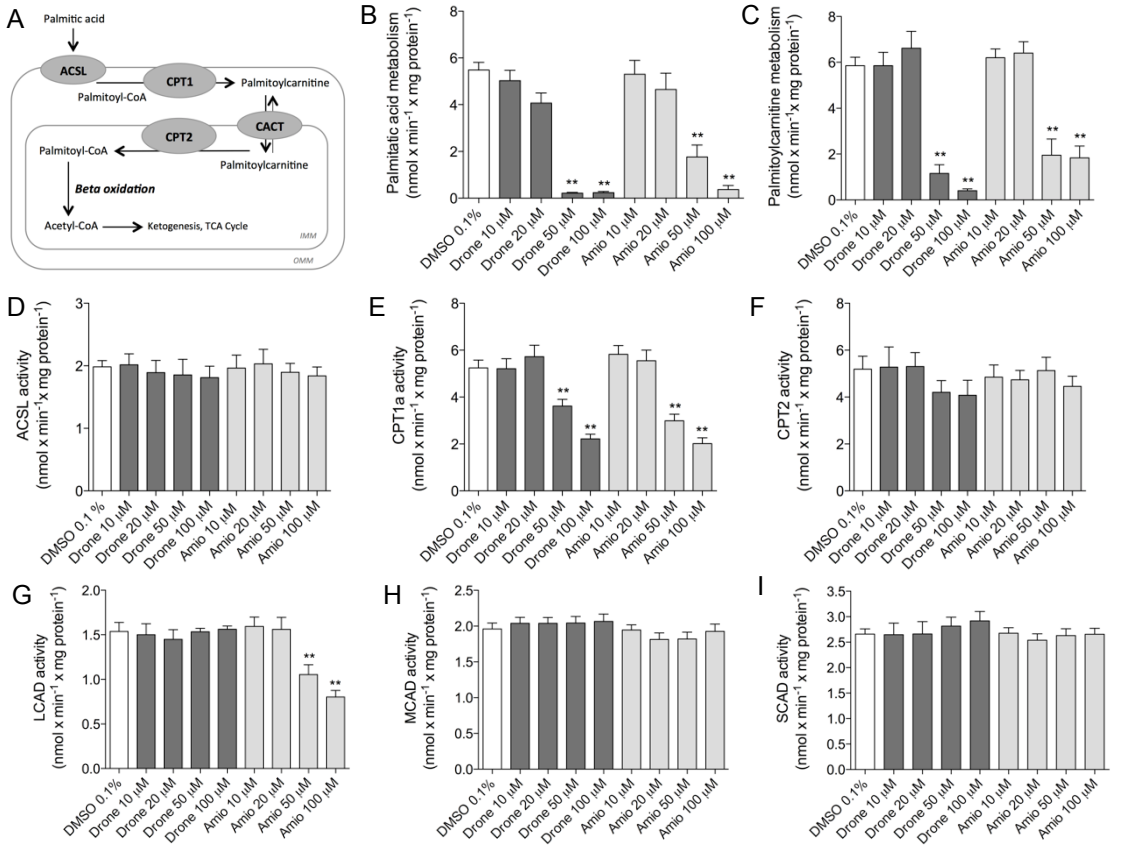

Figure 5. *Acute inhibition of fatty acid transport and metabolism.* Mouse liver mitochondria were acutely exposed to different concentrations of dronedarone and amiodarone. **A.** Schematic representation of mitochondrial fatty acid translocation and metabolism. **B, C.** Acute inhibition of 1-^{14}C-palmitic acid (B) or 1-^{14}C-palmitoylcarinitine (C) metabolism **D.** Activity of the long-chain acyl-CoA synthethase (ACSL). **E.** Activity of carnitine palmitoyltransferase 1a (CPT1a). **F.** Activity of carnitine palmitoyltransferase 2 (CPT2). **G, H, I.** Activities of long-chain, medium-chain, and short-chain acyl-CoA dehydrogenases (LCAD, MCAD, and SCAD). Values represent activities expressed in nmol x min^{-1} x mg protein^{-1} of at least three independent experiments. Statistical differences were calculated with a one-way ANOVA followed by a Dunnett's post test.

Discussion

Our study shows that a daily exposure to 200mg/kg dronedarone for 14 days was well tolerated by wild-type and $jvs^{+/-}$ mice and not associated with hepatic injury. In contrast, administration of 400mg/kg dronedarone daily was associated with a decrease in food consumption and body weight, impaired palmitate metabolism and hepatotoxic effects such as increased plasma transaminases and bilirubin as well as hepatocyte apoptosis in wild-type and $jvs^{+/-}$ mice.

We found that a daily exposure to 400mg/kg dronedarone inhibited hepatic β-oxidation of fatty acids in wild-type and $jvs^{+/-}$ mice both *in vivo* (impaired $^{14}CO_2$ exhalation of i.p. administered ^{14}C-palmitate) and *ex vivo* in liver mitochondria from mice treated with dronedarone. Our *ex vivo* results indicate that this reflects a direct inhibition of the mitochondrial β-oxidation pathway and not an indirect inhibition via an impaired activity of the respiratory chain. These results are in agreement with those reported by Serviddio et al., who also did not observe an inhibition of the respiratory chain in rats treated with dronedarone [9]. The findings are in contrast with our *in vitro* study showing that dronedarone impairs the activity of enzyme complex I and II of the respiratory chain starting at 20µM [8]. Since 98% of dronedarone is bound to albumin, it may be possible that differences in protein-binding between the *in vivo* and *in vitro* situation explain the lack of toxicity on the respiratory chain in the current study.

The reduced activity of mitochondrial β-oxidation in the presence of dronedarone can be explained by inhibition of CPT1a, which represents the rate-limiting enzyme in fatty acid oxidation [23] and controls the access of long-chain fatty acids to the mitochondrial matrix. Amiodarone, the structural analogue of dronedarone, is known to inhibit both CPT1a [21], as well as the long-chain acyl-CoA dehydrogenase (LCAD) [7], the first enzyme of the β-oxidation cycle in the mitochondrial matrix. In acute drug exposure experiments on isolated liver mitochondria, we confirmed the inhibition of CPT1a and LCAD by amiodarone and we demonstrate the inhibition of CPT1a by dronedarone. Furthermore, we found that the inhibition of fatty acid metabolism by dronedarone is also detectable with palmitoylcarnitine as a substrate, suggesting that dronedarone inhibits an additional target downstream to CPT1a, which is not located at the level of acyl-CoA dehydrogenases (LCAD, MCAD or SCAD) and needs further investigation. Since the protein content of CPT1a was not affected by treatment with dronedarone, our data support a direct toxic effect of dronedarone on the function of CPT1a. This assumption is supported by the acute toxicity of dronedarone of mitochondrial β-oxidation shown in the current and our previous investigation [8].

The inhibition of mitochondrial β-oxidation has several metabolic consequences for hepatocytes. First, it deprives hepatocytes of a major energy source, particularly during episodes of fasting. When hepatic mitochondrial fatty acid metabolism is severely inhibited, the impairment of β-oxidation causes hepatic accumulation of free fatty acids, which may be esterified into triglycerides and cause liver steatosis. Furthermore, the increasing pool of cellular free fatty acids may be associated with cytotoxic effects such as apoptosis and/or necrosis of hepatocytes [12, 24]. Amiodarone is a known inducer of steatosis in predisposed patients [25, 26] and also in mice [5]. In the current study, we did not observe a significant accumulation of lipids in the liver of wild-type or $jvs^{+/-}$ mice treated with 400mg/kg dronedarone. This observation may be a consequence of the decreased food intake and associated weight loss of the mice treated with 400mg/kg dronedarone per day, since it is known that weight loss can reverse hepatic steatosis [27].

Idiosyncratic drug-induced liver injury is rare and affected patients must have susceptibility factors [10]. Our previous study on $jvs^{+/-}$ mice developing liver injury when treated with a subtoxic dose of valproic acid revealed that reduced carnitine body stores represent a risk factor for hepatotoxicity [11]. $Jvs^{+/-}$ mice, but not wild-type mice, showed increased transaminases, impaired hepatic mitochondrial β-oxidation, and hepatocellular damage. In the current study, dronedarone induced numerically more pronounced elevations in plasma ALT and bilirubin and a stronger inhibition of *in vivo* metabolism of palmitic acid in $jvs^{+/-}$ as compared to wild-type mice treated with 400mg/kg daily. In isolated liver mitochondria, the impairment of palmitate metabolism and CPT1a activity was however comparable in mitochondria from wild-type and $jvs^{+/-}$ mice, since these assays were performed using saturating concentrations of all necessary cofactors, including L-carnitine. A comparison of the current with the former study [11] reveals, however, that carnitine deficiency is a more pronounced susceptibility factor for liver injury associated with valproate than with dronedarone. This may be due to differences in metabolic pathways and toxicological mechanisms of these drugs. While dronedarone is mainly metabolized by CYP3A4 through debutylation [28, 29], valproic acid is metabolized mainly by conjugation, including also conjugation with carnitine [30, 31]. Furthermore, oxidative metabolism of valproic acid is associated with toxic acidic metabolites (e.g. Δ2,4-diene valproic acid and other reactive metabolites, which can form carnitine esters and be excreted [32, 33]. Reduced hepatic carnitine stores may therefore be a more specific susceptibility factor for valproate-associated liver injury than for dronedarone, whose metabolism does not involve the production of carnitine conjugates. Based on the results of the current study, mice with impaired activity of CPT1a or enzymes involved in β-oxidation may be

a more suitable animal model than jvs$^{+/-}$ mice to investigate susceptibility factors for dronedarone-associated liver injury.

In conclusion, our results demonstrate that dronedarone acts as an inhibitor of mitochondrial fatty acid β-oxidation both *in vivo and in vitro*. Jvs$^{+/-}$ mice appear to be more sensitive to the hepatotoxic effects of dronedarone than wild-type mice. Inhibition of hepatic mitochondrial fatty acid β-oxidation may be an important mechanism of dronedarone-associated hepatotoxicity in humans and underlying defects in hepatic β-oxidation may represent susceptibility factors for this adverse drug reaction.

Financial support

This study was supported by a grant from the Swiss National Science Foundation to SK (SNF 31001A-132992).

References

1. Mason, J.W., *Amiodarone.* N Engl J Med, 1987. **316**(8): p. 455-66.
2. *In brief: FDA warning on dronedarone (Multaq).* Med Lett Drugs Ther, 2011. **53**(1359): p. 17.
3. Joghetaei, N., et al., *Acute liver failure associated with dronedarone.* Circ Arrhythm Electrophysiol, 2011. **4**(4): p. 592-3.
4. Lewis, J.H., et al., *Amiodarone hepatotoxicity: prevalence and clinicopathologic correlations among 104 patients.* Hepatology, 1989. **9**(5): p. 679-85.
5. Fromenty, B., et al., *Amiodarone inhibits the mitochondrial beta-oxidation of fatty acids and produces microvesicular steatosis of the liver in mice.* J Pharmacol Exp Ther, 1990. **255**(3): p. 1371-6.
6. Fromenty, B., et al., *Dual effect of amiodarone on mitochondrial respiration. Initial protonophoric uncoupling effect followed by inhibition of the respiratory chain at the levels of complex I and complex II.* J Pharmacol Exp Ther, 1990. **255**(3): p. 1377-84.
7. Kaufmann, P., et al., *Mechanisms of benzarone and benzbromarone-induced hepatic toxicity.* Hepatology, 2005. **41**(4): p. 925-35.

8. Felser, A., et al., *Mechanisms of hepatocellular toxicity associated with dronedarone--a comparison to amiodarone.* Toxicol Sci, 2013. **131**(2): p. 480-90.

9. Serviddio, G., et al., *Mitochondrial oxidative stress and respiratory chain dysfunction account for liver toxicity during amiodarone but not dronedarone administration.* Free Radic Biol Med, 2011. **51**(12): p. 2234-42.

10. Tujios, S. and R.J. Fontana, *Mechanisms of drug-induced liver injury: from bedside to bench.* Nat Rev Gastroenterol Hepatol, 2011. **8**(4): p. 202-11.

11. Knapp, A.C., et al., *Toxicity of valproic acid in mice with decreased plasma and tissue carnitine stores.* J Pharmacol Exp Ther, 2008. **324**(2): p. 568-75.

12. Fromenty, B. and D. Pessayre, *Inhibition of mitochondrial beta-oxidation as a mechanism of hepatotoxicity.* Pharmacol Ther, 1995. **67**(1): p. 101-54.

13. Lu, K., et al., *A missense mutation of mouse OCTN2, a sodium-dependent carnitine cotransporter, in the juvenile visceral steatosis mouse.* Biochem Biophys Res Commun, 1998. **252**(3): p. 590-4.

14. Kaido, M., et al., *Mitochondrial abnormalities in a murine model of primary carnitine deficiency. Systemic pathology and trial of replacement therapy.* Eur Neurol, 1997. **38**(4): p. 302-9.

15. Horiuchi, M., et al., *Cardiac hypertrophy in juvenile visceral steatosis (jvs) mice with systemic carnitine deficiency.* FEBS Lett, 1993. **326**(1-3): p. 267-71.

16. Knapp, A.C., et al., *Effect of carnitine deprivation on carnitine homeostasis and energy metabolism in mice with systemic carnitine deficiency.* Ann Nutr Metab, 2008. **52**(2): p. 136-44.

17. Reagan-Shaw, S., M. Nihal, and N. Ahmad, *Dose translation from animal to human studies revisited.* FASEB J, 2008. **22**(3): p. 659-61.

18. Morand, R., et al., *Quantification of plasma carnitine and acylcarnitines by high-performance liquid chromatography-tandem mass spectrometry using online solid-phase extraction.* Anal Bioanal Chem, 2013.

19. Hoppel, C., J.P. DiMarco, and B. Tandler, *Riboflavin and rat hepatic cell structure and function. Mitochondrial oxidative metabolism in deficiency states.* J Biol Chem, 1979. **254**(10): p. 4164-70.

20. Rottenberg, H., *Membrane potential and surface potential in mitochondria: uptake and binding of lipophilic cations.* J Membr Biol, 1984. **81**(2): p. 127-38.

21. Kennedy, J.A., S.A. Unger, and J.D. Horowitz, *Inhibition of carnitine palmitoyltransferase-1 in rat heart and liver by perhexiline and amiodarone.* Biochem Pharmacol, 1996. **52**(2): p. 273-80.

22. Reinartz, A., et al., *Lipid-induced up-regulation of human acyl-CoA synthetase 5 promotes hepatocellular apoptosis.* Biochim Biophys Acta, 2010. **1801**(9): p. 1025-35.

23. Kerner, J. and C. Hoppel, *Fatty acid import into mitochondria.* Biochim Biophys Acta, 2000. **1486**(1): p. 1-17.

24. Pessayre, D., et al., *Central role of mitochondria in drug-induced liver injury.* Drug Metab Rev, 2012. **44**(1): p. 34-87.

25. Jones, D.B., et al., *Reye's syndrome-like illness in a patient receiving amiodarone.* Am J Gastroenterol, 1988. **83**(9): p. 967-9.

26. Lewis, J.H., et al., *Histopathologic analysis of suspected amiodarone hepatotoxicity.* Hum Pathol, 1990. **21**(1): p. 59-67.

27. Petersen, K.F., et al., *Reversal of nonalcoholic hepatic steatosis, hepatic insulin resistance, and hyperglycemia by moderate weight reduction in patients with type 2 diabetes.* Diabetes, 2005. **54**(3): p. 603-8.

28. Patel, C., G.X. Yan, and P.R. Kowey, *Dronedarone.* Circulation, 2009. **120**(7): p. 636-44.

29. Ruan, H., et al., *Neuroprotective effects of (+/-)-catechin against 1-methyl-4-phenyl-1,2,3,6-tetrahydropyridine (MPTP)-induced dopaminergic neurotoxicity in mice.* Neurosci Lett, 2009. **450**(2): p. 152-7.

30. Boelsterli, U.A., *Animal models of human disease in drug safety assessment.* J Toxicol Sci, 2003. **28**(3): p. 109-21.

31. Spaniol, M., et al., *Development and characterization of an animal model of carnitine deficiency.* Eur J Biochem, 2001. **268**(6): p. 1876-87.

32. Rettenmeier, A.W., et al., *Studies on the biotransformation in the perfused rat liver of 2-n-propyl-4-pentenoic acid, a metabolite of the antiepileptic drug valproic acid. Evidence for the formation of chemically reactive intermediates.* Drug Metab Dispos, 1985. **13**(1): p. 81-96.

33. Silva, M.F., et al., *Differential effect of valproate and its Delta2- and Delta4-unsaturated metabolites, on the beta-oxidation rate of long-chain and medium-chain fatty acids.* Chem Biol Interact, 2001. **137**(3): p. 203-12.

Supplemental Figures

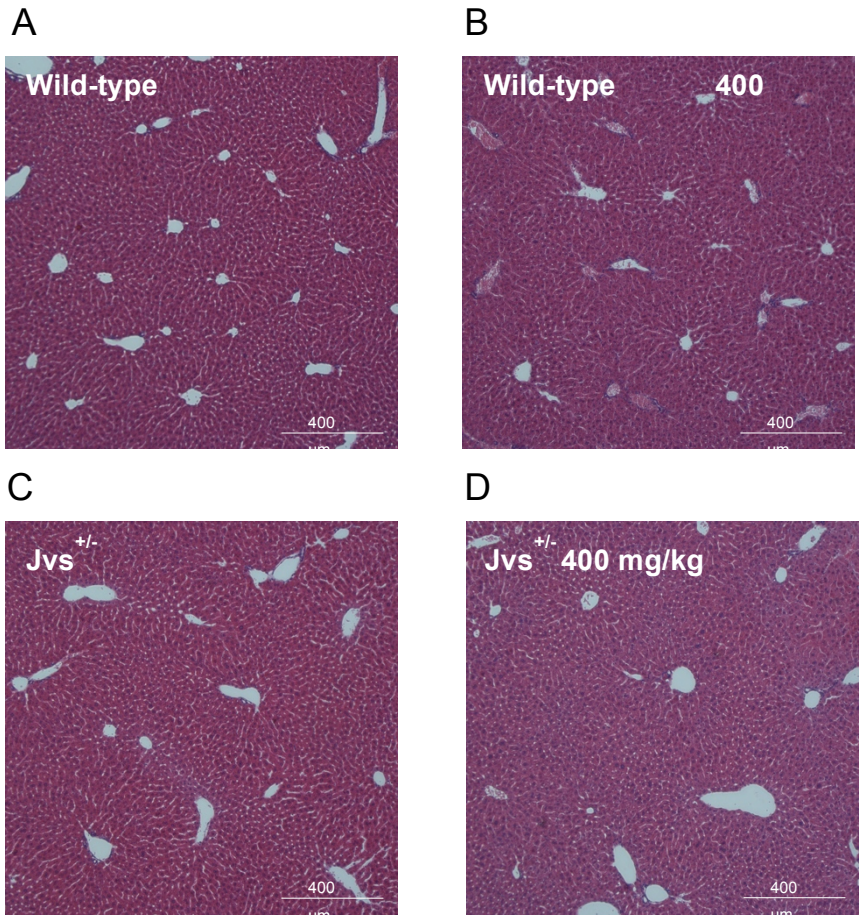

Suppl. Figure 1. *Liver sections stained for haematoxylin-eosin.* **A-D**. Liver sections stained for haematoxylin-eosin of wild-type animals treated with vehicle (A) or dronedarone 400mg/kg (B) and jvs$^{+/-}$ animals treated with vehicle (C) or dronedarone 400mg/kg (D). No gross pathological changes were detected in these sections.

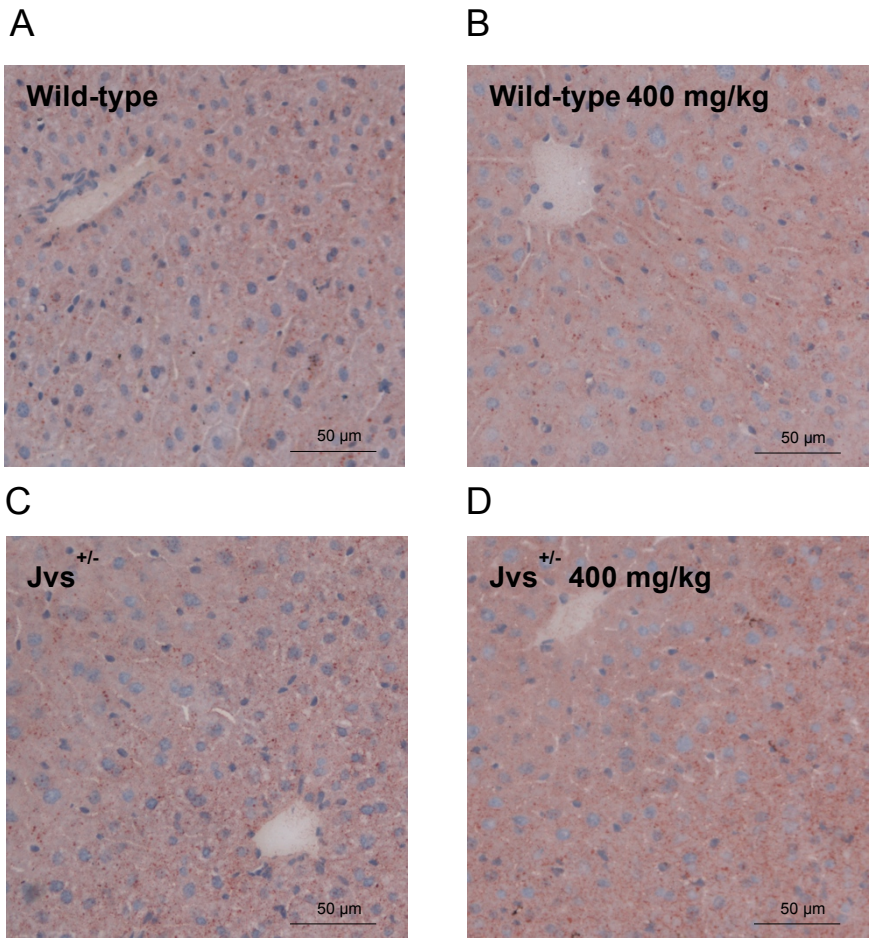

Suppl. Figure 2. *Liver sections stained for cellular lipids with Oil red O.* **A-D**. Wild-type animals treated with vehicle (A) or dronedarone 400mg/kg (B) and jvs$^{+/-}$ animals treated with vehicle (C) or dronedarone 400mg/kg (D). No significant fat accumulation was detected in these sections.

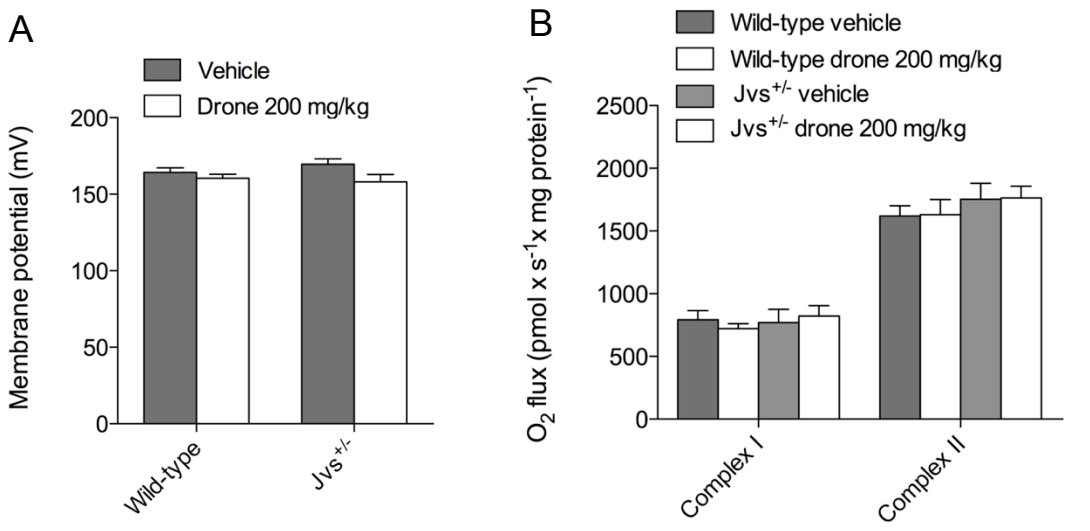

Suppl. Figure 3. *Characterization of isolated mouse liver mitochondria.* **A**. Mitochondrial membrane potential in mitochondria from animals treated with 200mg/kg. **B**. Respiratory capacity through complexes I and II in mitochondria from animals treated with 200mg/kg. Statistical differences were calculated with a two-way ANOVA followed by a Bonferroni post test.

Paper three

Hepatocellular toxicity of benzbromarone: effects on the mitochondrial function and structure

[1,2‡]Andrea Felser, [1,2,3‡]Peter W. Lindinger, [1,2]Dominik Schnell, [3,4]Denise V. Kratschmar, [3,4]Alex Odermatt, [5]Suzette Mies, [5]Paul Jenö, [1,2,3]Stephan Krähenbühl

[‡]contributed equally to the work

[1]Clinical Pharmacology & Toxicology, University Hospital Basel and [2]Department of Biomedicine, University of Basel, Switzerland

[3]Swiss Center of Applied Human Toxicology (SCAHT)

[4]Molecular and Systems Toxicology, Department of Pharmaceutical Sciences, University of Basel, Switzerland

[5]Biozentrum, University of Basel, Switzerland

Abstract

The aim of the study was to improve our understanding in the molecular mechanisms of benzbromarone associated liver toxicity. Benzbromarone is an uricosuric structurally related to amiodarone and is a known mitochondrial toxicant. HepG2 cells, a well characterized human hepatoma cell line lacking cytochrome P450 enzymes, were used for the experiments.

Cytotoxicity occurred at 100µM benzbromarone following incubation for 24 or 48h, whereas intracellular ATP started to decrease at 25 to 50µM, suggesting mitochondrial dysfunction. Benzbromarone was associated with a significant decrease in the mitochondrial membrane potential starting at 50µM. Furthermore, benzbromarone induced mitochondrial uncoupling, decreased mitochondrial ATP turnover and decreased maximal respiration of HepG2 cells starting at 50µM following incubation for 24h. This was accompanied by an increased lactate concentration in the cell culture supernatant, reflecting increased glycolysis. Investigation of the electron transport chain revealed a decreased activity of all relevant enzyme complexes. Treatment with benzbromarone was associated with increased cellular ROS production, which could be located to mitochondria using specific staining. Furthermore, benzbromarone inhibited palmitic acid metabolism due to a direct inhibition of the long-chain acyl CoA synthetase. Benzbromarone disrupted the mitochondrial network, leading to mitochondrial fragmentation and a decreased mitochondrial volume per cell. Cell death occurred by both apoptosis and necrosis.

The study clearly demonstrates that benzbromarone not only affects the function of mitochondria in HepG2 cells, but is also associated with profound changes in mitochondrial structure which may be associated with apoptosis.

Introduction

The liver represents an important target for drug-mediated toxicity. Accordingly, many drugs are associated with liver injury, which can be hepatocellular, cholestatic or mixed [1, 2]. Importantly, drug toxicity is one of the major causes for fulminant liver failure necessitating liver transplantation or leading to death [3, 4] and also for withdrawal of drugs from the market [3, 5]. The reason why the liver is a special target for drug toxicity is at least twofold. First, the liver is exposed to high drug concentrations after oral ingestion due to its location between the gut and the systemic circulation. Second, the liver is the major location of drug metabolism. Hepatic metabolism of drugs and other chemical compounds can be associated with the production of metabolites, which may be toxic to hepatocytes, and/or other cell types located in the liver [6, 7]. For most hepatotoxic drugs, the risk for drug-induced liver injury is small, non-predictable and does not occur in a clearly dose-dependent manner [2, 8].

Benzbromarone is an uricosuric used for the prophylaxis of acute gout attacks. For many years, benzbromarone was considered to be both effective and well-tolerated. However, after several reports of severe hepatotoxicity [9-11], the drug had to be withdrawn from the market in several countries, e.g. the USA, France and Switzerland. Histological findings in affected patients included microvesicular steatosis of liver [9], a finding compatible with inhibition of mitochondrial β-oxidation [12-14]. In a previous *in vitro* study using isolated rat liver mitochondria and rat hepatocytes, we have compared the hepatotoxicity associated with benzbromarone with that of amiodarone [15]. Relevant findings in this study were that benzbromarone uncouples hepatic mitochondria and inhibits the respiratory chain and β-oxidation.

Mitochondrial function can be disturbed by chemical compounds via multiple ways. Important mechanisms include inhibition and/or uncoupling of oxidative phosphorylation and inhibition of specific metabolic pathways such as the urea cycle, fatty acid oxidation and/or ketone body production and the citric acid cycle [16]. While it was clear from our previous study that benzbromarone impairs certain mitochondrial functions such as the respiratory chain and β-oxidation [15], it is currently unclear whether the findings in rodent mitochondria and hepatocytes are also present in human liver cell lines, by which mechanisms benzbromarone disturbs mitochondria and how mitochondria react after exposure to benzbromarone. We therefore studied the effect of benzbromarone on mitochondrial functions and mitochondrial structure in HepG2 cells after 24h or 48h drug exposure.

Material and Methods

Cell line and culture

The human hepatoma cell line HepG2 was purchased from ATCC (Manassas, USA). Benzbromarone was purchased from Sigma-Aldrich (Buchs, Switzerland). Cells were kept at 37°C in a humidified 5% CO_2 cell culture incubator and passaged according to the instructions provided by ATCC using trypsin. The cells were maintained in Dulbecco's Modified Eagle Medium (DMEM, containing 1.0g/l glucose, 4mM L-glutamine, and 1mM pyruvate, 10mM HEPES buffer) from Invitrogen (Basel, Switzerland), which was supplemented with 10% (v/v) heat-inactivated fetal calf serum. Protein concentrations of cells in culture plates were determined with the sulforhodamine B assay as described by Skehan et al. [17].

Isolation of mouse liver mitochondria

Male C57BL/6 mice were kept in the animal facility of the University Hospital Basel (Basel, Switzerland) with food and water *ad libitum*. Animal procedures were performed in accordance with the institutional guidelines for the care and use of laboratory animals. Liver mitochondria were isolated by differential centrifugation according to the method described by Hoppel et al. [18] and the mitochondrial protein content was determined using the bicinchoninic acid protein assay reagent from Thermo Scientific (Wohlen, Switzerland).

Cytotoxicity and intracellular ATP

Cytotoxicity was assessed using the Toxilight® assay from Lonza (Basel, Switzerland) and carried out according the manufacturer's manual. In brief, cells grown in 96-well plates were exposed to a range of benzbromarone concentrations for either 24 or 48h. All incubations contained the same amount of DMSO (0.1%, v:v), which has been shown not to be toxic to HepG2 cells [19]. The plate was centrifuged and 20µl of supernatant per well was transferred to a new 96 well plate. After addition of 100µl of Toxilight® solution and incubation in the dark at 37°C for 5min, luminescence was recorded using a Tecan M200 Pro Infinity plate reader (Tecan Traiding AG, Männedorf, Switzerland).

The intracellular ATP content was determined using the CellTiterGlo® Luminescent cell viability assay from Lonza (Basel, Switzerland) and carried out according to the manufacturer's manual. In brief, 100µl assay buffer was added to each 96-well

containing 100µl culture medium. After cell lysis at 37°C for 30min, the released ATP was detected by luminescence measurement.

Assessment of apoptosis and mitochondrial membrane potential

Apoptosis and necrosis of HepG2 cells was assessed by flow cytometry using annexin V/propidium iodide (PI) staining as described previously [20].

The mitochondrial membrane potential (Δψ) was determined using tetramethyl rhodamine methyl ester (TMRM, Invitrogen, Basel, Switzerland), a lipophilic cationic fluorescent probe which accumulates within mitochondria depending on their Δψ. Briefly, HepG2 cells were seeded in 24-well plates (200'000 cell/well) and treated with specified concentrations of benzbromarone for 24h. Cells were detached with trypsin-EDTA (0.05%), washed with Dulbecco's phosphate buffered saline (DPBS) and suspended in Hanks modified salt solution (HBSS). Cells were incubated with 10nM TMRM and Live/Dead® Near-IR dead cell stain kit (Invitrogen, Basel, Switzerland) for 30min at 37°C in the dark. Afterwards, cells were analyzed by flow cytometry using a CyAn ADP cytometer (Beckman coulter, Marseille, France). Dead cells were excluded in all measurements by gating the live-cell population and data were analyzed using FlowJo 9.3.2 software (Tree Star, Ashland, OR, USA). Incubations exposed to the uncoupler carbonyl cyanide-4-(trifluoromethoxy)phenylhydrazone (FCCP, 10µM, 5min) served as a positive control.

Oxygen consumption and activity of specific enzyme complexes of the respiratory chain

Cellular respiration of intact cells was measured using a Seahorse XF24 analyzer (Seahorse Biosciences, North Billerica, MA, USA). Two days prior the assessment of oxygen consumption, HepG2 cells were cultured in V7 Seahorse XF 24-well cell culture microplates by seeding 40'000 cells in 250µl Dulbecco's Modified Eagle's Medium (DMEM) per well.

Before assessing the respiratory capacities, the medium was replaced with 750µl unbuffered medium containing 4mM L-glutamate and 1mM pyruvate as described by the manufacturer of Seahorse. After equilibration of the cells to the unbuffered medium (30min at 37°C in a CO_2-free incubator), the plates were transferred to the XF24 analyzer. First, basal oxygen consumption rates (OCR) were measured, and then, sequentially 1µM oligomycin, 1µM FCCP and 1µM rotenone were injected for metabolic

characterization of the cells. The concentrations used in the final experiments had carefully been assessed in preliminary experiments.

Activity of complexes I, II, III and IV were analyzed as prescribed previously using an Oxygraph-2k high resolution respirometer (Oroboros Instruments, Innsbruck, Austria) [20]. Lactate concentrations in the cell culture supernatant were analyzed with an enzymatic assay after protein precipitation with PCA 5% [21].

Production of reactive oxygen species

Cellular reactive oxygen species (ROS) production was determined using 25µM dichlorofluorescein (DCF) as a probe as described previously [15].

Generation of mitochondrial ROS was assessed using MitoSox Red (Invitrogen, Basel, Switzerland). HepG2 cells were seeded into black costar 96-well plates and treated the following day with benzbromarone, DMSO (negative control) or doxorubicin (positive control). Upon incubation for 24h, culture medium was removed and 5µM MitoSox dissolved in HBSS was added and the plate was incubated for 20min. Afterwards, cells were washed with HBSS and fluorescence was recorded (excitation 510nm, emission 580nm) using a Tecan M200 Infinite Pro plate reader (Tecan Traiding AG, Männedorf, Switzerland).

For confocal microscopy, 80'000 HepG2 cells were seeded into Lab-Tek® chamber slides (Thermo Scientific, Wohlen, Switzerland) containing 2ml cell culture medium. The following day, the cells were treated with various concentrations of benzbromarone, DMSO (negative control) or doxorubicin (positive control). After 24h, the cells were washed with HBSS and incubated with HBSS containing 5µM MitoSox for 20min. Afterwards, the cells were washed twice with HBSS buffer containing 1% BSA, and confocal imaging was performed without cell fixation. The ROS-dependent emitted light was recorded using Zeiss Software (Zen) and confocal microscopy (Zeiss, LSM 710, Feldbach, Switzerland).

Oxidation of 1-^{14}C palmitic acid or 1-^{14}C palmitoylcarnitine

Metabolism of 1-^{14}C palmitic acid was assessed in isolated mouse liver mitochondria or permeabilized HepG2 cells via the formation of ^{14}C-acid-soluble β-oxidation products as described previously [20]. Metabolism of 1-^{14}C palmitoylcarnitine was assessed using a similar protocol with some modifications. Isolated liver mitochondria or HepG2 cells were preincubated for 10min in 225µl assay buffer (70mM sucrose, 43mM KCl,

3.6mM $MgCl_2$, 7.2mM KH_2PO_4, 36mM Tris, 10mg/ml BSA, 2mM ATP, 150µM coenzyme A, 5mM acetoacetate, pH 7.4) at 37°C in a thermomixer at 600rpm (Eppendorf, Schönenbuch, Switzerland). The assay buffer of HepG2 cells contained digitonin (10µg/million cells) in order to permeabilize the plasma membrane. The reaction was started by the addition of 25µl radioactive substrate mix containing L-palmitoylcarnitine (200µM final assay concentration), and 25pCi [1-^{14}C] palmitoylcarnitine. The reactions were stopped after 15min by adding 250µl 6% perchloric acid. After centrifugation (10'000rpm, 2min) the radioactivity was measured in the supernatant by liquid scintillation counting.

Activity of ACSL and CPT1α

The activity of the long-chain acyl-CoA synthetase (ACSL) was investigated by assessing the rate of ^{14}C-palmitoyl-CoA formation as described by Reinartz et al. [22] with some modifications. HepG2 cells or isolated liver mitochondria were incubated in 225µl assay buffer (70mM sucrose, 43mM KCl, 3.6mM $MgCl_2$, 7.2mM KH_2PO_4, 36mM Tris, 1mM ATP, 200µM coenzyme A, 5mM acetoacetate, pH 7.4) at 37°C for 10min in a thermomixer at 600rpm. The assay buffer of HepG2 cells contained digitonin (10µg/million cells). Then, the reaction was started by the addition of 25µl radioactive substrate mix containing 200µM Na-palmitate (final assay concentration), 25pCi [1-^{14}C] palmitic acid, and 170µM BSA (fatty acid free). The reaction was stopped after 4min by the addition of 1ml Dole's medium (isopropanol/n-heptane/H_2SO_4 0.5M, v/v/v 40:10:1), 0.4ml water and 0.6ml n-heptane. Next, each sample was transferred into an extraction vial and the upper n-heptane phase was renewed three times until the radioactivity was assessed in the water phase by liquid scintillation counting.

The activity of carnitine palmitoyltransferase (CPT) 1α was assessed as the formation of palmitoyl-^{14}C-carnitine from palmitoyl-CoA and ^{14}C-carnitine as described by Kennedy et al. [23] with some modifications. HepG2 cells or isolated liver mitochondria were incubated for 10min in 225µl assay buffer (80mM KCl, 50mM MOPS, 10mg BSA defatted, 5mM EGTA, 25mM *N*-ethylmaleimide and water, pH 7.4) at 37°C on a thermomixer at 600rpm. The assay buffer for HepG2 cells contained digitonin (10µg/million cells) in order to permeabilize the plasma membrane. The reaction was started by the addition of 25µl radioactive substrate mix containing 400µM L-carnitine (final concentration), 12.5pCi ^{14}C-L-carnitine and 200µM palmitoyl-CoA (final concentration). The reaction was terminated after 10min by adding 50µl of concentrated HCl. Next, the samples were transferred into an extraction vial, and 1.4ml n-butanol-saturated distilled water and 1ml water-saturated n-butanol was added. After

extraction, the upper (butanol) phase was transferred in a new extraction tube containing 2ml of butanol-saturated water. Finally, the upper butanol-phase containing the lipophilic palmitoyl-^{14}C-L-carnitine was removed and the radioactivity determined by liquid scintillation counting.

mRNA expression

Extraction of mRNA, synthesis of cDNA and real-time PCR were performed as described previously [24]. We used specific primers for SOD1 and SOD2 [20], for CPT1α (forward: 5'-GCCTCGTATGTGAGGCAAAA-3', reverse: 5'-TCATCAAGAAATGTCGCACG-3') and ACSL (forward: 5'-GGAGTGGGCTGCAGTGAC-3', reverse: 5'-GGGCTTGCATTGTCCTGT-3'), and for mitochondrial fission and fusion markers [25]. Quantification was performed using the comparative-threshold cycle method. GAPDH served as endogenous reference (forward: 5'- CATGGCCTTCCGTGTTCCTA -3', reverse: 5'-CCTGCTTCACCACCTTCTTGA-3').

Mitochondrial DNA content

DNA was extracted and purified using the Qiagen DNeasy blood and tissue kit (Qiagen, Hombrechtikon, Switzerland) following the manufacturer's instructions. DNA was quantified spectrophotometrically at 260nm with the NanoDrop 2000 (Thermo Scientific, Wohlen, Switzerland). The mitochondrial and nuclear DNA content was analysed by quantitative real-time PCR (qRT-PCR) as described recently, with some modifications [26]. DNA (10ng/µl) was analyzed in triplicate using SYBR Green dye (Roche Diagnostics, Rotkreuz, Basel) by determining the ratio between one mitochondrial gene (human NADH-ubiquinone oxidoreductase chain 1, forward: 5'-ATGGCCAACCTCCTACTCCT -3', reverse: 5'- CTACAACGTTGGGGCCTTT-3') and two nuclear reference genes (human polymerase γ accessory subunit, forward: 5'-GAGCTGTTGACGGAAAGGAG-3', reverse: 5'-CAGAAGAGAATCCCGGCTAAG-3', and beta-actin, forward: 5'-ACTCTTCCAGCCTTCCTTCC-3', reverse: 5'-GGCAGGACTTAGCTTCCACA-3') using the classical comparative-threshold cycle method.

Western blotting

Proteins were resolved by SDS-PAGE using commercially available 4-12% NuPAGE Bis-Tris gels (Invitrogen, Basel, Switzerland) which were run as described by the

producer. Western blotting was performed as described previously [7]. Specific monoclonal antibodies displaying one specific band at the appropriate molecular weight were used for CPT1α (Abcam, Cambridge, UK) and ACSL (Cell signalling technology, Danvers, USA). The five mitochondrial respiratory chain complexes were assessed using the MitoProfile® Total OXPHOS rodent antibody cocktail (MitoSciences, Eugene, USA). Appropriate secondary antibodies coupled to horseradish peroxidase were applied in order to visualize detected proteins. Densitometric analysis was performed using ImageJ software (Bethesda, USA).

Staining of mitochondrial network

HepG2 cells were seeded into Lab-Tek® chamber slides (Thermo Scientific, Wohlen, Switzerland). The following day, cells were treated with different concentrations of benzbromarone for 24h. Subsequently, cells were fixed using 4% paraformaldehyde/DPBS, followed by permeabilization using 0.2% Triton X-100. Afterwards, the slides were blocked using 10% BSA/DPBS for 1h. Subsequently, the cells were incubated with anti-TOMM22 (Sigma-Aldrich, Buchs, Switzerland) in 10% BSA/DPBS at 4°C for at least 15h. Afterwards, the samples were washed with 10% BSA/DPBS and treated with a secondary antibody (Alexa anti-mouse 488 in 10% BSA/DPBS) for 1h, followed by wash steps with DPBS and incubation with 4',6-diamidino-2-phenylindole (DAPI) dye for 5-10min. After a final wash step with DPBS, the chamber slides were used for confocal microscopy (Zeiss, LSM 710, Feldbach, Switzerland).

Transmission electron microscopy

HepG2 cells were cultured in 60cm^2 dishes. After reaching about 50% confluency, the cells were exposed to either 12.5µM or 50µM benzbromarone or 0.1% DMSO (v:v) for 24h. Subsequently, the cells were washed and fixed using a PBS solution with 3% paraformaldehyde and 0.5% glutaraldehyde for 1h. Afterwards, cells were collected by scraping, washed twice with PBS, treated with osmium tetroxide and dehydrated by ethanol. After an additional treatment with acetone, cells were embedded in epon and slices of 60 to 70nm (Ultracut microtome, Reichert-Jung, Germany) were obtained from these samples. Electron microscopy was performed using an FEI Morgagni 268D transmission electron microscope (Eindhoven, Netherlands).

Results

Cytotoxicity and mechanism of cell death

Benzbromarone caused release of adenylate kinase starting at 100µM and decreased intracellular ATP starting at 50µM after treatment for 24h in HepG2 cells (Fig. 1A and B). After treatment for 48h, cytotoxicity also started at 100µM, but the decrease in cellular ATP already at 25µM (Suppl. Fig. 1A and 1B).

The observation that the cellular ATP content was starting to decrease at lower concentrations than the appearance of cytotoxicity suggested mitochondrial toxicity, a finding compatible with our previous report [15]. To prove involvement of mitochondria also in HepG2 cells, we determined the mitochondrial membrane potential, which is a marker of mitochondrial integrity and function. Similar to the intracellular ATP content, the fraction of depolarized cells started to increase at a benzbromarone concentration of 50µM after drug exposure for 24h (Fig. 1C).

Impaired mitochondrial function can be associated with both apoptosis and/or necrosis [15]. As shown in Figure 1D, at the highest concentration investigated (100µM), treatment with benzbromarone was associated with an increase in annexin V positive cells, reflecting early apoptosis. This increase was also significant for annexin V and PI double stained populations, reflecting necrosis or later stages of apoptosis.

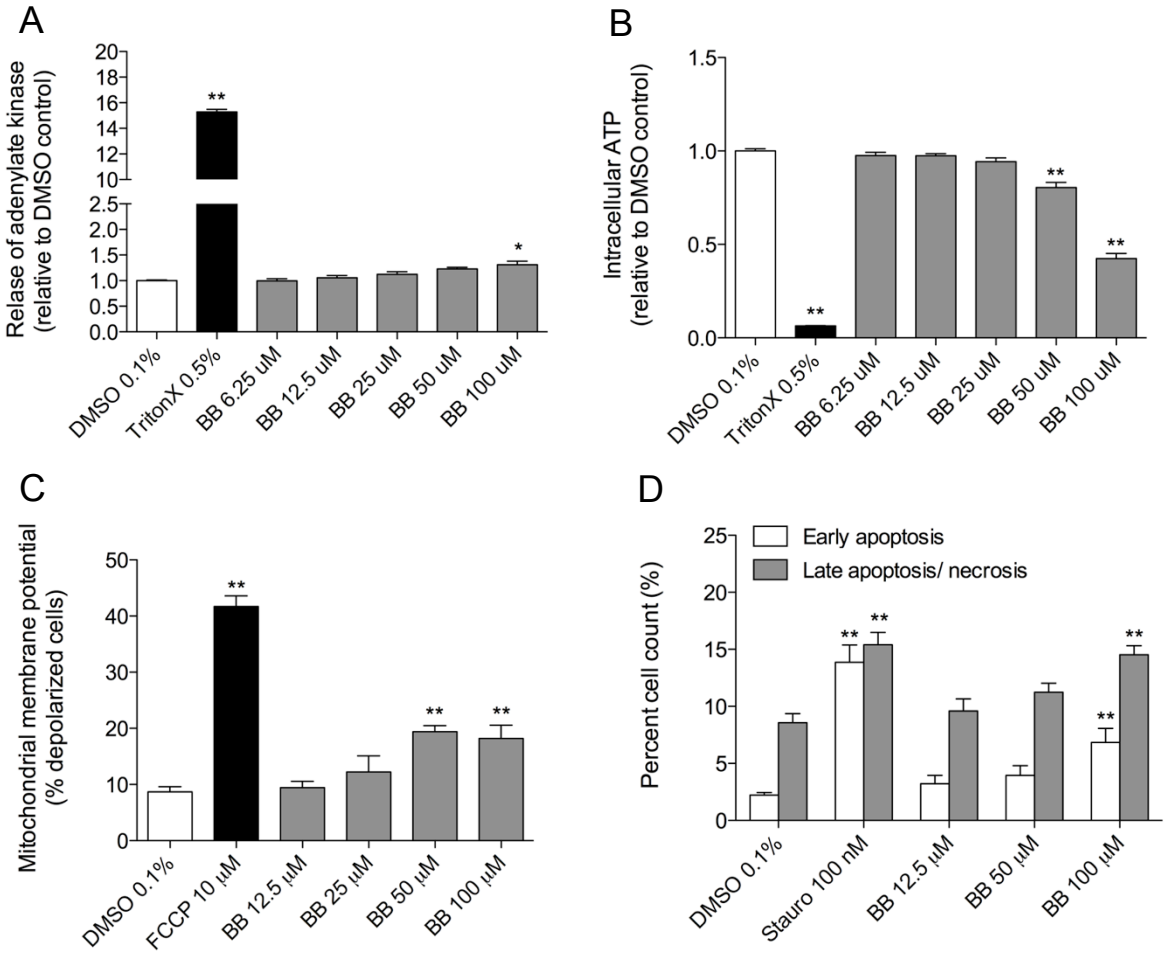

Figure 1. *Cytotoxicity and mechanism of cell death*. **A.** Cytotoxicity assessed by the release of adenylate kinase in HepG2 cells after 24h drug exposure. Data are expressed relative to control incubations containing 0.1% DMSO. **B.** Intracellular ATP content in HepG2 cells after 24h drug exposure. Data are expressed relative to control incubations containing 0.1% DMSO. **C.** Mitochondrial membrane potential assessed by means of TMRM fluorescent staining after 24h drug exposure. Samples were analyzed by flow cytometry and are presented as percent depolarized cells. Acute exposure to FCCP served as positive control. **D.** Annexin V binding and propidium iodide uptake in HepG2 cells after 24h drug exposure. Samples were analyzed using flow cytometry and presented as percent cell count. Early apoptotic populations are annexin V positive and late apoptotic or necrotic populations represent annexin V and PI double stained populations. Staurosporine was used as a positive control for apoptosis. Data represent the mean ± SEM of at least three independent experiments. *p<0.05 versus DMSO control. **p<0.01 versus DMSO control.

Effect on oxidative metabolism

The observed decrease in intracellular ATP and membrane potential can be caused by an impairment of the respiratory chain [15]. Incubation for 24h with benzbromarone had no effect on basal respiration of HepG2 cells up to 100µM benzbromarone (data not shown). However, the ATP turnover rate (see Fig. 2A for explanation) decreased by 40 to 50% starting at 50µM, whereas the leak respiration (indicating uncoupling) increased by the same extent at 50µM (Fig. 2B), explaining the observed decrease in the cellular ATP content. The maximal respiration (obtained by addition of the uncoupler FCCP) decreased by 60% starting at 100µM benzbromarone, demonstrating an impaired function of the electron transport chain.

In order to investigate the mechanism of decreased ATP turnover and maximal respiration, the activity of the complexes of the electron transport chain were analyzed using specific substrates for each complex. As shown in Figure 2C, after 24h exposure of HepG2 cells to 50µM benzbromarone, the respiratory capacity was decreased for all complexes with a more pronounced inhibition at the level of complexes I and II. In addition, after 24h benzbromarone treatment, the lactate concentration in the cell culture supernatant started to increase at 50µM, reflecting a compensatory increase of glycolysis (Fig. 2D).

In order to gain more information about the mechanism of the observed decrease in the activity of the enzyme complexes of the respiratory chain, Western blots of subunits of each enzyme complex were performed. As shown in suppl. Fig. 2, the protein content of selected subunits of enzyme complexes I to V of the respiratory chain revealed no change after benzbromarone treatment for up to 48h compared control incubations, compatible with a direct toxic effect of benzbromarone on the respiratory chain.

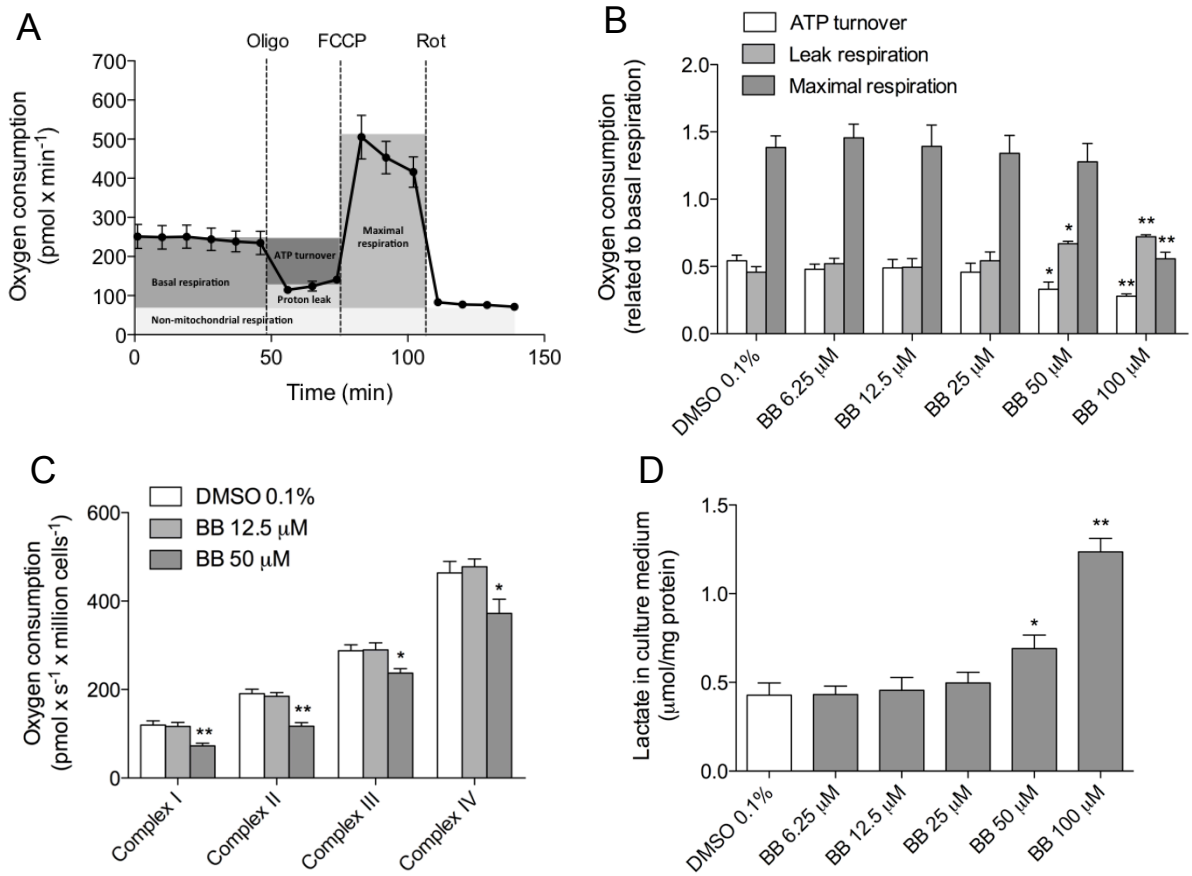

Figure 2. *Function of the respiratory chain and adaptive responses in HepG2 cells*. **A.** Schematic representation of ATP turnover, leak respiration, and maximal respiration. **B.** Oxygen consumption by HepG2 cells after 24h benzbromarone exposure measured by the Seahorse XF24 analyzer. Basal oxygen consumption rate by control incubations (0.1% DMSO) was 361 ± 14 pmol x min^{-1}. **C.** Respiratory capacity through complexes I, II, III, and IV after 24h benzbromarone treatment measured by the Oxygraph-2k high resolution respirometer. **D.** Lactate concentration in cell culture medium. Data represent the mean ± SEM of at least three independent experiments. *p<0.05 versus DMSO control. **p<0.01 versus DMSO control.

Effect on ROS production

Inhibition of the respiratory chain can be associated with increased ROS production [7, 15]. As shown in Figure 3A, treatment with benzbromarone was associated with an increased intracellular ROS accumulation in a concentration-dependent fashion, starting at 50µM and reaching statistical significance at 100µM.

To verify mitochondrial accumulation of ROS, a MitoSox red assay to detect superoxide formation was performed. As shown in Fig. 3B and 3C, mitochondrial ROS generation was evident starting at 50µM benzbromarone. In parallel, mRNA expression of the mitochondrial superoxide dismutase 2 (SOD2) increased starting at 50µM benzbromarone, whereas the cytoplasmic SOD1 showed a tendency to decrease (Fig. 3D). Increased expression of SOD2 as a consequence of mitochondrial ROS accumulation has been shown previously for dronedarone [20].

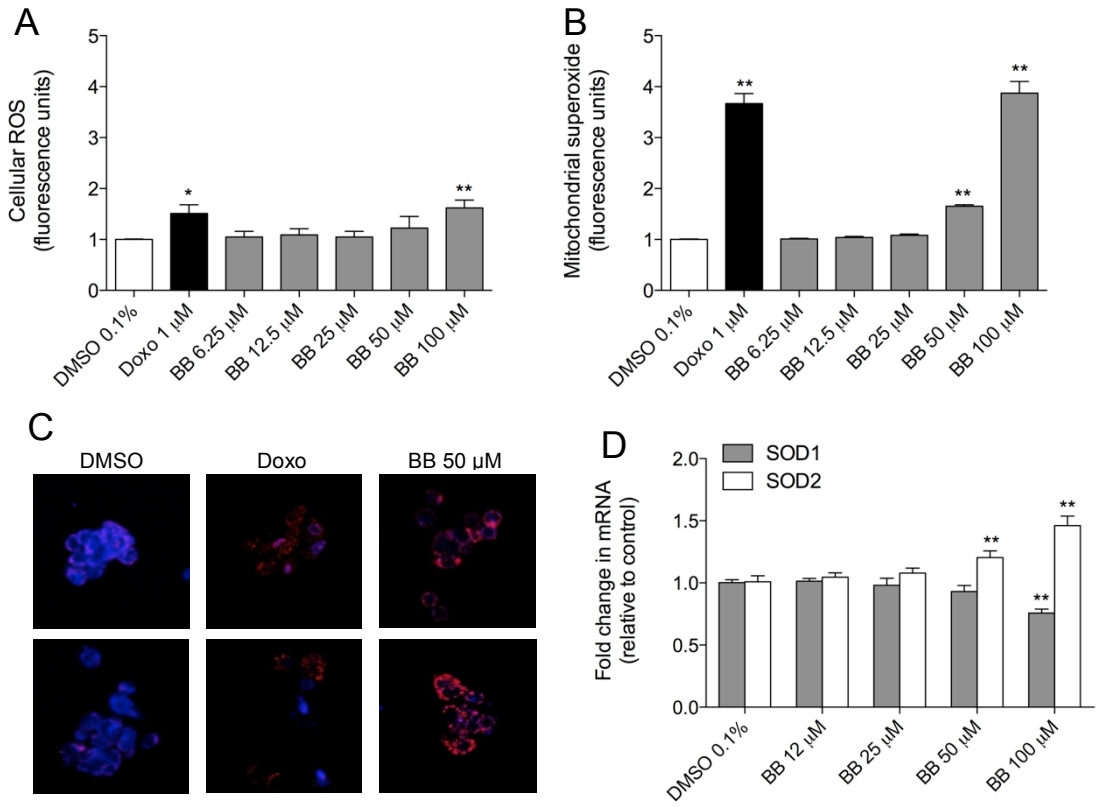

Figure 3. *ROS production and SOD expression by HepG2 cells*. **A.** Cellular accumulation of ROS in HepG2 cells after 24h drug treatment determined using dichlorofluorescein (DCF). **B.** Mitochondrial accumulation of superoxide in HepG2 cells after exposure to benzbromarone for 24h determined by staining with MitoSox red. **C.** Confocal microscopy of MitoSox red after 24h drug exposure. **D.** mRNA expression of SOD1 and SOD2 in HepG2 cells after exposure to benzbromarone for 24h. Data represent the mean ± SEM of at least three independent experiments. *p<0.05 versus DMSO control. **p<0.01 versus DMSO control.

Effect on mitochondrial β-oxidation

Previous studies in isolated rat liver mitochondria have shown that not only the mitochondrial respiratory chain, but also mitochondrial β-oxidation can be impaired by benzbromarone [15]. In order to localize the inhibition of fatty acid metabolism more precisely, we investigated the degradation of palmitic acid and palmitoylcarnitine by measuring the formation of acid soluble β-oxidation products. Long-chain fatty acids must first be transformed to acylcarnitines (e.g. palmitoylcarinitine) in order to be translocated into the mitochondrial matrix. In permeabilized HepG2 cells treated for 24h with different concentrations of benzbromarone, we found that 1-^{14}C-palmitic acid metabolism was inhibited starting at 50µM, whereas the metabolism of 1-^{14}C-palmitoylcarnitine remained unaffected up to 100µM benzbromarone (Fig. 4A). The findings in freshly isolated mouse liver mitochondria were qualitatively similar; benzbromarone started to inhibit 1-^{14}C palmitic acid metabolism already at 2µM, whereas the metabolism of 1-^{14}C-palmitoyl-carnitine remained unchanged (Fig. 4B).

These findings suggested that benzbromarone inhibits the conversion of palmitate to palmitoylcarnitine, but not the metabolism of palmitoylcarnitine. The conversion of palmitate to palmitoylcarnitine involves two enzymes, the long-chain acyl-CoA synthetase (ACSL) and carnitine palmitoyltransferase 1α (CPT1α). We directly assessed the activity of these two enzymes in permeabilized HepG2 cells and found that ACSL was inhibited whereas the activity of CPT1α was not impaired by benzbromarone (Fig. 4C,D).

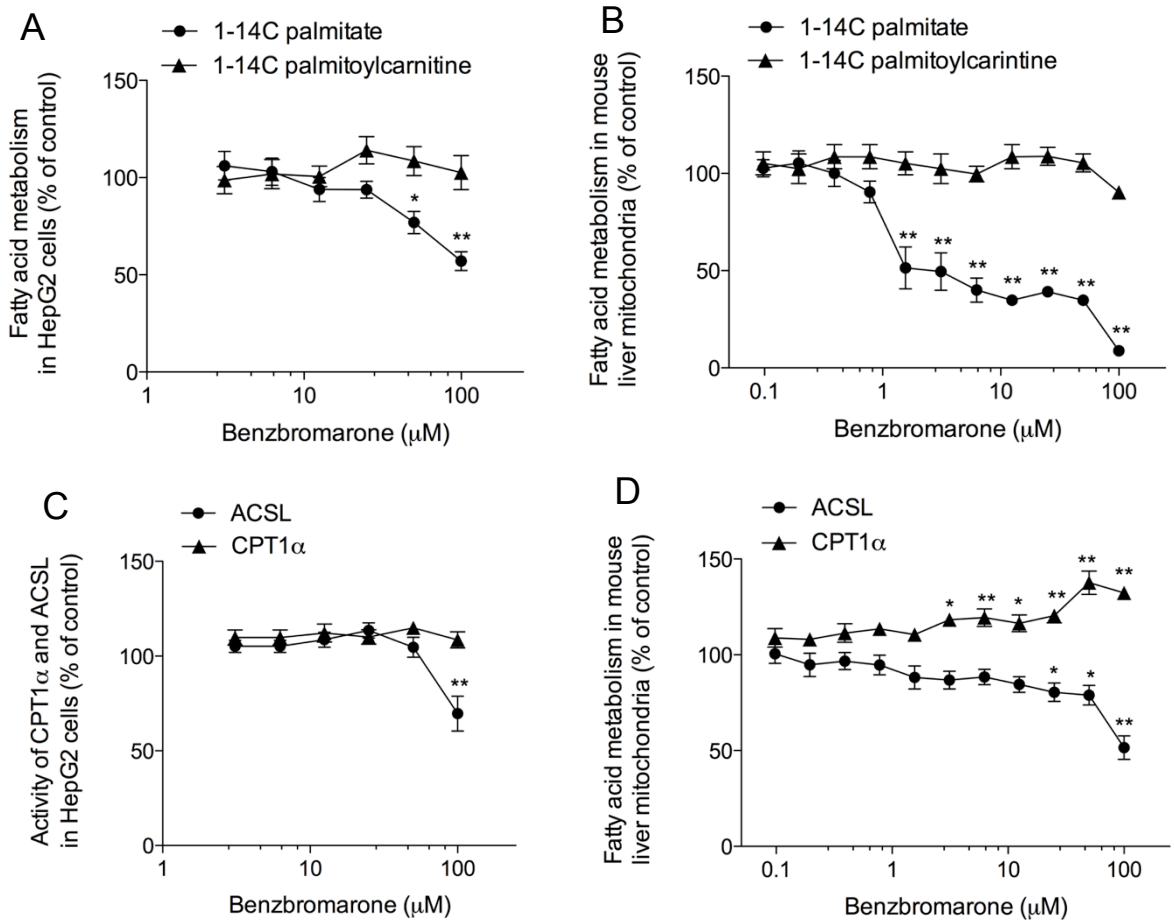

Figure 4. *Effect on fatty acid metabolism in HepG2 cells and freshly isolated mouse liver mitochondria*. **A.** HepG2 cells were exposed to benzbromarone for 24h and metabolism of palmitate or palmitoylcarnitine was determined in permeabilized cells. Basal β-oxidation activity of control incubations (0.1% DMSO) for palmitate or palmitoylcarnitine was 0.45 ± 0.03 or 0.49 ± 0.05 nmol x min^{-1} x mg $protein^{-1}$, respectively. **B.** Mouse liver mitochondria were exposed to benzbromarone and acute inhibition of palmitate and palmitoylcarnitine metabolism was determined. Basal β-oxidation activity of palmitate or palmitoylcarnitine was 4.93 ± 0.15 or 5.50 ± 0.20 nmol x min^{-1} x mg $protein^{-1}$, respectively. **C.** HepG2 cells were exposed to benzbromarone for 24h and activities of CPT1α and ACSL were determined in permeabilized HepG2 cells. Basal activities of ASCL and CPT1α were 0.15 ± 0.01 and 0.37 ± 0.02 nmol x min^{-1} x mg $protein^{-1}$, respectively. **D.** Mouse liver mitochondria were exposed to benzbromarone and acute inhibition of the activity of ACSL and CPT1α was determined. Basal activities of ASCL and CPT1α were 1.71 ± 0.09 and 4.21 ± 0.21 nmol x min^{-1} x mg $protein^{-1}$, respectively. Data represent the mean ± SEM of at least three independent experiments. *p<0.05 versus DMSO control. **p<0.01 versus DMSO control.

By inhibiting the long-chain acyl-CoA synthetase, benzbromarone is thus impairing the first step in mitochondrial β-oxidation of long-chain fatty acids. As shown in Fig. 5A, treatment with benzbromarone for 24h was associated with an increase in mRNA expression of CPT1α (but not ACSL) starting at 25µM. Analysis of protein expression revealed that treatment with benzbromarone up to 50µM and up to 48h did not affect ACSL expression (Fig. 5B and 5C), whereas expression of CPT1α was increased after incubation with 50µM benzbromarone for 48 h (Fig. 5B and 5D).

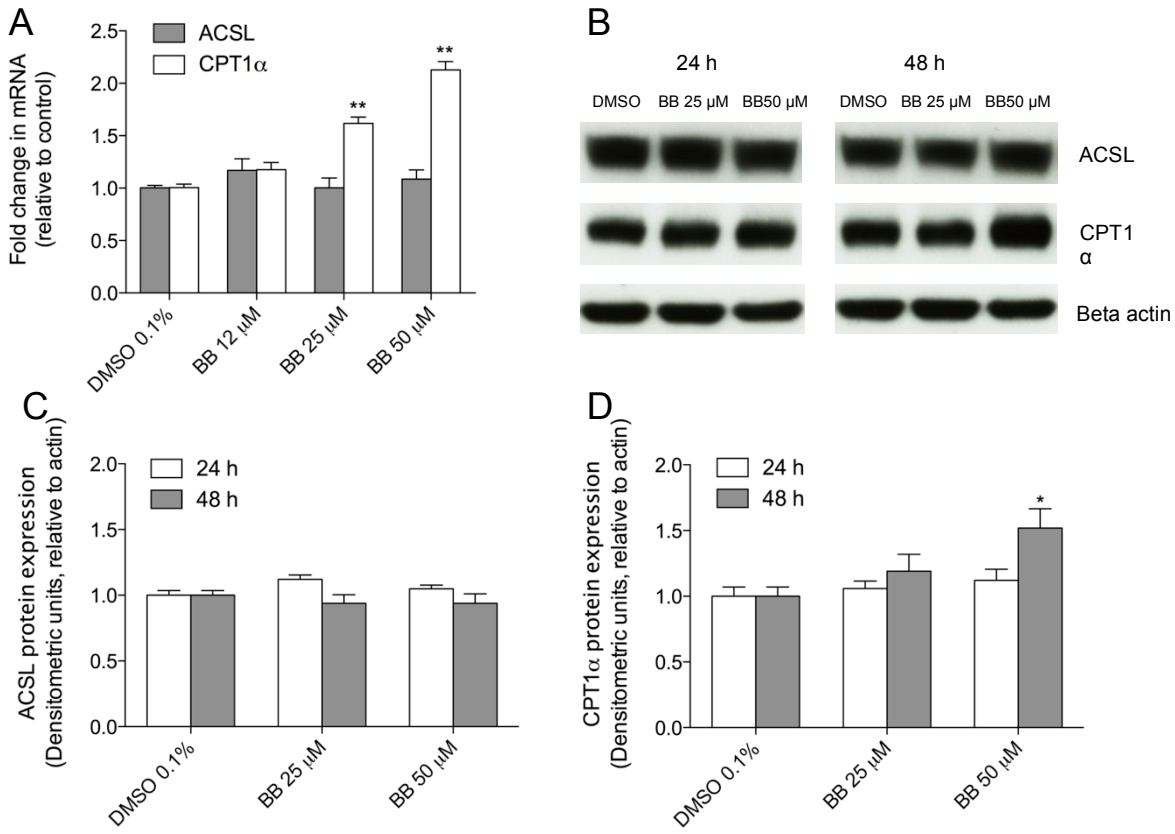

Figure 5. *Changes in mRNA and protein expression of CPT1α and ACSL*. **A.** mRNA expression of ACSL and CPT1α after 24h benzbromarone treatment of HepG2 cells. **B.** Western blot of ACSL and CPT1α of HepG2 cells after 24h and 48h exposure to benzbromarone. **C, D.** Densitometric quantification of ACSL and CPT1α expression of three independent experiments. Data represent the mean ± SEM. *p<0.05 versus DMSO control. **p<0.01 versus DMSO control.

Mitochondrial morphology and mitochondrial content

Mitochondrial morphology was assessed using confocal microscopy after labeling with anti-TOMM22 as well as with transmission electron microscopy (TEM). As shown in Figure 6A, mitochondria in HepG2 cells normally form a cellular network. After treatment with 12.5µM benzbromarone for 24h, this network was still intact. In contrast, treatment with 50µM benzbromarone for 24h disturbed the structure of the mitochondrial network, resulting in a granular appearance of the mitochondria.

To further investigate these alterations in mitochondrial structure, high-resolution transmission electron microscopy (TEM) was used (Fig. 6B). As already observed using confocal microscopy, treatment with 12.5µM benzbromarone for 24h did not change mitochondrial structure compared to DMSO-treated control incubations. In contrast, treatment with 50µM benzbromarone for 24h was associated with a fragmentation of mitochondria and a loss of mitochondrial cristae. Morphometric analysis revealed a decrease of the mitochondrial volume per cell volume (Fig. 6C), which could be observed already after treatment with 12.5µM benzbromarone for 24h.

In order to investigate possible reasons for this decrease in the mitochondrial volume fraction, we investigated the relative amount of mtDNA by real-time PCR as a marker for mitochondrial proliferation. As shown in Figure 6D, the ratio of mtDNA to nuclear DNA was not affected by treatment with benzbromarone. This is in agreement with the finding that the protein expression of the mitochondrially encoded subunit I of complex IV was not affected by benzbromarone treatment (Suppl. Fig. 2). In order to examine whether the observed changes in mitochondrial morphology may be associated with altered mRNA expression of genes involved in mitochondrial fission or fusion, we performed qRT-PCR of various genes. As shown in supplementary Fig. 3, we observed no significant differences in mRNA expression of genes involved in mitochondrial fusion (OPA1, Mfn1, Mfn2) or fission (Fis1, Drp1).

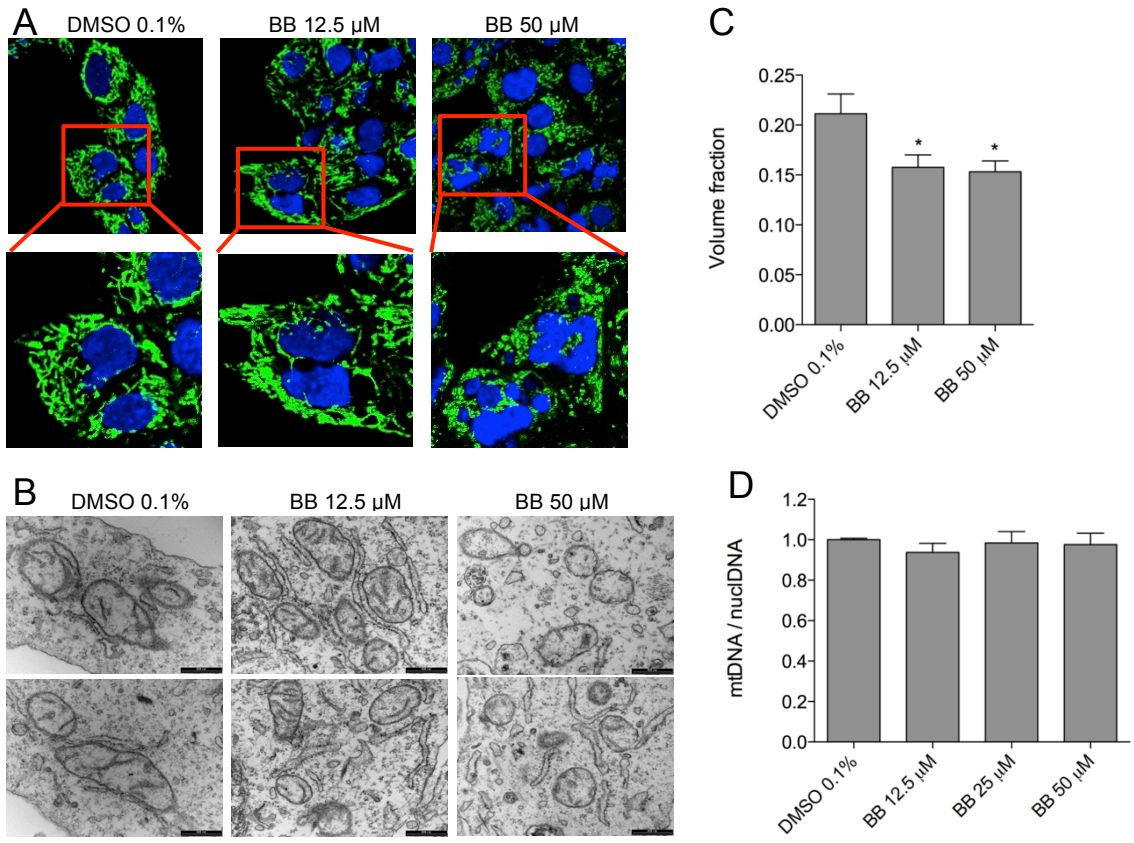

Figure 6. *Effect of benzbromarone on mitochondrial morphology and mitochondrial content*. **A.** Confocal microscopy of HepG2 cells stained with TOMM22 and treated for 24h with benzbromarone. **B.** Transmission electron microscopy (TEM) of HepG2 cells treated for 24h with benzbromarone. **C.** Volume fraction of mitochondria per HepG2 cell in TEM. **D.** Mitochondrial DNA content after 24h benzbromarone exposure in HepG2 cells. Data represent the mean ± SEM of at least three independent experiments. *p<0.05 versus DMSO control. **p<0.01 versus DMSO control.

Discussion

The principle aims of the current investigation were to uncover the specific mechanisms by which benzbromarone impairs mitochondrial function and to investigate possible effects on mitochondrial morphology in HepG2 cells. As known from previous investigations in isolated rat liver mitochondria [15], benzbromarone is a mitochondrial toxicant primarily affecting mitochondrial β-oxidation and the function of the respiratory chain. We could confirm these findings and provide evidence for mitochondrial ROS accumulation as an additional factor responsible for the hepatocellular toxicity of benzbromarone. Importantly, we performed the current studies primarily in HepG2 cells, showing directly that benzbromarone not only affects isolated mitochondria but also mitochondria in a more complex environment of human origin.

Benzbromarone impaired the function of the respiratory chain by uncoupling oxidative phosphorylation and by inhibiting complexes I to IV of the electron transport chain. This is in line with previous studies in rat liver mitochondria and isolated rat hepatocytes [15, 27], where impaired function of the respiratory chain and uncoupling of oxidative phosphorylation have also been described. From these early studies it is known that benzbromarone exerts an acute effect on the function of the respiratory chain. The current study is in agreement with these findings since exposure of HepG2 cells for up to 48h had no impact on the protein expression of subunits encoded by mitochondrial or nuclear DNA of the enzyme complexes of the respiratory chain. It is therefore most likely that benzbromarone directly inhibits the flow of electrons between the enzyme complexes of the respiratory chain. This may also be true for uncoupling of oxidative phosphorylation, since uncoupling was also described as an acute effect in our previous study [15]. Benzbromarone has a phenolic structure and is therefore a weak acid, possibly explaining the uncoupling effect of this compound.

Inhibition of the respiratory chain and uncoupling of oxidative phosphorylation are both associated with impaired mitochondrial ATP synthesis. In this situation, cells try to prevent a drop in intracellular ATP levels by increasing glycolysis. Since lactate is the end product of glycolysis, this was true also for the HepG2 cells exposed to benzbromarone (Fig. 2D), convincingly demonstrating the metabolic consequences of the inhibition of oxidative phosphorylation.

Impaired activity of the electron transport chain is usually associated with increased mitochondrial ROS production [15, 20]. In the current study, we showed that ROS accumulation is increased in mitochondria of HepG2 cells treated with benzbromarone. The observed ROS accumulation was associated with an increased mRNA expression of SOD2, a mitochondrial enzyme responsible for superoxide anion degradation [28]. Taking into account that we recently reported similar findings in HepG2 cells exposed to dronedarone, which is also associated with mitochondrial ROS accumulation, SOD2 upregulation seems to be a common mechanism to counteract mitochondrial ROS accumulation [20]. Importantly, mitochondrial ROS accumulation can be associated with apoptosis and/or necrosis, depending on the ATP content of the cells [29, 30]. Mitochondrial ROS accumulation is therefore a possible mechanism for hepatocyte death associated with benzbromarone exposure.

In our previous study with isolated liver mitochondria we have shown that benzbromarone inhibits mitochondrial β-oxidation more potently than the respiratory chain [15]. In the current study with HepG2 cells, benzbromarone started to inhibit both β-oxidation and the respiratory chain at 50µM. Interestingly, in contrast to HepG2 cells, in isolated mouse liver mitochondria, inhibition of β-oxidation started already at 2µM. The discrepancy between mitochondria and HepG2 cells may be explained by a better accessibility of the mitochondrial matrix for benzbromarone for isolated mitochondria compared to HepG2 cells. In addition, the original incubation buffer of the HepG2 cells containing benzbromarone was removed and replaced by the assay buffer containing no benzbromarone before the cells were investigated. The intramitochondrial concentration during the investigations may therefore have been lower than the benzbromarone concentration originally added.

In both assay systems, HepG2 cells and mouse liver mitochondria, inhibition of the long-chain acyl-CoA synthetase explains inhibition of β-oxidation. Interestingly, CPT1α, which is highly regulated and can therefore be considered as the rate-limiting enzyme of hepatic mitochondrial β-oxidation [31], showed an increased expression of both mRNA and protein, which was time- and concentration-dependent for benzbromarone exposure. Since benzbromarone impaired β-oxidation and the concentration of β-oxidation substrates and intermediates increases when β-oxidation is inhibited [14], CPT1α induction may be explained by accumulation of such intermediates. In support of this hypothesis, increased hepatocellular concentration of free fatty acids have been described to be associated with CPT1α induction [32]. Since benzbromarone did not impair CPT1 activity, a direct effect of benzbromarone on CPT1α expression is less likely but cannot be excluded.

Impaired mitochondrial β-oxidation explains well the clinical finding of microvesicular steatosis in a patient with liver injury associated with benzbromarone exposure [9]. Microvesicular steatosis is a typical histological finding in animals [13, 14] and humans [12, 33] with impaired hepatic β-oxidation.

Beside the exploration of the specific mechanisms how benzbromarone disturbs mitochondrial function in HepG2 cells, a second aim of the study was to investigate possible effects on mitochondrial morphology. Intact mitochondria perform active exchange of mitochondrial DNA and proteins through mutual interaction. Consequently, tight mitochondrial networks are formed and a highly controlled fission to fusion balance is maintained [34, 35]. Mitochondrial impairment, for instance by treatment with mitochondrial toxicants, can disturb this balance [36, 37]. Interestingly, as shown in Figure 6A, we observed a decrease in mitochondrial interconnectivity in TOMM22-stained HepG2 cells with increasing benzbromarone concentrations. The network structures gradually disappeared and were replaced by more granulated structures. This was also clearly visible on transmission electron microscopy images, where mitochondria appeared smaller with fewer cristae. Loss of the mitochondrial network structure with a granular appearance and formation of short, round mitochondria occurs in early apoptosis [38, 39], which is favoring mitochondrial fission over fusion. Furthermore, dissipation of the inner membrane potential was shown to inhibit mitochondrial fusion and may induce fragmentation of mitochondrial filaments [37]. The amount of mitochondrial DNA did not change, indicating that benzbromarone had no effect on mitochondrial DNA synthesis.

Cell death occurred by both apoptosis and necrosis. As mentioned above, apoptosis can be induced by mitochondrial accumulation of ROS [30]. In addition, hepatocellular accumulation of fatty acids has also been described to be associated with apoptosis [40]. As described above, the development of apoptosis is most probably responsible for the destruction of the mitochondrial network associated with benzbromarone. Apoptosis is dependent on a high enough cellular ATP concentration, whereas cells with a too low ATP level undergo necrosis [29], which was also observed in HepG2 cells treated with benzbromarone (Fig. 1D).

A pharmacokinetic study in healthy volunteers has shown that peak plasma benzbromarone concentrations after a single dose of 100mg can reach 5 to 15µmol/L, depending on the CYP2C9 genotype [41]. This concentration is most likely also reached in the liver and is close to the concentrations associated with cytotoxicity in the current study. Interestingly, recently Kobayashi et al. [42] have shown that both the parent substance (benzbromarone) and 1'-OH-benzbromarone, which is formed by

CYP3A4 [43], are hepatotoxic. Since HepG2 cells do not contain CYP3A4 [7], a conversion to 1'-OH-benzbromarone can be excluded in the current studies. The molecular mechanism of the hepatocellular toxicity associated with 1'-OH-benzbromarone has therefore to be investigated in future studies.

In conclusion, our investigations show that benzbromarone is causing mitochondrial dysfunction in HepG2 cells already after 24h of exposure at clinically relevant concentrations. Benzbromarone is associated with uncoupling of oxidative phosphorylation, inhibition of the respiratory chain and impaired β-oxidation. Most of these effects can be explained by a direct toxic effect of benzbromarone, since they occur also with acute exposure. Benzbromarone induces mitochondrial ROS accumulation and breakdown of the mitochondrial network which are associated with the development of apoptosis and necrosis.

References

1. Navarro, V.J. and J.R. Senior, *Drug-related hepatotoxicity.* N Engl J Med, 2006. **354**(7): p. 731-9.

2. Suzuki, A., et al., *Drugs associated with hepatotoxicity and their reporting frequency of liver adverse events in VigiBase: unified list based on international collaborative work.* Drug Saf, 2010. **33**(6): p. 503-22.

3. Kaplowitz, N., *Idiosyncratic drug hepatotoxicity.* Nat Rev Drug Discov, 2005. **4**(6): p. 489-99.

4. Ostapowicz, G., et al., *Results of a prospective study of acute liver failure at 17 tertiary care centers in the United States.* Ann Intern Med, 2002. **137**(12): p. 947-54.

5. Kaplowitz, N., *Drug-induced liver disorders: implications for drug development and regulation.* Drug Saf, 2001. **24**(7): p. 483-90.

6. Zahno, A., et al., *Hepatocellular toxicity of clopidogrel: Mechanisms and risk factors.* Free Radic Biol Med, 2013. **65C**: p. 208-216.

7. Zahno, A., et al., *The role of CYP3A4 in amiodarone-associated toxicity on HepG2 cells.* Biochem Pharmacol, 2011. **81**(3): p. 432-41.

8. de Abajo, F.J., et al., *Acute and clinically relevant drug-induced liver injury: a population based case-control study.* Br J Clin Pharmacol, 2004. **58**(1): p. 71-80.

9. Arai, M., et al., *Fulminant hepatic failure associated with benzbromarone treatment: a case report.* J Gastroenterol Hepatol, 2002. **17**(5): p. 625-6.

10. van der Klauw, M.M., et al., *Hepatic injury caused by benzbromarone.* J Hepatol, 1994. **20**(3): p. 376-9.

11. Wagayama, H., et al., *Fatal fulminant hepatic failure associated with benzbromarone.* J Hepatol, 2000. **32**(5): p. 874.

12. Fromenty, B. and D. Pessayre, *Inhibition of mitochondrial beta-oxidation as a mechanism of hepatotoxicity.* Pharmacol Ther, 1995. **67**(1): p. 101-54.

13. Spaniol, M., et al., *Development and characterization of an animal model of carnitine deficiency.* Eur J Biochem, 2001. **268**(6): p. 1876-87.

14. Spaniol, M., et al., *Mechanisms of liver steatosis in rats with systemic carnitine deficiency due to treatment with trimethylhydraziniumpropionate.* J Lipid Res, 2003. **44**(1): p. 144-53.

15. Kaufmann, P., et al., *Mechanisms of benzarone and benzbromarone-induced hepatic toxicity.* Hepatology, 2005. **41**(4): p. 925-35.

16. Krahenbuhl, S., *Mitochondria: important target for drug toxicity?* J Hepatol, 2001. **34**(2): p. 334-6.

17. Skehan, P., et al., *New colorimetric cytotoxicity assay for anticancer-drug screening.* J Natl Cancer Inst, 1990. **82**(13): p. 1107-12.

18. Hoppel, C., J.P. DiMarco, and B. Tandler, *Riboflavin and rat hepatic cell structure and function. Mitochondrial oxidative metabolism in deficiency states.* J Biol Chem, 1979. **254**(10): p. 4164-70.

19. Waldhauser, K.M., et al., *Hepatocellular toxicity and pharmacological effect of amiodarone and amiodarone derivatives.* J Pharmacol Exp Ther, 2006. **319**(3): p. 1413-23.

20. Felser, A., et al., *Mechanisms of hepatocellular toxicity associated with dronedarone--a comparison to amiodarone.* Toxicol Sci, 2013. **131**(2): p. 480-90.

21. Olsen, C., *An enzymatic fluorimetric micromethod for the determination of acetoacetate, -hydroxybutyrate, pyruvate and lactate.* Clin Chim Acta, 1971. **33**(2): p. 293-300.

22. Reinartz, A., et al., *Lipid-induced up-regulation of human acyl-CoA synthetase 5 promotes hepatocellular apoptosis.* Biochim Biophys Acta, 2010. **1801**(9): p. 1025-35.

23. Kennedy, J.A., S.A. Unger, and J.D. Horowitz, *Inhibition of carnitine palmitoyltransferase-1 in rat heart and liver by perhexiline and amiodarone.* Biochem Pharmacol, 1996. **52**(2): p. 273-80.

24. Mullen, P.J., et al., *Susceptibility to simvastatin-induced toxicity is partly determined by mitochondrial respiration and phosphorylation state of Akt.* Biochim Biophys Acta, 2011. **1813**(12): p. 2079-87.

25. Hoffmann, R.F., et al., *Prolonged cigarette smoke exposure alters mitochondrial structure and function in airway epithelial cells.* Respir Res, 2013. **14**(1): p. 97.

26. Pieters, N., et al., *Decreased mitochondrial DNA content in association with exposure to polycyclic aromatic hydrocarbons in house dust during wintertime: from a population enquiry to cell culture.* PLoS One, 2013. **8**(5): p. e63208.

27. Kramar, R. and M.M. Muller, *[Inhibition of enzymes of the internal mitochondrial membrane by benzbromarone].* Experientia, 1973. **29**(4): p. 391-2.

28. Inoue, M., et al., *Mitochondrial generation of reactive oxygen species and its role in aerobic life.* Curr Med Chem, 2003. **10**(23): p. 2495-505.

29. Leist, M., et al., *Intracellular adenosine triphosphate (ATP) concentration: a switch in the decision between apoptosis and necrosis.* J Exp Med, 1997. **185**(8): p. 1481-6.

30. Sinha, K., et al., *Oxidative stress: the mitochondria-dependent and mitochondria-independent pathways of apoptosis.* Arch Toxicol, 2013. **87**(7): p. 1157-80.

31. Kerner, J. and C. Hoppel, *Fatty acid import into mitochondria.* Biochim Biophys Acta, 2000. **1486**(1): p. 1-17.

32. Le May, C., et al., *Fatty acids induce L-CPT I gene expression through a PPARalpha-independent mechanism in rat hepatoma cells.* J Nutr, 2005. **135**(10): p. 2313-9.

33. Krahenbuhl, S., et al., *Plasma and hepatic carnitine and coenzyme A pools in a patient with fatal, valproate induced hepatotoxicity.* Gut, 1995. **37**(1): p. 140-3.

34. Karbowski, M. and R.J. Youle, *Dynamics of mitochondrial morphology in healthy cells and during apoptosis.* Cell Death Differ, 2003. **10**(8): p. 870-80.

35. Westermann, B., *Mitochondrial fusion and fission in cell life and death.* Nat Rev Mol Cell Biol, 2010. **11**(12): p. 872-84.

36. Detmer, S.A. and D.C. Chan, *Functions and dysfunctions of mitochondrial dynamics.* Nat Rev Mol Cell Biol, 2007. **8**(11): p. 870-9.

37. Legros, F., et al., *Mitochondrial fusion in human cells is efficient, requires the inner membrane potential, and is mediated by mitofusins.* Mol Biol Cell, 2002. **13**(12): p. 4343-54.

38. Arnoult, D., *Mitochondrial fragmentation in apoptosis.* Trends Cell Biol, 2007. **17**(1): p. 6-12.

39. Palmer, C.S., et al., *The regulation of mitochondrial morphology: intricate mechanisms and dynamic machinery.* Cell Signal, 2011. **23**(10): p. 1534-45.

40. Belosludtsev, K., et al., *On the mechanism of palmitic acid-induced apoptosis: the role of a pore induced by palmitic acid and Ca2+ in mitochondria.* J Bioenerg Biomembr, 2006. **38**(2): p. 113-20.

41. Uchida, S., et al., *Benzbromarone pharmacokinetics and pharmacodynamics in different cytochrome P450 2C9 genotypes.* Drug Metab Pharmacokinet, 2010. **25**(6): p. 605-10.

42. Kobayashi, K., et al., *Cytotoxic effects of benzbromarone and its 1'-hydroxy metabolite in human hepatocarcinoma FLC4 cells cultured on micro-space cell culture plates.* Drug Metab Pharmacokinet, 2013. **28**(3): p. 265-8.

43. Kobayashi, K., et al., *Identification of CYP isozymes involved in benzbromarone metabolism in human liver microsomes.* Biopharm Drug Dispos, 2012. **33**(8): p. 466-73.

Supplemental Figures

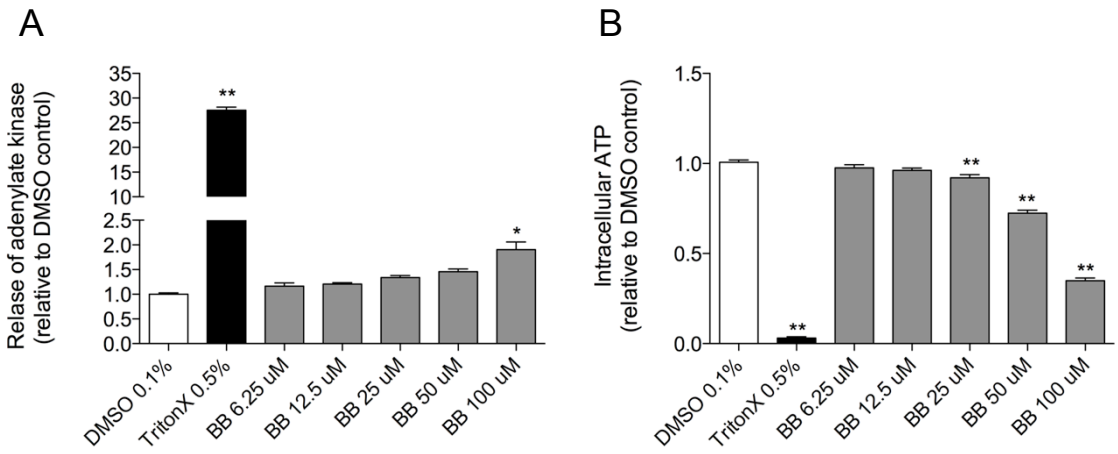

Suppl. Figure 1. *Cytotoxicity and intracellular ATP*. **A**. Cytotoxicity in HepG2 cells after drug exposure for 48 h assessed by the release of adenylate kinase. Data are expressed relative to control incubations containing 0.1% DMSO. **B**. Intracellular ATP content in HepG2 cells after drug exposure for 48h. Data are expressed relative to control incubations containing 0.1% DMSO. Data represent the mean ± SEM of at least three independent experiments. *p<0.05 versus DMSO control. **p<0.01 versus DMSO control.

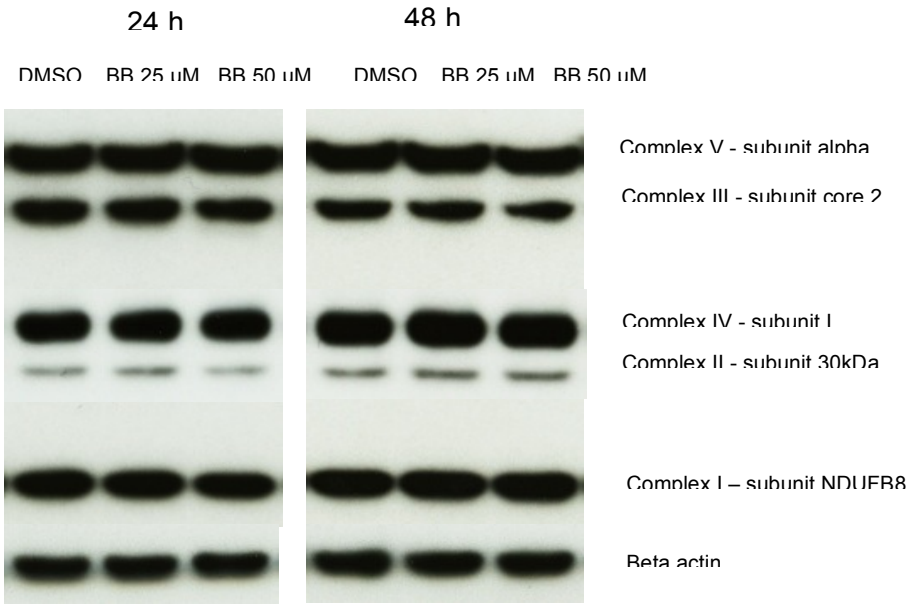

Suppl. Figure 2. *Protein expression of subunits of mitochondrial respiratory chain complexes*. The protein expression of the five mitochondrial respiratory chain complexes was assessed by Western blotting using using the MitoProfile® Total OXPHOS antibody cocktail.

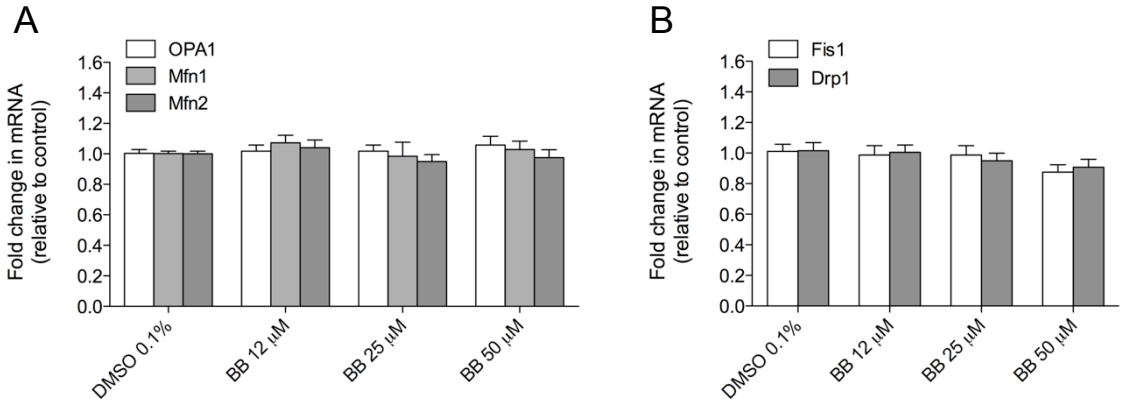

Suppl. Figure 3. *mRNA expression of mitochondrial fusion and fission markers*. HepG2 cells were exposed for 24h with benzbromarone and mRNA of fission and fusion markers was quantified by RT-PCR. **A**. Markers involved in mitochondrial fusion, e.g. OPA1, Mfn1, Mfn2. **B**. Markers involved in mitochondrial fission, e.g. Fis1, Drp1. Data represent the mean ± SEM of at least three independent experiments. *p<0.05 versus DMSO control. **p<0.01 versus DMSO control.

General discussion

Drug-induced liver injury is an important adverse drug reaction and a challenge for the pharmaceutical industry as well as for health care professionals. The reasons for the unique susceptibility of a few patients to idiosyncratic DILI are not completely understood, but mitochondrial dysfunction and reactive metabolite formation are believed to be major contributors [47]. Over the last years, drugs with mitochondrial liability have been withdrawn from the market (e.g. troglitazone, benzbromarone) or have been given warnings by drug agencies restricting their use (e.g. valproic acid, amiodarone, dronedarone) [3, 13, 97]. Numerous mitochondrial targets might be responsible for a metabolic failure, and often one drug impairs several mitochondrial targets [18].

Molecular mechanisms of dronedarone-induced hepatotoxicity

Previous studies of our laboratory have described that chemicals containing a benzofuran structure coupled to a p-hydroxybenzolring are prone to induce mitochondrial dysfunction [76, 77]. Since the chemical structure of dronedarone contains these structural properties, we hypothesized, that mitochondrial dysfunction might account for dronedarone-induced hepatotoxicity.

The aim of our first study therefore was to understand the molecular mechanism of dronedarone-induced hepatotoxicity *in vitro*. Our investigations in isolated rat liver mitochondrial and HepG2 cells demonstrate, that similar to amiodarone, dronedarone inhibited the ETC and β-oxidation and uncoupled Ox/Phos. The mitochondrial dysfunction led to an accumulation of superoxide and intracellular lipids that might have triggered hepatocyte apoptosis. Reactive metabolites play an important role in amiodarone-induced hepatotoxicity, and previous studies have shown that N-dealkylated metabolites of amiodarone are more hepatotoxic than the parent compound [78, 81]. Our data in primary human hepatocytes suggested that in the case of dronedarone mainly the parent compound caused the toxicity. In order to clearly address the question if reactive metabolites may play a role, we recently performed a toxicological study directly with the main N-dealkylated metabolite of dronedarone, desbutyl dronedarone, and found that the metabolite did not further increase

cytotoxicity *in vitro* (Felser et al., unpublished data). We thus conclude that dronedarone is, in contrast to amiodarone, most probably not associated with reactive metabolite formation. Since the effects on mitochondrial function were observed at pre-cytotoxic concentrations and were clearly dose-dependent, it is likely that mitochondrial dysfunction is a major reason for dronedarone-associated hepatotoxicity *in vitro*.

In our second study we investigated dronedarone-associated hepatotoxicity in wild-type and $jvs^{+/-}$ mice, and exposed the animals to two different doses of dronedarone. Whereas the lower dose was not hepatotoxic, the higher induced apoptosis of hepatocytes. We found that dronedarone inhibited β-oxidation of 1-^{14}C palmitic acid *in vivo*, as well as *ex vivo* in isolated liver mitochondria. In contrast, inhibition or uncoupling of Ox/Phos could not be demonstrated. These results are in agreement with a study performed by Serviddio et al., who did not observe inhibition of Ox/Phos in rats treated with dronedarone [88]. In order to fully uncover where the inhibition of fatty acid oxidation is located, further research is still required. We found that the rate-limiting enzyme in fatty acid oxidation, CPT1a, was inhibited. In spite of this we also demonstrated that the acute inhibition of fatty acid oxidation could not be restored with palmitoylcarnitine as substrate, suggesting that an additional target downstream to CPT1a must be inhibited as well. Overall, the experiments show that inhibition of mitochondrial β-oxidation might play a leading role in dronedarone-induced hepatotoxicity *in vivo*.

Taken together, the first two studies of the thesis have characterized a possible mechanism of dronedarone-induced hepatotoxicity *in vitro* and *in vivo*. We showed that dronedarone is a mitochondrial toxicant and that inhibition of mitochondrial β-oxidation is a major mechanism of liver toxicity associated with dronedarone. Hepatotoxicity caused by dronedarone can be fatal in rare cases, and our observations contribute to the understanding that patients with mitochondrial β-oxidation defects might be at risk of developing dronedarone-associated severe liver injury in the clinics. In order to validate susceptibility factors for dronedarone-associated hepatotoxicity, it would be interesting to test affected patients for genetic mitochondrial abnormalities [7]. Indeed, in the past years, a great progress has been made in the collection of biological samples from patients experiencing unexpected liver reactions in response to a given drug and novel observations are starting to emerge from their work [98, 99]. Such approaches will help to further enlarge our knowledge about idiosyncratic hepatotoxicity and identify new susceptibility factors of patients.

Animal models for idiosyncratic liver injuries – future directions

Preclinical safety assessments are usually performed in young and healthy wild-type animals. However, idiosyncratic drug-induced liver injuries are rare, and affected patients have susceptibility factors [3, 7, 47, 100]. So far, only two models with pre-existing mitochondrial alterations in liver and other tissues, namely $SOD2^{+/-}$ and $jvs^{+/-}$ mice, have been tested for their sensitivity towards drug-induced mitochondrial hepatotoxicity [58, 62, 66, 67]. In our study on dronedarone-associated hepatotoxicity in mice, elevations in plasma ALT and bilirubin, and inhibition of *in vivo* metabolism of palmitic acid were more accentuated in $jvs^{+/-}$ mice as compared to wild-type mice. However, the hepatotoxicity observed in our study was rather modest compared to the pronounced liver injuries that have been observed in some dronedarone-treated patients [86, 87].

New models for underlying defects in hepatic β-oxidation that reflect clinical manifestations of mitochondrial dysfunction more faithfully are thus necessary [101]. An animal model that could be interesting to use are medium-chain acyl-CoA dehydrogenase ($MCAD^{+/-}$) deficient mice [102]. This deficiency is the most frequent metabolic disorder of genetic origin among Caucasians [103, 104]. MCAD deficiency is inherited in an autosomal recessive manner and newborn screening for homozygous mutations of MCAD ($MCAD^{-/-}$) is well-established [105, 106], since affected children would remain undiagnosed until an episode of increased energy demand and fasting occurs [107-109]. $MCAD^{+/-}$ are asymptomatic and so far, it has never been investigated whether the MCAD carrier state may be sufficient to increase the risk of DILI in patients receiving drugs that impair mitochondrial function [47]. Alternatively, another mouse model with partial carnitine palmitoyltransferase 1a deficiency ($CPT1a^{+/-}$) might be interesting to test, especially for dronedarone-associated hepatotoxicity. Since CPT1 is a rate-limiting enzyme in fatty acid oxidation and highly regulated [30], it might represent a stronger bottleneck situation for inhibitors of fatty acid oxidation than $MCAD^{+/-}$. This is underlined by the fact that homozygous knockout was lethal in early gestation, whereas the heterozygous phenotype resulted in a significant reduced CPT1a activity in liver (54.7% compared to wild-type activity) [110].

In addition, also improved mouse models with underlying Ox/Phos dysfunction are necessary. A next approach could be to test models with direct impairment of the ETC [111, 112], such as for example a model with partial knockout of the mitochondrial transcription factor A ($TFAM^{+/-}$). As explained earlier, the ETC complexes are composed of several subunits, which are encoded either by the mitochondrial

DNA or the nuclear DNA. The mitochondrial transcription machinery consists of a three proteins, namely the mitochondrial RNA polymerase, mitochondrial transcription factor A (TFAM) and mitochondrial transcription factor B2 and is essential for the biogenesis of 13 subunits of the respiratory chain complexes I, III, IV and V. Whereas a homozygous TFAM knockout is lethal in early gestation, heterozygous mice are born at normal frequency but have reduced levels of mitochondrial encoded ETC proteins [113] and could therefore be more susceptible for inhibitors of mitochondrial Ox/Phos.

In conclusion, animal models with a higher susceptibility to drug-induced mitochondrial effects that reflect clinical manifestations of mitochondrial dysfunction more faithfully should be established. Further studies are needed to assess if any of the animal models mentioned above provide progress and hold promise for increasing the prediction and understanding of human mitochondrial dysfunction-mediated DILI. Furthermore, greater understanding of the mechanisms of DILI will help to develop more effective *in vitro* screening strategies [58].

Investigation of drug-induced mitochondrial dysfunction *in vitro*

In the third project of the thesis we aimed to improve our understanding of the molecular mechanisms of benzbromarone associated liver toxicity *in vitro*. We found that benzbromarone inhibited the ETC and uncoupled Ox/Phos, which led to a compensatory increase in lactate and accumulation of superoxide. Furthermore, we found that benzbromarone inhibited mitochondrial β-oxidation, most probably at the level of the long-chain acyl-CoA synthetase, and we observed that benzbromarone not only impaired mitochondrial function in HepG2 cells, but also induced profound changes in mitochondrial morphology.

Together with our first study on dronedarone-induced mitochondrial toxicity *in vitro*, we demonstrated that there are a plethora of possibilities how to demonstrate mitochondrial dysfunction *in vitro*. Although our approaches are useful to test specific hypotheses, not all of them might be applicable for routine high-throughput preclinical safety assessments in industry. The assessment of mitochondrial dysfunction during the lead discovery phase could for example be organized in a two-step approach [3]. In a first step a high-throughput screen for mitochondrial dysfunction could be preformed and if mitochondrial liability would be identified in a lead structure of interest, in a

second step, more mechanistic studies would need to be performed. Investigations to set up and validate high-throughput assays for mitochondrial toxicity involve the use of oxygen-sensitive probes (fluorescent-based 96-well approach, Seahorse bioscience) [114, 115] or multiplexed assays in sensitive cell lines, which measure several endpoints such as cytotoxicity, ATP, ROS, membrane potential, etc. [51, 56, 116].

But how severe does mitochondrial impairment have to be before it yields frank toxicity *in vivo*? As mentioned earlier, *in vitro* systems such as isolated mitochondria and tumor-derived cell lines, might over- or underreport drug effects, since they lack cytochrome P450 and do not take into account detoxifying mechanisms or formation of reactive metabolites. Furthermore, screening concentrations might often include a multiple of anticipated maximum serum concentration and not reflect physiological reality. In order to define the range of mitochondrial impairment that can be tolerated clinically, a retrospective analysis of correlations between adverse drug events in humans and mitochondrial toxicity *in vitro* would help to establish a guideline. Indeed, many beneficial drugs have mitochondrial liabilities, but they might not be clinically significant in terms of risk-to-benefit ratio if the dysfunction is merely modest. Therefore, finding a drug-induced mitochondrial liability does not necessarily lead to the abandoning of the drug, but to increased safety vigilance and investigation of the potency in mechanistic assays.

In conclusion, although testing for mitochondrial dysfunction is not mandatory in preclinical safety assessments, pharmaceutical companies should consider systematically investigating mitochondrial dysfunction during the routine screening for preclinical safety in the early lead selection phase, in order to be aware of the hepatotoxic potential and to allow an early selection of safer compounds for the subsequent development process [3, 47].

Conclusion

In summary, we provide important mechanisms of dronedarone-induced idiosyncratic hepatotoxicity *in vitro* and *in vivo*. Patients with mitochondrial β-oxidation defects might be at risk of developing dronedarone-associated severe liver injury. However, a reliable preclinical model to safely predict disruptors of mitochondrial β-oxidation is still missing. In addition, we have shown that benzbromarone induced mitochondrial dysfunction and structural changes in the mitochondrial network *in vitro*. Further studies are still necessary to investigate whether these findings are relevant for benzbromarone-induced hepatotoxicity *in vivo*. Over all, this thesis contributes to our knowledge of how dronedarone and other mitochondrial disruptors cause toxicity, provides evidence that mitochondrial testing is important in preclinical research and shows that the area of idiosyncratic drug reactions still needs intense research in order to improve preclinical predictivity.

References

1. Ghabril, M., N. Chalasani, and E. Bjornsson, *Drug-induced liver injury: a clinical update.* Curr Opin Gastroenterol, 2010. **26**(3): p. 222-6.

2. Larrey, D., *Epidemiology and individual susceptibility to adverse drug reactions affecting the liver.* Semin Liver Dis, 2002. **22**(2): p. 145-55.

3. Dykens, J.A. and Y. Will, *The significance of mitochondrial toxicity testing in drug development.* Drug Discov Today, 2007. **12**(17-18): p. 777-85.

4. Lammert, C., et al., *Oral medications with significant hepatic metabolism at higher risk for hepatic adverse events.* Hepatology, 2010. **51**(2): p. 615-20.

5. Navarro, V.J. and J.R. Senior, *Drug-related hepatotoxicity.* N Engl J Med, 2006. **354**(7): p. 731-9.

6. Temple, R., *Hy's law: predicting serious hepatotoxicity.* Pharmacoepidemiol Drug Saf, 2006. **15**(4): p. 241-3.

7. Tujios, S. and R.J. Fontana, *Mechanisms of drug-induced liver injury: from bedside to bench.* Nat Rev Gastroenterol Hepatol, 2011. **8**(4): p. 202-11.

8. Begriche, K., et al., *Drug-induced toxicity on mitochondria and lipid metabolism: mechanistic diversity and deleterious consequences for the liver.* J Hepatol, 2011. **54**(4): p. 773-94.

9. Shaw, P.J., P.E. Ganey, and R.A. Roth, *Idiosyncratic drug-induced liver injury and the role of inflammatory stress with an emphasis on an animal model of trovafloxacin hepatotoxicity.* Toxicol Sci, 2010. **118**(1): p. 7-18.

10. Walgren, J.L., M.D. Mitchell, and D.C. Thompson, *Role of metabolism in drug-induced idiosyncratic hepatotoxicity.* Crit Rev Toxicol, 2005. **35**(4): p. 325-61.

11. Hawkins, M.T. and J.H. Lewis, *Latest advances in predicting DILI in human subjects: focus on biomarkers.* Expert Opin Drug Metab Toxicol, 2012. **8**(12): p. 1521-30.

12. Watanabe, I., et al., *A study to survey susceptible genetic factors responsible for troglitazone-associated hepatotoxicity in Japanese patients with type 2 diabetes mellitus.* Clin Pharmacol Ther, 2003. **73**(5): p. 435-55.

13. Pessayre, D., et al., *Mitochondrial involvement in drug-induced liver injury.* Handb Exp Pharmacol, 2010(196): p. 311-65.

14. Krahenbuhl, S., et al., *Mitochondrial diseases represent a risk factor for valproate-induced fulminant liver failure.* Liver, 2000. **20**(4): p. 346-8.

15. Lam, C.W., et al., *Mitochondrial myopathy, encephalopathy, lactic acidosis and stroke-like episodes (MELAS) triggered by valproate therapy.* Eur J

Pediatr, 1997. **156**(7): p. 562-4.

16. Kottlors, M., et al., *Valproic acid triggers acute rhabdomyolysis in a patient with carnitine palmitoyltransferase type II deficiency.* Neuromuscul Disord, 2001. **11**(8): p. 757-9.

17. Njolstad, P.R., et al., *Medium chain acyl-CoA dehydrogenase deficiency and fatal valproate toxicity.* Pediatr Neurol, 1997. **16**(2): p. 160-2.

18. Wallace, K.B., *Mitochondrial off targets of drug therapy.* Trends Pharmacol Sci, 2008. **29**(7): p. 361-6.

19. Wojtczak, L. and K. Zablocki, *Basic mitochondrial physiology in cell viability and death.* In: Dykens JA., Will Y., eds. Drug-induced mitochondrial dysfunction, 2008. **1st ed.** (Hoboken, New Jersey: John Wiley and Sons, Inc.): p. 3-36.

20. Cuperus, R., et al., *Fenretinide induces mitochondrial ROS and inhibits the mitochondrial respiratory chain in neuroblastoma.* Cell Mol Life Sci, 2010. **67**(5): p. 807-16.

21. Goncharov, N.V., R.O. Jenkins, and A.S. Radilov, *Toxicology of fluoroacetate: a review, with possible directions for therapy research.* J Appl Toxicol, 2006. **26**(2): p. 148-61.

22. Balaban, R.S., S. Nemoto, and T. Finkel, *Mitochondria, oxidants, and aging.* Cell, 2005. **120**(4): p. 483-95.

23. Liu, Y., G. Fiskum, and D. Schubert, *Generation of reactive oxygen species by the mitochondrial electron transport chain.* J Neurochem, 2002. **80**(5): p. 780-7.

24. Adam-Vizi, V. and C. Chinopoulos, *Bioenergetics and the formation of mitochondrial reactive oxygen species.* Trends Pharmacol Sci, 2006. **27**(12): p. 639-45.

25. Li, Y., et al., *Dilated cardiomyopathy and neonatal lethality in mutant mice lacking manganese superoxide dismutase.* Nat Genet, 1995. **11**(4): p. 376-81.

26. Sena, L.A. and N.S. Chandel, *Physiological roles of mitochondrial reactive oxygen species.* Mol Cell, 2012. **48**(2): p. 158-67.

27. Adjeitey, C.N., et al., *Mitochondrial uncoupling in skeletal muscle by UCP1 augments energy expenditure and glutathione content while mitigating ROS production.* Am J Physiol Endocrinol Metab, 2013. **305**(3): p. E405-15.

28. Fromenty, B. and D. Pessayre, *Inhibition of mitochondrial beta-oxidation as a mechanism of hepatotoxicity.* Pharmacol Ther, 1995. **67**(1): p. 101-54.

29. Bonnefont, J.P., et al., *Carnitine palmitoyltransferases 1 and 2: biochemical, molecular and medical aspects.* Mol Aspects Med, 2004. **25**(5-6): p. 495-520.

30. Kerner, J. and C. Hoppel, *Fatty acid import into mitochondria.* Biochim Biophys

Acta, 2000. **1486**(1): p. 1-17.

31. Pessayre, D., et al., *Central role of mitochondria in drug-induced liver injury.* Drug Metab Rev, 2012. **44**(1): p. 34-87.

32. Fulgencio, J.P., et al., *Troglitazone inhibits fatty acid oxidation and esterification, and gluconeogenesis in isolated hepatocytes from starved rats.* Diabetes, 1996. **45**(11): p. 1556-62.

33. Kennedy, J.A., S.A. Unger, and J.D. Horowitz, *Inhibition of carnitine palmitoyltransferase-1 in rat heart and liver by perhexiline and amiodarone.* Biochem Pharmacol, 1996. **52**(2): p. 273-80.

34. Ponchaut, S., F. van Hoof, and K. Veitch, *In vitro effects of valproate and valproate metabolites on mitochondrial oxidations. Relevance of CoA sequestration to the observed inhibitions.* Biochem Pharmacol, 1992. **43**(11): p. 2435-42.

35. Millington, D.S., et al., *Valproylcarnitine: a novel drug metabolite identified by fast atom bombardment and thermospray liquid chromatography-mass spectrometry.* Clin Chim Acta, 1985. **145**(1): p. 69-76.

36. Letteron, P., et al., *Glucocorticoids inhibit mitochondrial matrix acyl-CoA dehydrogenases and fatty acid beta-oxidation.* Am J Physiol, 1997. **272**(5 Pt 1): p. G1141-50.

37. Rial, E., et al., *Lipotoxicity, fatty acid uncoupling and mitochondrial carrier function.* Biochim Biophys Acta, 2010. **1797**(6-7): p. 800-6.

38. Saudubray, J.M., et al., *Recognition and management of fatty acid oxidation defects: a series of 107 patients.* J Inherit Metab Dis, 1999. **22**(4): p. 488-502.

39. Han, D., et al., *Regulation of drug-induced liver injury by signal transduction pathways: critical role of mitochondria.* Trends Pharmacol Sci, 2013. **34**(4): p. 243-53.

40. Sano, M. and K. Fukuda, *Activation of mitochondrial biogenesis by hormesis.* Circ Res, 2008. **103**(11): p. 1191-3.

41. St-Pierre, J., et al., *Suppression of reactive oxygen species and neurodegeneration by the PGC-1 transcriptional coactivators.* Cell, 2006. **127**(2): p. 397-408.

42. Han, D., et al., *Dynamic adaptation of liver mitochondria to chronic alcohol feeding in mice: biogenesis, remodeling, and functional alterations.* J Biol Chem, 2012. **287**(50): p. 42165-79.

43. Gomes, L.C., G. Di Benedetto, and L. Scorrano, *During autophagy mitochondria elongate, are spared from degradation and sustain cell viability.* Nat Cell Biol, 2011. **13**(5): p. 589-98.

44. Chen, H. and D.C. Chan, *Emerging functions of mammalian mitochondrial fusion and fission.* Hum Mol Genet, 2005. **14 Spec No. 2**: p. R283-9.

45. Kim, J.S., T. Qian, and J.J. Lemasters, *Mitochondrial permeability transition in the switch from necrotic to apoptotic cell death in ischemic rat hepatocytes.* Gastroenterology, 2003. **124**(2): p. 494-503.

46. Eguchi, Y., S. Shimizu, and Y. Tsujimoto, *Intracellular ATP levels determine cell death fate by apoptosis or necrosis.* Cancer Res, 1997. **57**(10): p. 1835-40.47. Labbe, G., D. Pessayre, and B. Fromenty, *Drug-induced liver injury through mitochondrial dysfunction: mechanisms and detection during preclinical safety studies.* Fundam Clin Pharmacol, 2008. **22**(4): p. 335-53.

48. Brand, M.D. and D.G. Nicholls, *Assessing mitochondrial dysfunction in cells.* Biochem J, 2011. **435**(2): p. 297-312.

49. Hengstler, J.G., et al., *Cryopreserved primary hepatocytes as a constantly available in vitro model for the evaluation of human and animal drug metabolism and enzyme induction.* Drug Metab Rev, 2000. **32**(1): p. 81-118.

50. Castell, J.V., et al., *Hepatocyte cell lines: their use, scope and limitations in drug metabolism studies.* Expert Opin Drug Metab Toxicol, 2006. **2**(2): p. 183-212.

51. Marroquin, L.D., et al., *Circumventing the Crabtree effect: replacing media glucose with galactose increases susceptibility of HepG2 cells to mitochondrial toxicants.* Toxicol Sci, 2007. **97**(2): p. 539-47.

52. O'Brien, P.J., et al., *High concordance of drug-induced human hepatotoxicity with in vitro cytotoxicity measured in a novel cell-based model using high content screening.* Arch Toxicol, 2006. **80**(9): p. 580-604.

53. Diaz-Ruiz, R., M. Rigoulet, and A. Devin, *The Warburg and Crabtree effects: On the origin of cancer cell energy metabolism and of yeast glucose repression.* Biochim Biophys Acta, 2011. **1807**(6): p. 568-76.

54. Swiss, R. and Y. Will, *Assessment of mitochondrial toxicity in HepG2 cells cultured in high-glucose- or galactose-containing media.* Curr Protoc Toxicol, 2011. **Chapter 2**: p. Unit2 20.

55. Gomez-Lechon, M.J., et al., *A human hepatocellular in vitro model to investigate steatosis.* Chem Biol Interact, 2007. **165**(2): p. 106-16.

56. Donato, M.T., et al., *Cytometric analysis for drug-induced steatosis in HepG2 cells.* Chem Biol Interact, 2009. **181**(3): p. 417-23.

57. Rossignol, R., et al., *Energy substrate modulates mitochondrial structure and oxidative capacity in cancer cells.* Cancer Res, 2004. **64**(3): p. 985-93.

58. Roth, R.A. and P.E. Ganey, *Animal models of idiosyncratic drug-induced liver injury--current status.* Crit Rev Toxicol, 2011. **41**(9): p. 723-39.

59. Boelsterli, U.A., *Animal models of human disease in drug safety assessment.* J Toxicol Sci, 2003. **28**(3): p. 109-21.

60. Boelsterli, U. and Y. Lee, *Development of animal models of drug-induced mitochondrial toxicity.* In: Dykens JA., Will Y., eds. Drug-induced mitochondrial dysfunction, 2008. **1st ed.** (Hoboken, New Jersey: John Wiley and Sons, Inc.): p. 539-554.

61. Miele, L., et al., *Hepatic mitochondrial beta-oxidation in patients with nonalcoholic steatohepatitis assessed by 13C-octanoate breath test.* Am J Gastroenterol, 2003. **98**(10): p. 2335-6.

62. Knapp, A.C., et al., *Toxicity of valproic acid in mice with decreased plasma and tissue carnitine stores.* J Pharmacol Exp Ther, 2008. **324**(2): p. 568-75.

63. Freneaux, E., et al., *Stereoselective and nonstereoselective effects of ibuprofen enantiomers on mitochondrial beta-oxidation of fatty acids.* J Pharmacol Exp Ther, 1990. **255**(2): p. 529-35.

64. Spaniol, M., et al., *Development and characterization of an animal model of carnitine deficiency.* Eur J Biochem, 2001. **268**(6): p. 1876-87.

65. Spaniol, M., et al., *Mechanisms of liver steatosis in rats with systemic carnitine deficiency due to treatment with trimethylhydraziniumpropionate.* J Lipid Res, 2003. **44**(1): p. 144-53.

66. Ong, M.M., C. Latchoumycandane, and U.A. Boelsterli, *Troglitazone-induced hepatic necrosis in an animal model of silent genetic mitochondrial abnormalities.* Toxicol Sci, 2007. **97**(1): p. 205-13.

67. Lee, Y.H., et al., *Troglitazone-induced hepatic mitochondrial proteome expression dynamics in heterozygous Sod2(+/-) mice: two-stage oxidative injury.* Toxicol Appl Pharmacol, 2008. **231**(1): p. 43-51.

68. Huang, Y.S., et al., *Genetic polymorphisms of manganese superoxide dismutase, NAD(P)H:quinone oxidoreductase, glutathione S-transferase M1 and T1, and the susceptibility to drug-induced liver injury.* J Hepatol, 2007. **47**(1): p. 128-34.

69. Julian, D.G., et al., *Randomised trial of effect of amiodarone on mortality in patients with left-ventricular dysfunction after recent myocardial infarction: EMIAT. European Myocardial Infarct Amiodarone Trial Investigators.* Lancet, 1997. **349**(9053): p. 667-74.

70. Morse, R.M., et al., *Amiodarone-induced liver toxicity.* Ann Intern Med, 1988. **109**(10): p. 838-40.

71. Mason, J.W., *Amiodarone.* N Engl J Med, 1987. **316**(8): p. 455-66.

72. Stelfox, H.T., et al., *Monitoring amiodarone's toxicities: recommendations, evidence, and clinical practice.* Clin Pharmacol Ther, 2004. **75**(1): p. 110-22.

73. Lewis, J.H., et al., *Histopathologic analysis of suspected amiodarone hepatotoxicity.* Hum Pathol, 1990. **21**(1): p. 59-67.

74. Simon, J.B., et al., *Amiodarone hepatotoxicity simulating alcoholic liver disease.* N Engl J Med, 1984. **311**(3): p. 167-72.

75. Fromenty, B., et al., *Dual effect of amiodarone on mitochondrial respiration. Initial protonophoric uncoupling effect followed by inhibition of the respiratory chain at the levels of complex I and complex II.* J Pharmacol Exp Ther, 1990. **255**(3): p. 1377-84.

76. Kaufmann, P., et al., *Mechanisms of benzarone and benzbromarone-induced hepatic toxicity.* Hepatology, 2005. **41**(4): p. 925-35.

77. Spaniol, M., et al., *Toxicity of amiodarone and amiodarone analogues on isolated rat liver mitochondria.* J Hepatol, 2001. **35**(5): p. 628-36.

78. Waldhauser, K.M., et al., *Hepatocellular toxicity and pharmacological effect of amiodarone and amiodarone derivatives.* J Pharmacol Exp Ther, 2006. **319**(3): p. 1413-23.

79. Pirovino, M., et al., *Amiodarone-induced hepatic phospholipidosis: correlation of morphological and biochemical findings in an animal model.* Hepatology, 1988. **8**(3): p. 591-8.

80. Fromenty, B., et al., *Amiodarone inhibits the mitochondrial beta-oxidation of fatty acids and produces microvesicular steatosis of the liver in mice.* J Pharmacol Exp Ther, 1990. **255**(3): p. 1371-6.

81. Zahno, A., et al., *The role of CYP3A4 in amiodarone-associated toxicity on HepG2 cells.* Biochem Pharmacol, 2011. **81**(3): p. 432-41.

82. Hoy, S.M. and S.J. Keam, *Dronedarone.* Drugs, 2009. **69**(12): p. 1647-63.

83. Dobrev, D. and S. Nattel, *New antiarrhythmic drugs for treatment of atrial fibrillation.* Lancet, 2010. **375**(9721): p. 1212-23.

84. Anonymous, *In brief: FDA warning on dronedarone (Multaq).* Med Lett Drugs Ther, 2011. **53**(1359): p. 17.

85. *In brief: FDA warning on dronedarone (Multaq).* Med Lett Drugs Ther, 2011. **53**(1359): p. 17.

86. Joghetaei, N., et al., *Acute liver failure associated with dronedarone.* Circ Arrhythm Electrophysiol, 2011. **4**(4): p. 592-3.

87. Jahn, S., et al., *Severe toxic hepatitis associated with dronedarone.* Curr Drug Saf, 2013. **8**(3): p. 201-2.

88. Serviddio, G., et al., *Mitochondrial oxidative stress and respiratory chain dysfunction account for liver toxicity during amiodarone but not dronedarone*

administration. Free Radic Biol Med, 2011. **51**(12): p. 2234-42.

89. Patel, C., G.X. Yan, and P.R. Kowey, *Dronedarone.* Circulation, 2009. **120**(7): p. 636-44.

90. van der Klauw, M.M., et al., *Hepatic injury caused by benzbromarone.* J Hepatol, 1994. **20**(3): p. 376-9.

91. Arai, M., et al., *Fulminant hepatic failure associated with benzbromarone treatment: a case report.* J Gastroenterol Hepatol, 2002. **17**(5): p. 625-6.

92. Wagayama, H., et al., *Fatal fulminant hepatic failure associated with benzbromarone.* J Hepatol, 2000. **32**(5): p. 874.

93. Haring, B., et al., *Benzbromarone: a double-edged sword that cuts the liver?* Eur J Gastroenterol Hepatol, 2013. **25**(1): p. 119-21.

94. Kramar, R. and M.M. Muller, *Inhibition of enzymes of the internal mitochondrial membrane by benzbromarone.* Experientia, 1973. **29**(4): p. 391-2.

95. Kobayashi, K., et al., *Cytotoxic effects of benzbromarone and its 1'-hydroxy metabolite in human hepatocarcinoma FLC4 cells cultured on micro-space cell culture plates.* Drug Metab Pharmacokinet, 2013. **28**(3): p. 265-8.

96. Kobayashi, K., et al., *Identification of CYP isozymes involved in benzbromarone metabolism in human liver microsomes.* Biopharm Drug Dispos, 2012. **33**(8): p. 466-73.

97. Krahenbuhl, S., *Mitochondria: important target for drug toxicity?* J Hepatol, 2001. **34**(2): p. 334-6.

98. Stewart, J.D., et al., *Polymerase gamma gene POLG determines the risk of sodium valproate-induced liver toxicity.* Hepatology, 2010. **52**(5): p. 1791-6.

99. Daly, A.K., et al., *HLA-B*5701 genotype is a major determinant of drug-induced liver injury due to flucloxacillin.* Nat Genet, 2009. **41**(7): p. 816-9.

100. Boelsterli, U.A. and P.L. Lim, *Mitochondrial abnormalities--a link to idiosyncratic drug hepatotoxicity?* Toxicol Appl Pharmacol, 2007. **220**(1): p. 92-107.

101. Dixit, R. and U.A. Boelsterli, *Healthy animals and animal models of human disease(s) in safety assessment of human pharmaceuticals, including therapeutic antibodies.* Drug Discov Today, 2007. **12**(7-8): p. 336-42.

102. Tolwani, R.J., et al., *Medium-chain acyl-CoA dehydrogenase deficiency in gene-targeted mice.* PLoS Genet, 2005. **1**(2): p. e23.

103. de Vries, H.G., et al., *Prevalence of carriers of the most common medium-chain acyl-CoA dehydrogenase (MCAD) deficiency mutation (G985A) in The Netherlands.* Hum Genet, 1996. **98**(1): p. 1-2.

104. Grosse, S.D., et al., *The epidemiology of medium chain acyl-CoA dehydrogenase deficiency: an update.* Genet Med, 2006. **8**(4): p. 205-12.

105. Chace, D.H., et al., *Rapid diagnosis of MCAD deficiency: quantitative analysis of octanoylcarnitine and other acylcarnitines in newborn blood spots by tandem mass spectrometry.* Clin Chem, 1997. **43**(11): p. 2106-13.

106. Lindner, M., G.F. Hoffmann, and D. Matern, *Newborn screening for disorders of fatty-acid oxidation: experience and recommendations from an expert meeting.* J Inherit Metab Dis, 2010. **33**(5): p. 521-6.

107. Schatz, U.A. and R. Ensenauer, *The clinical manifestation of MCAD deficiency: challenges towards adulthood in the screened population.* J Inherit Metab Dis, 2010. **33**(5): p. 513-20.

108. Rinaldo, P., D. Matern, and M.J. Bennett, *Fatty acid oxidation disorders.* Annu Rev Physiol, 2002. **64**: p. 477-502.

109. Fromenty, B., et al., *Most cases of medium-chain acyl-CoA dehydrogenase deficiency escape detection in France.* Hum Genet, 1996. **97**(3): p. 367-8.

110. Nyman, L.R., et al., *Homozygous carnitine palmitoyltransferase 1a (liver isoform) deficiency is lethal in the mouse.* Mol Genet Metab, 2005. **86**(1-2): p. 179-87.

111. Vempati, U.D., A. Torraco, and C.T. Moraes, *Mouse models of oxidative phosphorylation dysfunction and disease.* Methods, 2008. **46**(4): p. 241-7.

112. Lee, K.K., et al., *Isoniazid-induced cell death is precipitated by underlying mitochondrial complex I dysfunction in mouse hepatocytes.* Free Radic Biol Med, 2013. **65**: p. 584-94.

113. Larsson, N.G., et al., *Mitochondrial transcription factor A is necessary for mtDNA maintenance and embryogenesis in mice.* Nat Genet, 1998. **18**(3): p. 231-6.

114. Hynes, J., et al., *Investigation of drug-induced mitochondrial toxicity using fluorescence-based oxygen-sensitive probes.* Toxicol Sci, 2006. **92**(1): p. 186-200.

115. Will, Y., et al., *Analysis of mitochondrial function using phosphorescent oxygen-sensitive probes.* Nat Protoc, 2006. **1**(6): p. 2563-72.

116. Rana, P., S. Nadanaciva, and Y. Will, *Mitochondrial membrane potential measurement of H9c2 cells grown in high-glucose and galactose-containing media does not provide additional predictivity towards mitochondrial assessment.* Toxicol In Vitro, 2011. **25**(2): p. 580-7.

Acknowledgments

This work could only be performed with the help and support of several people.

I would like to thank Prof. Stephan Krähenbühl for mentoring my work and his constant support and advices during my PhD studies. I profited from your extensive knowledge in pharmacology and toxicology and you offered me a great opportunity to advance my scientific knowledge in the master program in Toxicology. Thanks also to Prof. Jörg Huwyler for his availability as co-referee for the evaluation of this work, and to Prof. Alex Odermatt for his presence as chairman of the faculty.

I am grateful to all my colleagues in the Clinical Pharmacology and Toxicology Laboratory 410 and 411 at the University Hospital of Basel. I would like to thank Dr. Peter Lindinger and Dr. Jamal Bouitbir for introducing me to mitochondrial function and for teaching me essentials in *in vitro* and *in vivo* experimentation. A special thank also goes to Andrea Marisa Stoller and Réjane Morand Bourqui for their support during the animal study, and to Kim Blum and Dominik Schnell who performed their master thesis under my supervision and helped me to get a lot of assays done, I couldn't have done it on my own. Thank you Annalisa, Benji, Anna, Riccardo, Franziska, Patrizia, Massimiliano, Karin, Linda, Swarna, Estelle and all the master students for the good working climate and for valuable discussions.

Finally, I would like to thank my family and friends for their support and encouragement. Thanks to my parents and sisters for supporting my in every possible way and thank you my dear Stefan for backing me up all along.